Evaluation of SERA seismic hazard assessment results using Bayesian approaches

Work Package 5 "PSHA"

AUTHORS		REVIEW		APPROVAL	
Name	Date	Name	Date	Name	Date
Stéphane Drouet Ramon Secanell	2021/08/31	R. Musson *Roger Musson* P. Bazzurro	2022/02/18	JP.Tardivel T.Rukavina ***Public-access*** ☒ ***SIGMA-2 restricted*** ☐	20…./…./…..

Evaluation of SERA seismic hazard assessment results using Bayesian approaches

Report | France

159486_REP01_ORA20_Bayesian-update-PSHA 02 | 31 August 2021
Final report – First revision
ORANO

Document Control

Document Information

Project Title	Evaluation of SERA seismic hazard assessment results using Bayesian approaches
Document Title	Evaluation of SERA seismic hazard assessment results using Bayesian approaches
Fugro Project No.	159486
Fugro Document No.	159486_REP01_ORA20_Bayesian-update-PSHA
Issue Number	02
Issue Status	Final report – First revision
Fugro Legal Entity	FUGRO France SAS
Issuing Office Address	20 ZAC du Pujol 1 – Les Artauds Est – Auriol13390, France

Client Information

Client	ORANO
Client Address	125 Avenue de Paris, 92320 Châtillon
Client Contact	Tea RUKAVINA
Client Document No.	[Client Document No.]

Document History

Issue	Date	Status	Comments on Content	Prepared By	Checked By	Approved By
00	April 9, 2021	Final report – For review		SDR, RSE	RSE	SDR
01	April 19, 2021	Final report – first emmission	Integration of comments by E. Viallet and G. Daniel	SDR, RSE	RSE	SDR
02	August 31, 2021	Final report – first revision	Integration of comments by SIGMA2 reviewers P. Bazzurro and R. Musson	SDR, RSE	RSE	SDR

Project Team

Initials	Name	Role
SDR	Stéphane Drouet	Project Manager
RSE	Ramon Secanell	Senior Seismologist

FUGRO
FUGRO France SAS
20 ZAC du Pujol 1
Les Artauds Est
13390 AURIOL
FRANCE

ORANO Support

125 avenue de Paris

92320 Chatillon

France

31 August 2021

Dear Madam Rukavina,

We are pleased to deliver the final report regarding the Bayesian evaluation of the seismic European hazard models ESHM13 (SHARE) and ESHM20 (SERA). The database compilation is presented as well as evaluation results.

This report has been be submitted to SIGMA-2 for review and results presented during the Scientific Committee in June 2021. This final version includes additional modification of the content of the report following SIGMA-2 reviewers P. Bazzurro and R. Musson suggestions.

Yours faithfully,

Stéphane Drouet
Seismic Hazard & Monitoring team Manager
Fugro
T +33 4 42 36 08 62 | **M** +33 6 81 95 88 87 | **E** s.drouet@fugro.com | **W** fugro.com
A 20 ZAC du Pujol 1 - Les Artauds Est, 13390 Auriol, France

Executive Summary

Two databases have been built in order to apply a testing procedure to PSHA model based on a Bayesian approach. Several sites with instrumental or macroseismic observations have been considered in Western Europe complemented by a couple of sites in more active regions (Italy, Greece, Turkey). Considering several sites is necessary in order to obtain a meaningful observation period. In order to avoid correlations between the different observations, a minimum inter-site distance of 200 km has been considered. For consistency with the PSHA calculations, only observations from events with magnitude above 4.5 (minimum magnitude used in the PSHA calculations) and located at distance lower than 200 km (consistent with the maximum integration distance used in the PSHA) are considered.

In addition to observations, i.e. exceedances of a given acceleration threshold or a given intensity level, the completeness period for the observations are also needed. Most of the information related to completeness is taken from the literature with exception of the completeness for Italian sites which have been computed by Pr. Albarello (pers. com.). For instrumental data the completeness is evaluated based on station metadata information downloaded from the FDSN webservices of RESIF, INGV and ETH.

The PSHA results from two versions of the European Seismic Hazard Model are considered: ESHM13 developed in the framework of the SHARE project, and ESHM20 being currently finalized in the framework of the SERA project. For the ESHM13 model, calculations have been performed at the sites of interest while for ESHM20, hazard curves have been provided by L. Danciu for points at a distance lower than 5 km from the points of interest.

The Viallet et al. (2019) Bayesian evaluation approach is applied. For instrumental data, the likelihoods of the various hazard curves are computed from Poisson distribution with mean equal to the cumulated rate of exceedance over all the sites (taking into account the completeness period). For macroseismic data a preliminary step is necessary to convert the hazard curve in acceleration into hazard curve in intensity. However, the likelihoods are then computed in a similar way considering the cumulated rate of occurrence of intensity.

The testing procedure is applied to a sub-set of data covering only France and to the complete set of data. Both ESHM13 and ESHM20 are tested. The results can be summarised as follows:

- Evaluation of the ESHM13 model with French data:
  - Based on macroseismic observations, the ESHM13 model seems to slightly over-estimate observations for intensities VII and VIII. For intensity VI, the model is relatively close to observations;
  - The evaluation based on macroseismic data is strongly dependent on the Intensity-to-PGA relationship. From the list of models compiled we selected a subset of 4 models representative of the uncertainty in the intensity-PGA conversion;

- The evaluation at intensity VII also leads to different results compared to intensity VI and VIII due to the fact that no observations exist at I=VII, but this random occurrence process is taken into consideration in the evaluation;
  - Based on instrumental data (for 0.1 m/s² threshold), the ESHM13 seems to largely overestimate observations (overestimation of seismic hazard).
  - Since there are no observations for acceleration thresholds 0.2, 0.5, 1.0 m/s², the results of the Bayesian update must be used with caution, but predictions seem to slightly over-estimate observation because predictions lead to expect some occurrences;
- Evaluation of the ESHM20 model with French data:
  - Based on macroseismic observations, the ESHM20 model seems to slightly underpredict observations (underestimation of seismic hazard) but the agreement is better compared to that obtained with ESHM13;
  - The evaluation at intensity VII also leads to different results compared to intensity VI and VIII due to the fact that no observations exist at intensity VII, but this random occurrence process is taken into consideration in the evaluation;
  - The evaluation based on macroseismic data is again very dependent on the Intensity-to-PGA relationship;
  - Based on instrumental data, the ESHM20 seems to overpredict slightly observations;
- Evaluation of the ESHM20 model with data from Europe:
  - Based on macroseismic observations, the ESHM20 model seems to be consistent with observations, for intensities VI and VII. For intensity VIII, the predictions of ESHM20 model overestimate the observations;
  - Based on instrumental data, the ESHM20 seems to overpredict slightly the observations but the agreement is rather good.

Contents

FUGRO

Appendices

Roger Musson

Figures in the Main Text

Tables in the Main Text

1.   Introduction

1.1   Scope of work and objective

The main objective of this study is the evaluation of the seismic hazard assessment performed in the framework of the SERA project based on observed seismicity.

The overall objective of SERA is to give a significant contribution to improve the access to data, services and research infrastructures, and deliver solutions based on innovative R&D in seismology and earthquake engineering, aiming at reducing the exposure of our society to the risk posed by natural and anthropogenic earthquakes. To this end, one of the tasks of SERA is to revise the European Seismic Hazard reference model for potential consideration in the ongoing revision of the Eurocode 8 (possibly as part as an informative annex).

Then, the main objective of this study is the comparison between observations (in some selected European sites) and predictions of the SERA seismic hazard assessment (seismic hazard curves). This comparison will be performed using Bayesian methodologies recently developed by several teams in France.

During the last decade, new methodologies to evaluate probabilistic seismic hazard analysis (PSHA) results appeared, mainly in France and Italy, particularly within the framework of the SIGMA project. Two published methodologies (Viallet et al, 2019 and Secanell et al, 2018) are based on a Bayesian approach and present many similitudes. A larger panel of existing methodologies and applications is given in the proceedings of the OECD/NEA Workshop on Testing Probabilistic Seismic Hazard Analysis Results and the Benefits of Bayesian Techniques held in Pavia, Italy, 2015 (OECD/NEA/CSNI workshop, 2015).

These methods used in this study were developed in parallel by EDF and FUGRO France. A tool was developed in Python by EDF, called "Phebus", to apply the Viallet et al. (2019) method. FUGRO France developed its own tool in Delphi, called "Bayac", to apply the Secanell et al. (2018) method.

The study proposed here aims at the evaluation of the SERA seismic hazard assessment results using mainly the Viallet et al. (2019) method (using "Phebus"). The FUGRO France software and the Secanell et al. (2018) method will be also used to evaluate the coherence between both methods.

A second objective of the project is the improvement of "Phebus". It will be updated incorporating the graphical representation and outputs of "Bayac". "Phebus" will also be checked (V & V process) and will be improved during the project, as much as possible, to create a user-friendly tool which could be distributed to the community.

1.2 Main existing evaluations of the seismic hazard

This chapter presents the main projects developed in France during the last 15 years to test and to update a seismic hazard assessment based on the comparison between observations (instrumental and historical recorded information) and predictions (seismic hazard curves of a PSHA).

Historically, the firsts PSHA performed in France (i.e. the seismic hazard map performed during the MEDD 2002 project, that was used as a basis for the national annex of the EC8) showed a poor agreement between predictions and observations. Many reasons were behind this disagreement: Ms-ML conversions, selection of GMPEs, etc.

Then, some studies were performed in order to "test" the PSHAs and to try to refine the initial PSHA using Bayes theorem. These studies are summarized here below.

1.2.1 Report GTR_EDF_0907_396.pdf

In 2007, a PSHA study was performed in France, at a national scale, developed in terms of macroseismic intensity (Carbon et al 2007). Using this PSHA study, a comparison of predictions and historical observations (French Sisfrance database) was performed and resulted in a rather good agreement. However, this consistency is not observed when the PSHA is developed in terms of acceleration.

When conducting the PSHA developed in terms of intensity, the intensity prediction equations were calculated using the local macroseismic data from the national database and the seismic distribution relations (Gutenberg-Richter model) were developed using the earthquake catalogue homogenized in intensity.

In a PSHA developed in terms of acceleration, the seismic distribution relations (Gutenberg-Richter model) are always developed using local data. However, in a context of moderate activity, the ground motion prediction equations (GMPE) are imported from worldwide databases or from regional databases representative of other seismotectonic contexts. There were not enough seismic records in stable seismotectonic regions (such as France) to develop a local GMPE. This could be one of the reasons of the discrepancies between predictions and observations. Of course, in the case of intensities, we have a longer period of observation (some centuries). In the case of accelerations, the period of observation is only some tens of years. This short period of observation could also be a reason of the discrepancies between predictions and observations.

1.2.2 Report GTR_EDF_0508_458.pdf

This report developed and implemented a testing method based on Bayes' theory. A software developed during the project allowed its implementation for any further project.

For the project a new probabilistic model was developed for the France, with a logic tree of 400 branches. The instrumental observations (PGA) on 38 sites (19 NPPs and 19 seismic stations spread around France) were compiled and the testing method was applied.

In the a priori method an equivalent weight was assigned to each of the 400 branches of the logic tree and the application of the Bayesian method allowed to update the weights of the different branches of the logic tree.

1.2.3 Report GTR_EDF_1014_1216.pdf

The objective of this report was to present the Bayesian methodology developed previously and presented in report GTR_EDF_0508_458.pdf, to update a probabilistic seismic hazard assessment based on a prior logic tree, and to conduct sensitivity analyses to check if the Bayesian update, based on observed data, may be used in the PSHA, to calibrate the weights of the different branches of a logic tree.

The PSHA carried out at the beginning of the SIGMA project was considered to generate the prior distribution of hazard curves at several selected sites.

The predictions of acceleration exceedance rates were compared with the observations. In addition to accelerations recorded during the instrumental period, in this case also the historical observations were used (in GTR_EDF_0508_458.pdf only instrumental information was used). The historical observations were obtained using intensity-PGA correlations applied to historical events. In the case of historical observations, only epistemic uncertainty associated to I-PGA relations was considered (different I-PGA were tested). The aleatory uncertainty was not considered and only the mean PGA predicted by the I-PGA relation was used.

Applying the Bayes theory, the conditional probability of occurrence of the predicted accelerations, given that instrumental or historical accelerations were produced and were used to calculate a posterior distribution of the weights of the different branches of the logic tree.

The method was tested as an alternative to the classic weight assignment based on expert judgement. The posterior weights allow defining a posterior seismic hazard assessment (mean and centiles seismic hazard curves), which was assumed in better agreement with the observations, and for which a reduction of the uncertainties is expected.

1.2.4 Viallet et al. 2019

The Viallet et al. 2019 publication presents, essentially, a similar Bayesian method used in reports GTR_EDF_0508_458.pdf and GTR_EDF_1014_1216.pdf. If only the instrumental observations are used, the methods are essentially equivalents. However, if historical information is used, the Viallet et al. 2019 method introduced a new approach allowing to take into account the epistemic and aleatory uncertainty associated to the I-PGA relations.

The method developed was based on a Bayesian inference technique used in order to quantify the likelihood of the prior estimation, and finally update the PSHA.

FUGRO

Moreover, a case of application was presented on the French metropolitan territory to demonstrate the efficiency of that updating method and draw perspectives for further applications. A new software (Phebus) was developed to apply the methodology described.

Viallet at al. 2019 represents the most recent evolution of testing tools based on Bayes theorem developed in France during the last 10 years approximately. Therefore, Phebus was adopted and improved for the present study.

2. Compilation of Input data

To perform the evaluation of a Probabilistic Seismic Hazard Assessment, 2 types of input data are required:

- <u>Observations</u> which may include paleoseismic data, macroseismic information and instrumental information, available in a number of geographical locations (observation points);
- <u>Seismic hazard curves</u> at given geographical locations (observation points). Depending on the complexity of the logic-tree, all the curves corresponding to all the branches, or a sub-set of branches representative of the logic-tree can be considered.

Regarding observations, this study considers instrumental and macroseismic data (even if some examples of evaluation based on paleoseismic data are given in OECD/NEA/CSNI workshop, 2015).

Regarding Seismic hazard curves, ideally, evaluation process should be performed based on the results from the whole logic tree of the PSHA study in order to provide PSHA actors with useful feedback in order to let them adjust weight of the whole logic tree (even reconsider some branches), based on the comparison to observations. In this study, using the SERA results, only percentiles 5, 15, 50, 85 and 95 were used due to time delay and organizational issues. But a complementary action could be done in a future stage by exploring the whole logic tree (or at least a sub-set of it).

2.1 Observation database. Selection criteria

The observation database can be composed of historical information and instrumental information. For the evaluation of SERA seismic hazard results, we compiled both types of information. For the historical data, the selection points are mainly big cities, with a long seismic history (i.e. Lyon, Grenoble, Basel, Barcelona, etc.). For the instrumental data, the observation points are mainly seismic stations. Additionally, the nuclear power plants (NPP), which have accelerometers installed in free field since many years, are also very useful observation points. A data collection of the recorded data in NPP facilities has been compiled in the framework of an OECD/NEA activity related to the Assessment of the Safe Shutdown Earthquake Robustness Against on Site Observations described in OECD/NEA/CSNI/WGIAGE (2019), the official report being currently under publishing process.

The selection of the observation points is a key aspect of any reliable evaluation process. Some criteria will be considered for their selection:

1. *Consideration of seismotectonic context:* Our main region of interest is Western Europe (France, Spain, Switzerland, Belgium and Germany) where seismic activity is low to moderate. However, the seismic hazard model that will be tested (ESHM20 from SERA and ESHM13 from SHARE) cover the whole Euro-Mediterranean region. Hence a couple

of points in Southern and Eastern Europe (Italy Greece, Turkey) are also considered. Combining different seismotectonic contexts might be complicated since the hazard model can be quite different from one region to the other. PSHA evaluation is usually done using observation points located in the same seismotectonic context.

2. *Territory under consideration in the evaluation process*: Ideally, the evaluation process should cover the whole territory under consideration and then multiple comparisons might be performed. For instance, evaluation of results from sub-regions of the whole territory or evaluation of results from all regions with similar seismotectonic contexts. The former would give insights of possible inconsistency between PSHA results and observations in a specific area which may encourage PSHA actors to reconsider their assumptions (or logic tree branches) related to this particular area. The latter would allow to gather more sites and then evaluate a longer return period range of the PSHA which may encourage PSHA actors to reconsider some of their general assumptions (or logic tree branches) that may have an impact on the PSHA results among the whole territory.

3. *Correlation between observations*: Special attention must be paid to the distance between observation points, in order to address possible correlation issues between observed data. This issue is well described in OECD/NEA/CSNI workshop, 2015. This means that if two sites are close to each other, observation data will be correlated (most of seismic events will be observed by both the 2 sites). Then, this correlation has to be considered when comparing with PSHA results, but usual Poisson's occurrence model does not consider this correlation. Consequently, either the site selection has to consider an appropriate separation distance in order to avoid correlation or the evaluation process has to include correlation.

4. *Time of observation*: Finally, the evaluation process considers the time of observation in order to transform an annual rate of exceedance of a given ground motion parameter into a rate of exceedance along a certain period of observation. This means that a special attention has to be paid to this parameter, depending on the type of observation under consideration.

5. *Instrumental data*: For the selection of instrumental sites, the following criteria are considered:
   a. Priority will be given to rock station sites (for coherency with the hazard calculation results).
   b. The distance between stations will be considered to avoid correlations.
   c. The time of operation (removing maintenance time) of the seismic stations will be considered.

6. *Historical data:* For the selection of historical sites, the following criteria are considered:
   a. Priority will be given to well documented sites (meaning big cities with well documented historical seismicity).
   b. The distance between cities will be considered to avoid correlations.
   c. The time of observation will be based on completeness period of the catalogue of historical seismicity.

2.2 Macroseismic database

2.2.1 France

2.2.1.1 Source of information

AHEAD (European Archive of Historical EArthquake Data) is a pan-European, common, and open platform to support the research on historical earthquake data. It is the most reliable source of macroseismic data in Europe. For France the portal https://www.emidius.eu/AHEAD/ leads to the link https://sisfrance.irsn.fr/ . The SISFRANCE portal shows an interface allowing request for information. We observed that, sometimes, the data in this portal does not correspond to the SISFRANCE2017 database. For this project, we retained the information existing in SISFRANCE2017 database provided by EDF under Microsoft Access format.

To develop the macroseismic database in France for the study, we used 2 sources:

- SISFRANCE2017: The Access file containing the macroseismic database of France was provided by EDF. It contains the macroseismic data up to 2007. However, the last modifications of the database were performed in 2017.
- The FCAT-17 seismic catalogue (Manchuel et al., 2017) developed in the framework of the SIGMA project. Moment magnitude of earthquakes included in the SISFRANCE database are taken from FCAT-17.

2.2.1.2 Selection of observation points:

The criteria to select the French cities with macroseismic information are:

1. Cities with a long history where macroseismic information is available since a long time.
2. Cities covering almost homogeneously the whole territory.
3. In 2007, a PSHA in terms of intensity was performed by Fugro for EDF (report GTR/EDF/0907-396). Fugro developed 7 attenuation laws in terms of intensity for 7 regions with different seismotectonic characteristics (Pyrenees, Rhine, Alps, Armorican Massif, Northern France, Provence and stable regions) (Figure 2.1). The predictions of PSHA in terms of intensity were very coherent with observations. In the present study, at least one city for each "seismotectonic" region in France is considered.
4. A minimum distance between cities of approximately 200 km is considered to avoid correlations (i.e., one earthquake producing simultaneously several observations in different cities).
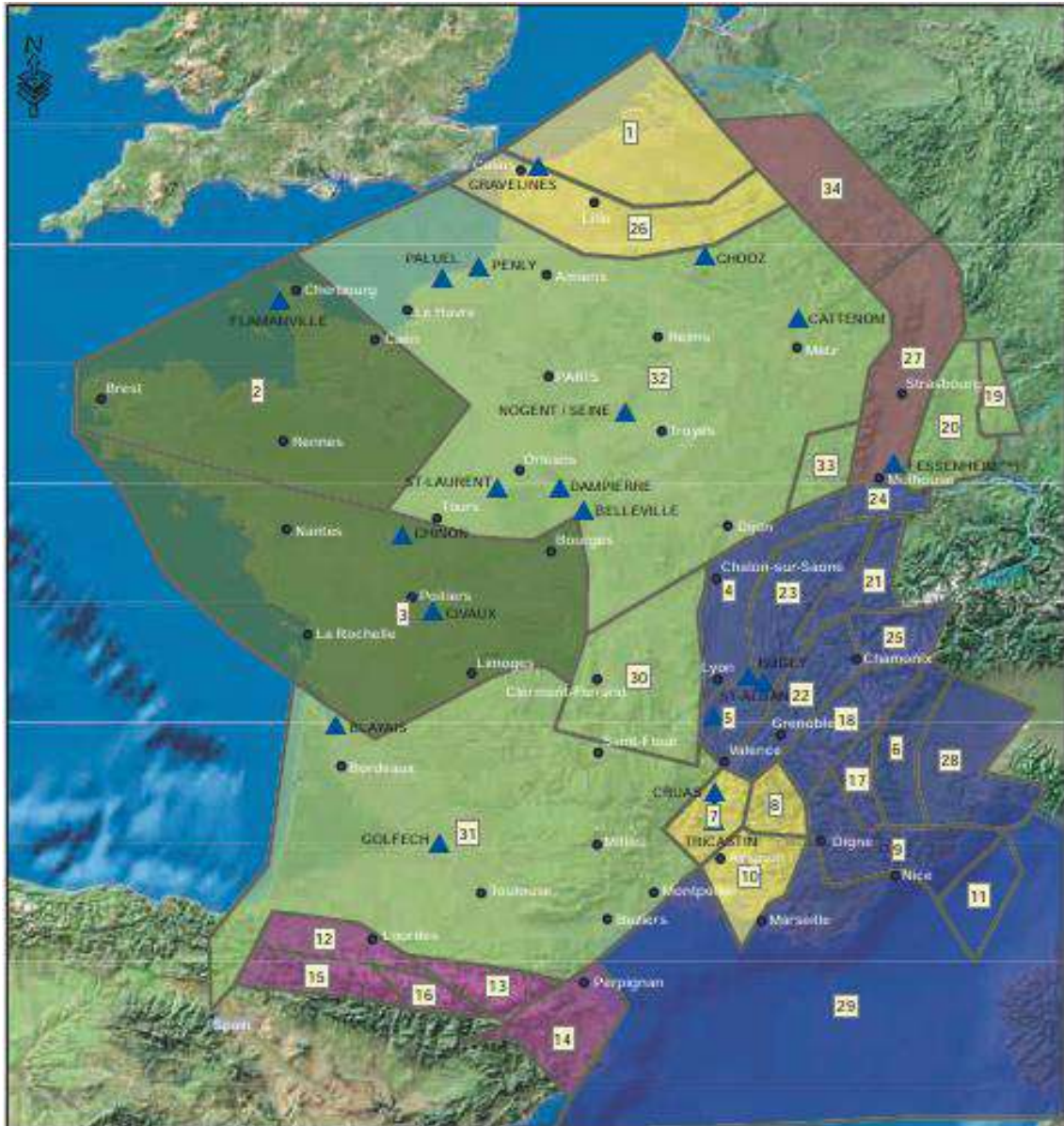
FUGRO

Figure 2.1: Seven seismic regions defined for France in Fugro 2007 report GTR/EDF/0907-396.

The selected 15 cities in France are :

- Grenoble and Nice in the Alps region.
- La Rochelle, Brest and Cherbourg in the Armoricain Massif region.
- Lille in Northern France.
- Marseille in Provence.
- Mulhouse in the Rhine region.
- Lourdes and Perpignan in the Pyrenees.
- Paris, Orleans, Limoges, Toulouse and Clermont-Ferrand in the so-called stable region in the 2007 study.

Figure 2.2 and Figure 2.3 show the macroseismic observations in France, epicentral intensity and observed punctual intensities, respectively (source: SISFRANCE database 2017), as well as the 15 selected sites. Epicentral intensities are associated to a quality index which can take

values A, B, C, E, I, and K. The SisFrance website provides a short description of quality indexes A, B, C and K. A corresponds to an estimation based on a large number and precise values of intensity observation, B to a smaller number of observation but still precise, C to sparse and imprecise intensity observations and K based on an estimation based on an intensity attenuation model (Sponheuer). No precision is provided however regarding quality indexes E and K. Punctual observations are also associated to a quality index A, B or C, corresponding to good, fairly good and imprecise évaluation.

Epicentral intensity

·	<= 2
∘	2 - 4
∘	4 - 6
O	6 - 9
O	9 - 12
O	> 9

Quality of epicentral intensity

🔴	A
🟠	B
🟡	C
🟢	E
🔵	I
⚫	K

☑ Selected city
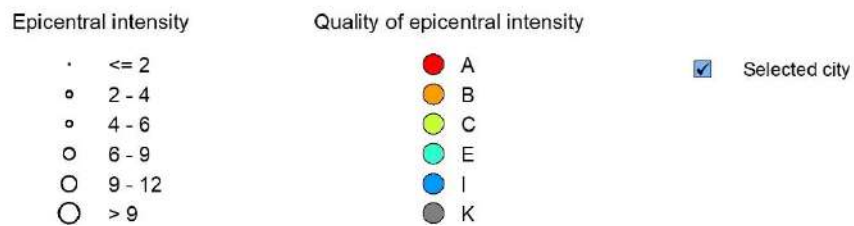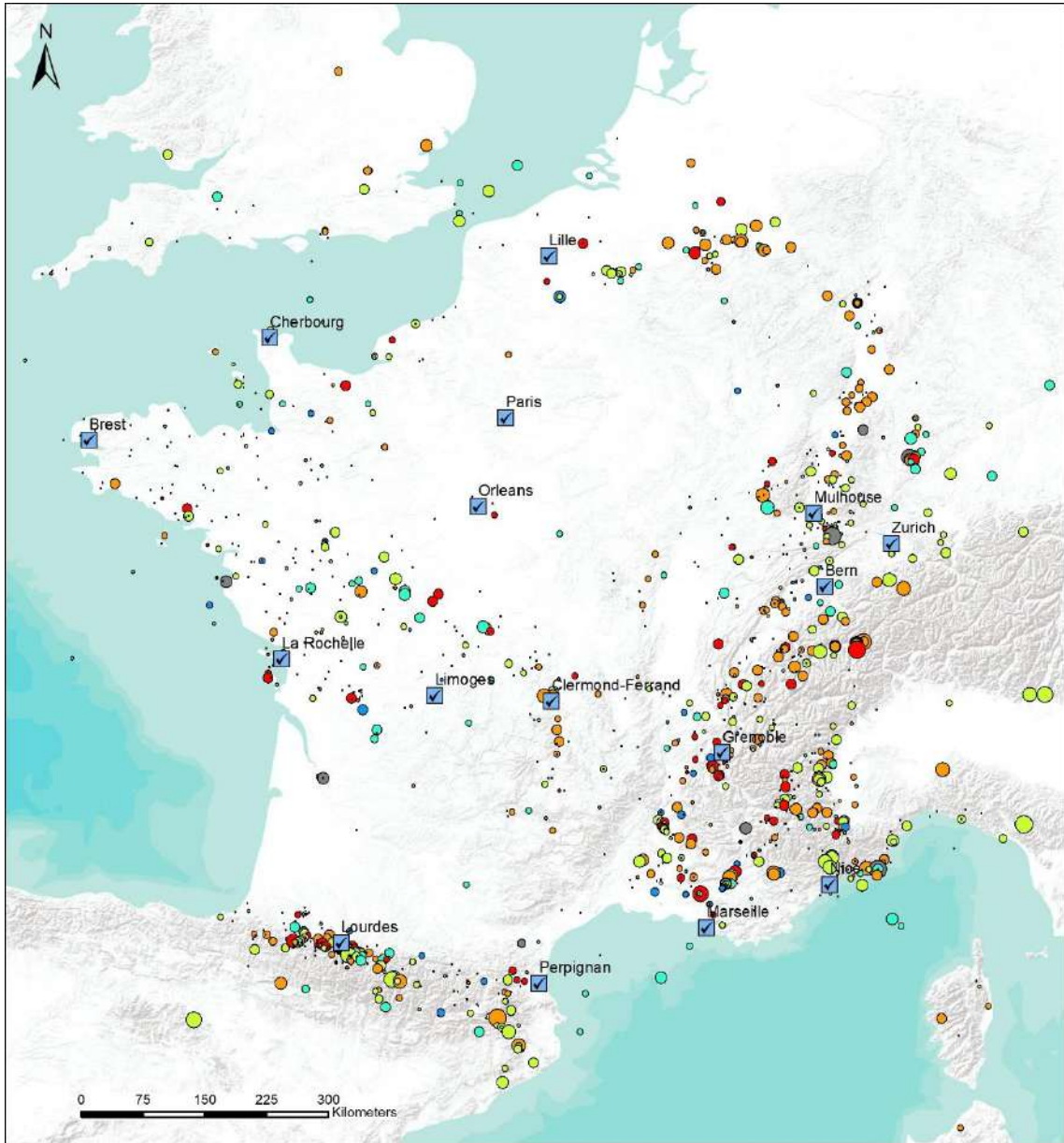
Figure 2.2: Map of epicentral intensities in the SisFrance (2017) database with the 15 cities selected for the creation of the macroseismic database in France.
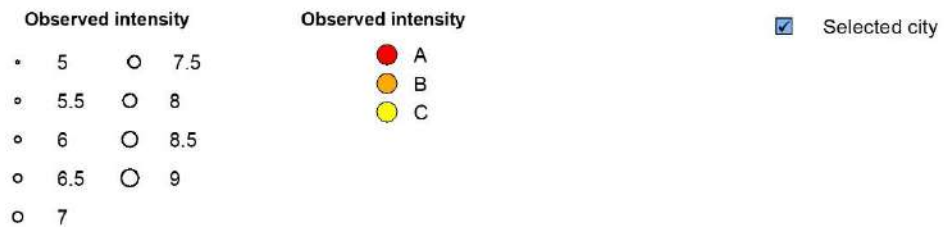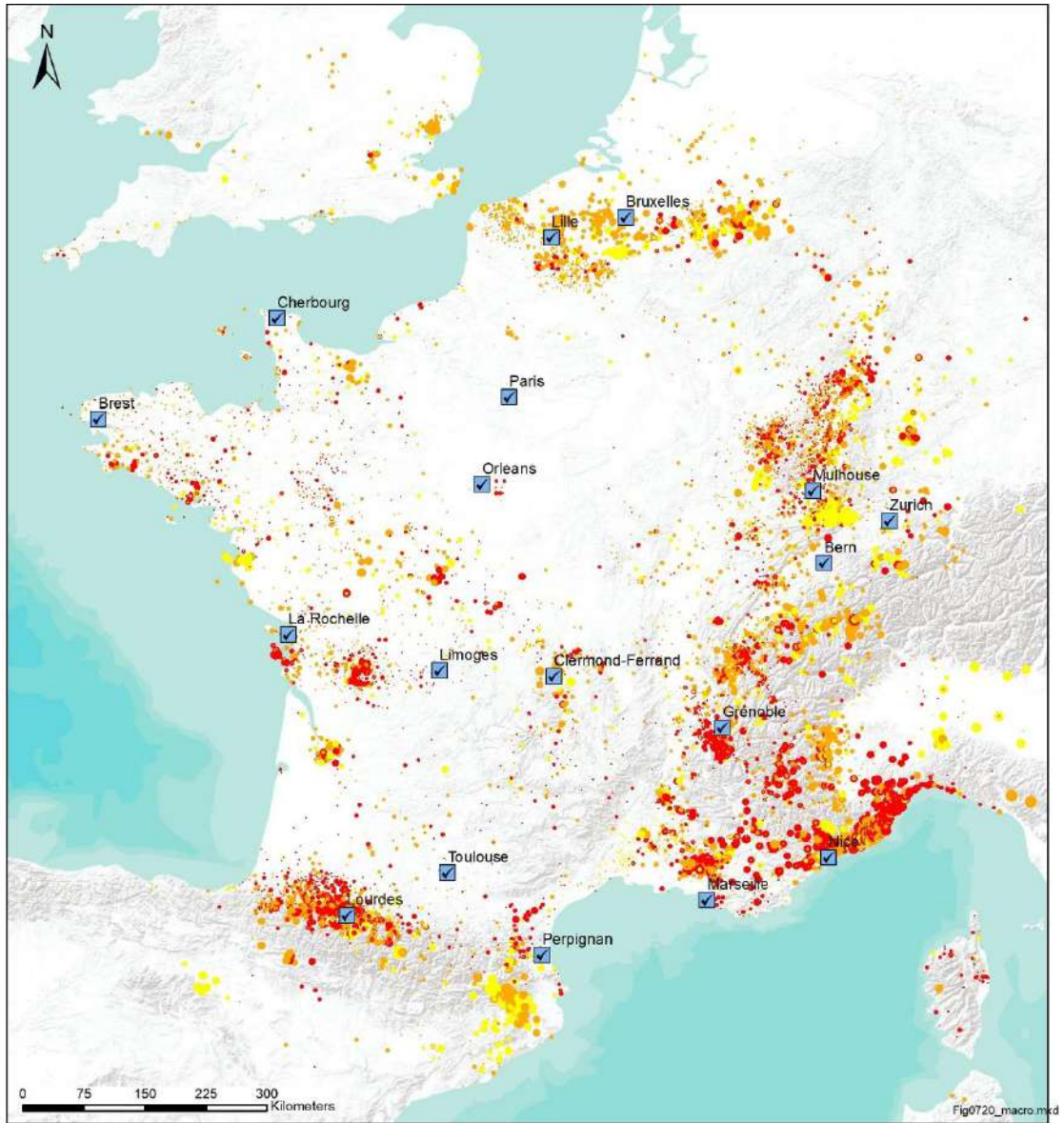
Figure 2.3: Map of observed intensities in the SisFrance (2017) database (punctual observation points) with the 15 cities selected for the creation of the macroseismic database in France.

2.2.1.3 Completeness of observation

Completeness of observations must be taken into account such that the computed rate of exceedances is robust.

Ideally, the completeness should be defined for each city. However, often the lack of data (mainly of high intensities) does not allow to define a reliable completeness period for each city.

As an alternative a regional approach is used. In the present study specific completeness evaluation is not performed, the evaluation made in the 2007 study (report GTR/EDF/0907-396) is used. The period of completeness can be different in different regions. Globally, the populated regions should have longer completeness periods than regions with a low density of population. For each city, we considered the completeness period defined in the region where the city is located.

The periods of completeness adopted are shown in Table 2.1 for the seven regions defined in the 2007 report.

Table 2.1: Completeness periods adopted in 7 regions in France for different intensity bins (from report GTR/EDF/0907-396).

Intensity	Alps	Armorican Massif	Northern France	Provence	Pyrenees	Rhine region	Stable regions
[V-VI[	1880	1880	1880	1880	1910	1870	1850
[VI-VII[	1830	1750	1850	1850	1910	1750	1750
[VII-VIII[	1800	1700	1750	1750	1750	1630	1750
[VIII-XI[	1500	1500	1500	1500	1500	1500	1500
[IX-X[	1300	1300	1300	1300	1300	1300	1300

The years of observation are then computed considering the period from the beginning of completeness periods (the year from which we do not miss seismic information) and 2007, the last year considered in SISFRANCE2017 database provided by EDF. In SISFRANCE2017, some information is updated up to 2017, however no new information is included since 2007.

2.2.1.4 Analysis of the database

The macroseismic information in 15 cities was extracted from the Access version of the SISFRANCE database (version 2017) provided by EDF for the project. From this Access database, we created some request to extract the observations recorded in the 15 cities. Appendix A shows the earthquakes felt and recorded in the 15 cities. The main information extracted from SISFRANCE is:

- Epicentral intensity.
- Quality of the epicentral intensity.
- Date of occurrence (year, month, day, hour, minute, seconde).
- Intensity felt in the city.

▪ Quality of the intensity felt in the city.

The magnitude of the earthquakes is not provided in SISFRANCE. The magnitude was extracted from the seismic catalogue FACT-17 (Manchuel et al., 2017), developed in the framework of the SIGMA project. The magnitude is needed to compute the number of exceedances considering only events with magnitude greater than the minimum magnitude used in the hazard analysis to compare with observation.

The epicentral distance from the epicenter to the city was also computed. Similar to the minimum magnitude, a maximum distance is considered corresponding to the integration distance used in the hazard model to compare with observations.

Number of exceedances of intensities V, VI, VII and VIII for each of the 15 cities have been counted in the database.

Appendix A presents maps with the intensity observations recorded in the selected cities. Figures showing the distribution of observations over time are also included.

Table 2.2 shows the number of occurrences of the different intensity thresholds (number of observations in the intensity bin), taking into consideration the completeness periods as well as the criteria on magnitude and epicentral distance (minimum magnitude and maximum distance considered in the hazard calculation to be compared with the observations). In agreement with the ESHM20 hazard model a minimum magnitude Mw=4.5 and a maximum distance Repi=200 km are considered.

Table 2.3 presents the cumulated number of occurrences of the intensities V, VI, VII and VIII in the 15 selected cities in France. Table 2.3 also presents the cumulated number of years of observation for the 4 intensities considered.

Table 2.2: Number of occurrences of intensity bins for sites located in France.

Site	Intensity	Number of occurrences	Observation period (Years)	Completeness year (Year)
Brest (Armorican Massif)	[V-VI[	1	127	1880
	[VI-VII[	0	257	1750
	[VII-VIII[	0	307	1700
	[VIII-XI[	0	507	1500
Cherbourg (Armorican Massif)	[V-VI[	1	127	1880
	[VI-VII[	1	257	1750
	[VII-VIII[	0	307	1700
	[VIII-XI[	0	507	1500
Clermond-Ferrand (Other regions)	[V-VI[	1	157	1850
	[VI-VII[	1	257	1750
	[VII-VIII[	0	257	1750
	[VIII-XI[	0	507	1500

Site	Intensity	Number of occurrences	Observation period (Years)	Completeness year (Year)
Grenoble (Alps)	[V-VI[	7	127	1880
	[VI-VII[	1	177	1830
	[VII-VIII[	0	207	1800
	[VIII-XI[	0	507	1500
La Rochelle (Armorican Massif)	[V-VI[	1	127	1880
	[VI-VII[	1	257	1750
	[VII-VIII[	0	307	1700
	[VIII-XI[	0	507	1500
Lille (Northern France)	[V-VI[	0	127	1880
	[VI-VII[	1	157	1850
	[VII-VIII[	0	257	1750
	[VIII-XI[	0	507	1500
Limoges (Other regions)	[V-VI[	0	157	1850
	[VI-VII[	0	257	1750
	[VII-VIII[	0	257	1750
	[VIII-XI[	0	507	1500
Lourdes (Pyrenees)	[V-VI[	4	97	1910
	[VI-VII[	0	97	1910
	[VII-VIII[	0	257	1750
	[VIII-XI[	1	507	1500
Marseille (Provence)	[V-VI[	2	127	1880
	[VI-VII[	1	157	1850
	[VII-VIII[	0	257	1750
	[VIII-XI[	0	507	1500
Mulhouse (Rhine)	[V-VI[	3	137	1870
	[VI-VII[	1	257	1750
	[VII-VIII[	0	377	1630
	[VIII-XI[	0	507	1500
Nice (Alps)	[V-VI[	5	127	1880
	[VI-VII[	1	177	1830
	[VII-VIII[	0	207	1800
	[VIII-XI[	1	507	1500
Orléans (Other regions)	[V-VI[	0	157	1850
	[VI-VII[	0	257	1750
	[VII-VIII[	0	257	1750
	[VIII-XI[	0	507	1500

Site	Intensity	Number of occurrences	Observation period (Years)	Completeness year (Year)
Paris (Other regions)	[V-VI[	0	157	1850
	[VI-VII[	0	257	1750
	[VII-VIII[	0	257	1750
	[VIII-XI[	0	507	1500
Perpigan (Pyrenees)	[V-VI[	0	97	1910
	[VI-VII[	1	97	1910
	[VII-VIII[	0	257	1750
	[VIII-XI[	0	507	1500
Toulouse (Other regions)	[V-VI[	2	157	1850
	[VI-VII[	0	257	1750
	[VII-VIII[	0	257	1750
	[VIII-XI[	0	507	1500

Table 2.3: Cumulated number of occurrences of intensity thresholds in 15 cities considered in France.

Intensity	Number of occurrences	Observation period (Years)
Total [V-VI[	27	1995
Total [VI-VII[	9	3095
Total [VII-VIII[	0	3855
Total [VIII-XI[	2	7605

2.2.2   Spain

2.2.2.1   Source of information

To develop the macroseismic database for the study in Spain, we used the AHEAD portal developed within the framework of the NERIES project and improved during the SHARE project. AHEAD relies on an application called MIDOP (https://emidius.eu/MIDOP/). This tool allows to request the macroseismic information recorded in some cities. Some institutions involved in NERIES and SHARE used MIDOP to present the macroseismic data.

For Spain, 2 institutions provide macroseismic information, using MIDOP software:

- IGN (Instituto Geográfico nacional). The AHEAD portal lead to http://www.ign.es/web/ign/portal/sismicidad-historica . From here the macroseismic data of selected cities can be extracted. Epicentral coordinates and magnitudes of earthquakes producing the macroseismic information are not included in the downloaded file.
- ICGC (Institut Cartogràfic I Geològic de Catalunya). The AHEAD portal lead to https://www.icgc.cat/Administracio-i-empresa/Serveis/Terratremols-enregistrats-i-

informacio-sismica/Reculls-d-informacio-sismica-i-mapes/Base-de-dades-macrosismica-de-Catalunya. Magnitudes of earthquakes producing the macroseismic information are not included in the downloaded file.

Epicentral coordinates and magnitudes of earthquakes producing the macroseismic information not included in the downloaded files were obtained from SHARE catalogue (version 3.3).

2.2.2.2 Selection of observation points:

The objective in Spain was to define 4 cities, 2 of them located in seismic areas and 2 cities located in more stable areas. Based on the analysis of the location of earthquakes associated to macroseismic data in Spain (Figure 2.4), and on data availability, the four selected cities are:

- Madrid and Barcelona in relatively seismically quiet regions;
- Sevilla and Malaga in more active regions.
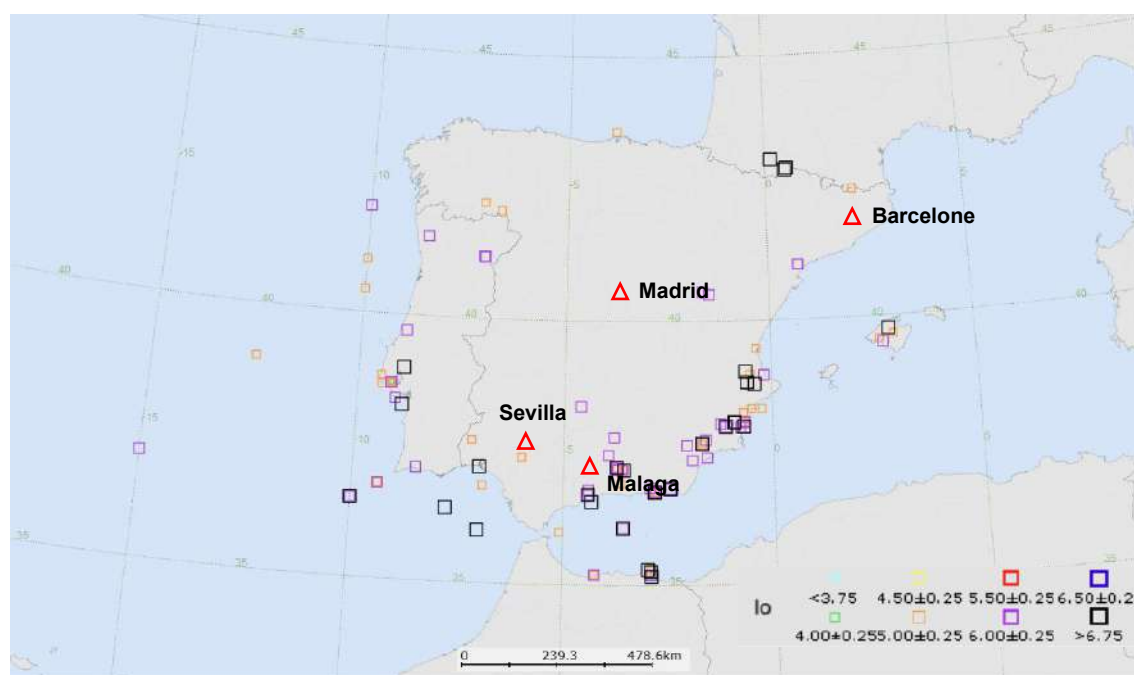
Figure 2.4: Epicentres of earthquakes with macroseismic data in Spain. Source: (IGN).

In Madrid, Sevilla and Malaga, only the IGN provides macroseismic information.

In Barcelona, both institutions (IGN and ICGC) provide macroseismic information. In this case, we coupled both information in order to cover a longer observation period. The information provided by both institutions covers different periods.

2.2.2.3 Completeness of observation

The periods of completeness adopted in Barcelona were adopted from Secanell (1999), who defined the periods of completeness for some regions in Catalonia, including Barcelona region. For Madrid, Malaga and Sevilla no specific evaluations were found and completeness

period for the whole Spain determined using IGN databases by Mezcua et al. (2004) are used. Completeness years for the four cities in Spain are presented in Table 2.4.

Table 2.4: Completeness years adopted in Spain.

Intensity	Completeness year	
	Barcelona Region	Spain
V	1899	1925
VI	1849	1900
VII	1749	1825
VIII	1249	1750
IX	1249	1525

Again, ideally specific periods of completeness for each city would be better. Periods of completeness defined for bigger regions can be considered as a conservative hypothesis, because the selected cities have a long history and specific completeness would probably be longer than regional estimates.

The periods of observation are then computed considering the years from the beginning of completeness periods (the year from which we do not miss seismic information) but also the limited time span over which data are included in the database. Figure 2.5 shows the recorded felt intensities in Barcelona versus time according to the ICGC and IGN databases. The ICGC database include records for two periods of time: 1373-1448 and 1917-2007. Between 1448 and 1917 the database seems not populated (it is under construction). For the IGN database, records from 1755 to 1873 are reported as well as two events in 1373 and 1428 (both included in the ICGC database). Combining ICGC and IGN data, the observation period for Barcelona combines three periods of time: 1373-1448, 1755-1873 and 1917-2007. The IGN portal however indicates that data up to 1899 are collected so the final observation period for Barcelona is the combination of: 1373-1448, 1755-1899 and 1917-2007. For Malaga, Sevilla and Madrid, the database covers the period before 1900 with apparently no gaps.
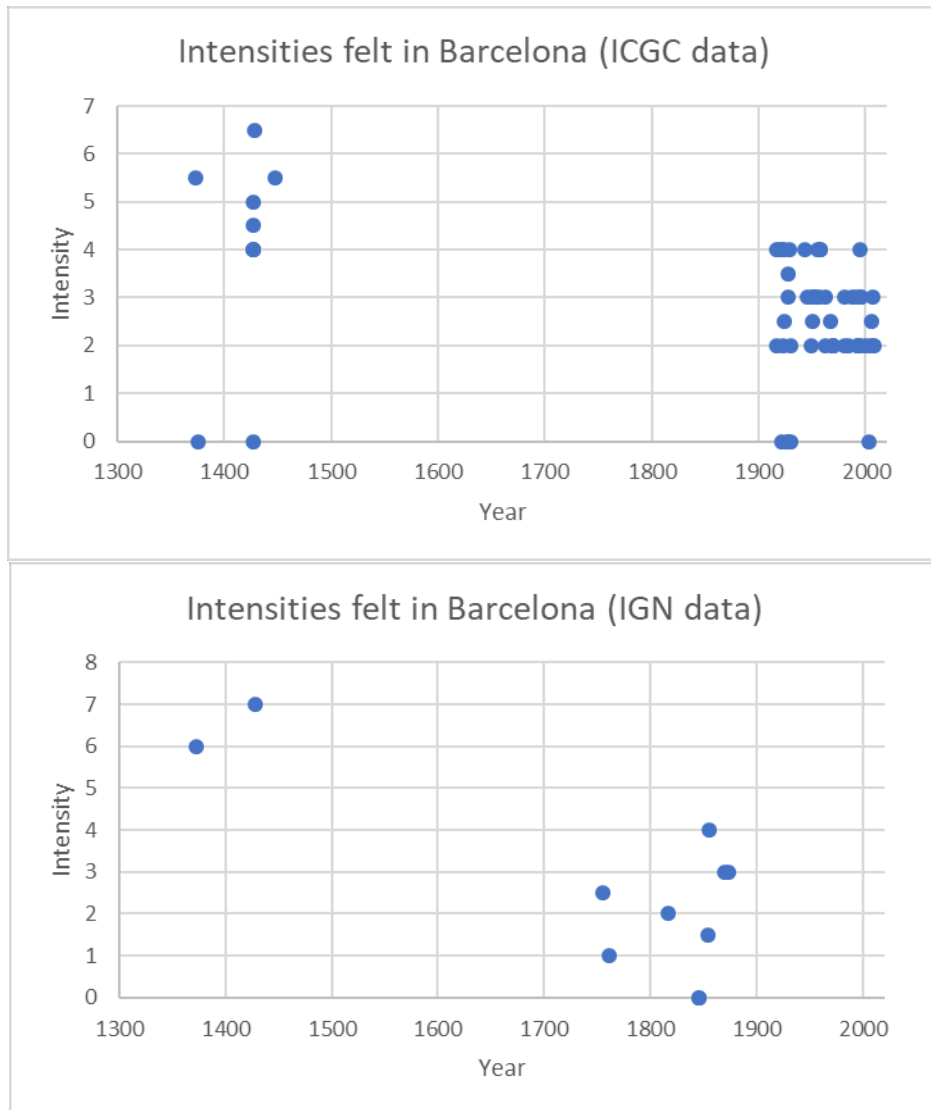
Figure 2.5: Felt intensities in Barcelona versus time based on the ICGC database (top) and IGN database (bottom).

2.2.2.4 Analysis of the database

The AHEAD Spanish database is not very complete, and it does not include all macroseismic information.

The ICGC provides a more detailed information on macroseismic data recorded in Catalonia region (north-eastern part of Spain). The extraction of macroseismic data using the ICGC portal provides:

- Epicentral intensity.
- Date of occurrence (year, month, day, hour, minute, second).
- Intensity felt in the city.
- Longitude and latitude of the epicenter of the earthquake.
- Number of macroseismic data.

The magnitude of the earthquakes is not provided. It was defined using the SHARE catalogue (version 3.3).

The IGN provides less detailed information. The extraction of macroseismic data using the IGN portal provides:

- Epicentral intensity.
- Date of occurrence (year, month, day, hour, minute, second).
- Intensity felt in the city.
- Number of macroseismic data.

The location of the epicenters and the moment magnitude of the earthquakes was defined using the SHARE catalogue (version 3.3).

Appendix A shows the tables (with felt seismicity on the cities) and seismic maps with the observations recorded in the 4 cities. A table and a figure are presented for each city.

Table 2.5 indicates the number of occurrences for different intensity bins.

Table 2.5: Number of exceedances of intensity thresholds for sites located in Spain. Note that observation period for Barcelona takes into account gaps in the database.

Site	Intensity	Number of occurrences	Observation period (Years)	Completeness year (Year)
Barcelona (Catalonia)	[V-VI[	0	90	1899
	[VI-VII[	0	142	1849
	[VII-VIII[	0	237	1749
	[VIII-XI[	0	437	1249
Madrid (Spain)	[V-VI[	-	-	1925
	[VI-VII[	-	-	1900
	[VII-VIII[	0	74	1825
	[VIII-XI[	0	150	1750
Malaga (Spain)	[V-VI[	-	-	1925
	[VI-VII[	-	-	1900
	[VII-VIII[	1	74	1825
	[VIII-XI[	0	149	1750
Sevilla (Spain)	[V-VI[	-	-	1925
	[VI-VII[	-	-	1900
	[VII-VIII[	0	74	1825
	[VIII-XI[	1	149	1750

2.2.3   Italy

2.2.3.1   Source of information

For Italy, the main source of information for macroseismic information is the AHEAD portal which direct the request towards the INGV site. In the case of INGV, this tool allows the selection of all macroseismic data recorded for some locations, mainly big cities (https://emidius.mi.ingv.it/CPTI15-DBMI15/query_place/).

The extraction of data from AHEAD portal does not include the location and the moment magnitudes of earthquakes included in the AHEAD extracted file. Then, these data were selected from the SHARE catalogue (version 3.3).

2.2.3.2   Selection of observation points

We decided to select 4 cities in Italy. The criteria used for the selection of cities were mainly:

- Selection of cities located in regions with different levels of seismic activity.
- Minimum distance between cities fixed at 200 km.
- Availability of macroseismic information in AHEAD database.

According to these criteria, 4 cities were selected:

- Catania, which was selected as representative of the southern part of Italy. Catania has a large seismic history, with large historical earthquakes and the macroseismic data is quite complete.
- Roma was selected as representative of central part of Italy and it is probably the city with the longest seismic history in Europe.
- Bologna, which is situated in the north-eastern part of Italy and was selected because the macroseismic database is quite large.
- Milan, which is also representative of the northern part of Italy, but the seismic activity is quite lower than in Bologna. Milan was selected as representative of the most stable part of Italy.

2.2.3.3   Completeness of observation

A first estimation of periods of completeness for Italy can be extracted from Albarello et al. (2001), who defined the periods of completeness for the whole Italian catalogue. They are presented in Table 2.6.

However, the periods of completeness defined in Albarello et al. (2001) seem to be conservative considering the large seismic history of the selected Italian cities. Consequently, specific completeness estimation for each city was performed by Pr. Albarello who applied his method to better estimate the completeness periods of the 4 selected cities (personal communication, 2020). The specific periods of completeness are presented in Table 2.6.

Table 2.6: Completeness periods adopted for Italy.

Intensity	Completeness year Albarello (2001)	Completeness year albarello (2020)			
	Italy	Catania	Roma	Milan	Bologna
V	---	1775	1695	1635	1715
VI	1875	1665	1705	1265	1595
VII	1850	1485	1045	1165	1295
VIII	1800	1415	1000	1000	1165
IX	1625	1365	1000	1000	1085

2.2.3.4 Analysis of the database

The AHEAD Italian database is very complete, and it contains all macroseismic information from 1000 AC to 2017.

Table 2.7 indicates the number of occurrences for different intensity bins.

Table 2.7: Number of exceedances of intensity thresholds for sites located in Italy.

Site	Intensity	Number of occurrences	Observation period (Years)	Completeness year (Year)
Bologna	[V-VI[	18	302	1715
	[VI-VII[	11	422	1595
	[VII-VIII[	3	722	1295
	[VIII-XI[	1	852	1165
Catania	[V-VI[	7	242	1775
	[VI-VII[	6	352	1665
	[VII-VIII[	4	532	1485
	[VIII-XI[	2	602	1415
Milan	[V-VI[	3	382	1635
	[VI-VII[	0	752	1265
	[VII-VIII[	0	852	1165
	[VIII-XI[	0	1017	1000
Roma	[V-VI[	10	322	1695
	[VI-VII[	5	312	1705
	[VII-VIII[	4	972	1045
	[VIII-XI[	0	1017	1000

2.2.4 Switzerland

2.2.4.1 Source of information

The catalogue of observed intensities for Zürich and Bern has been provided by Donät Faeh (personal communication). The database covers all the historical period and is completed up to end of 2007.

2.2.4.2 Selection of observation points

Bern and Zürich are the two cities considered in the data compilation. They are however very close to each other and only Zürich will be considered in the final database. Indeed, as explained earlier, we are compiling uncorrelated observations.

2.2.4.3 Completeness of observation

Completeness for Switzerland has been taken from ECOS-02 report (see Figure 2.6). The values for Zürich and Bern are given in Table 2.8.

Completeness	Swiss regions							
Time span	1 (InnerCH)	2 (ZH/SG)	3 (BE/WestCH)	4 (Basel)	5 (Wallis)	6 (Tessin)	7 (GR)	8 (GL)
563–799	n	n	n	n	u	n	n	n
800–899	u	u	n	n	n	n	n	n
900–999	n	u	n	n	n	n	n	n
1000–1099	n	u	n	n	n	n	n	n
1100–1199	n	VII	n	n	n	n	n	n
1200–1299	n	n	n	u	n	n	VIII	n
1300–1399	n	n	u	VIII	n	n	n	n
1400–1499	n	VII	n	VII	n	n	n	n
1500–1599	n	VII	VII	n	VIII	VIII	n	n
1600–1679	VIII	VII	n	VIII	n	VIII	n	n
1680–1730	VII	V	VII	VI	VIII	VIII	VII	VI
1730–1750	VII	VI	VII	VI	VIII	VIII	VII	V
1751–1800	VI	VI	VI	VI	VII	VII	VI	V
1801–1850	VI	V	VI	VI	VII	VI	VI	VI
1851–1878	VI	V	VI	VI	VI	VI	VI	VI
1878–1963	V	V	V	V	V	V	V	V
1964–1974	IV	IV	IV	IV	IV	IV	IV	IV

Table 3.1. Completeness of observed intensities for different regions in Switzerland over given time periods. n: no primary sources found; u: completeness unknown. The Swiss regions are illustrated in Figure 3.1. The table is taken from the ECOS-02 report (see Appendix A).
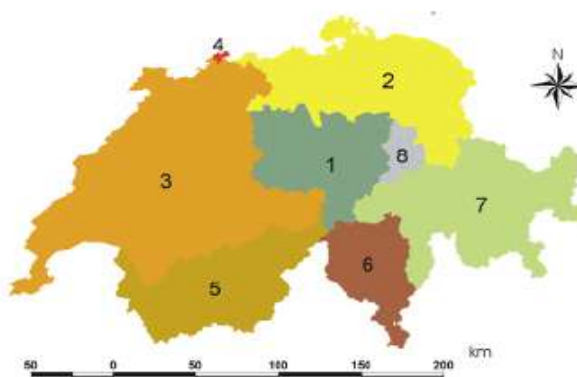
Figure 3.1. Geographical distribution of catalogue completeness, according to Table 3.1. The figure is taken from the ECOS-02 report (see Appendix A).

Figure 2.6: Regional completeness years for different intensity levels for Switzerland (from ECOS-02).

Table 2.8: Completeness periods adopted for Switzerland.

Intensity	Completeness year	
	Zürich	Bern
V	1801	1878
VI	1730	1751
VII	1400	1680
VIII	1400	1680
IX	1400	1680

2.2.4.4 Analysis of the database

Table 2.9 indicates the number of occurrences for different intensity bins.

Table 2.9: Number of exceedances of intensity thresholds for sites located in Switzerland.

Site	Intensity	Number of occurrences	Observation period (Years)	Completeness year (Year)
Zürich	[V-VI[	12	206	1801
	[VI-VII[	4	277	1730
	[VII-VIII[	1	607	1400
	[VIII-XI[	0	607	1400
Bern	[V-VI[	12	129	1878
	[VI-VII[	4	256	1751
	[VII-VIII[	1	327	1680
	[VIII-XI[	0	327	1680

2.2.5 Belgium

2.2.5.1 Source of information

The catalogue of observed intensities for Belgium has been provided by Thierry Cameelbeck (personal communication). Data from 1382 to 2015 are compiled. As expected, due to the low activity level in the region, only few data are compiled.

2.2.5.2 Selection of observation points

Only the city of Bruxels is considered.

2.2.5.3 Completeness of observation

No specific information was found regarding intensity completeness for Bruxels nor for Belgium. Since the city has a long history, we made the assumption that the completeness

defined for Barcelona can approximate completeness for Bruxels. Note that using the same completeness as for Lille which is the closest French city to Bruxels as no impact on the number of observations.

2.2.5.4 Analysis of the database

Table 2.10 indicates the number of occurrences for different intensity bins.

Table 2.10: Number of exceedances of intensity thresholds for sites located in Belgium.

Site	Intensity	Number of occurrences	Observation period (Years)	Completeness year (Year)
Bruxels	[V-VI[	0	108	1899
	[VI-VII[	1	158	1849
	[VII-VIII[	0	258	1749
	[VIII-XI[	0	758	1249

2.2.6 Greece

2.2.6.1 Source of information

As for Spain and Italy, the main source of information is the AHEAD database.

2.2.6.2 Selection of observation points

The two main cities of Greece Athens to the South and Thessaloniki to the North are selected.

2.2.6.3 Completeness of observation

The database includes very few events from 1859 to 1894 for Athens and from 1737 to 1898 for Thessaloniki.

No specific information on the completeness is available and a completeness year equal to 1850 is selected for all intensity levels.

2.2.6.4 Analysis of the database

Table 2.11 indicates the number of occurrences for different intensity bins.

Table 2.11: Number of exceedances of intensity thresholds for sites located in Greece.

Site	Intensity	Number of occurrences	Observation period (Years)	Completeness year (Year)
Athens	[V-VI[	3	49	1850
	[VI-VII[	0	49	1850
	[VII-VIII[	0	49	1850
	[VIII-XI[	0	49	1850
Thessaloniki	[V-VI[	1	49	1850

Site	Intensity	Number of occurrences	Observation period (Years)	Completeness year (Year)
	[VI-VII[	0	49	1850
	[VII-VIII[	0	49	1850
	[VIII-XI[	0	49	1850

2.2.7   Turkey

2.2.7.1   Source of information

As for Spain and Italy, the main source of information is the AHEAD database.

2.2.7.2   Selection of observation points

Two large cities in Western Turkey: Istanbul and Izmir are selected.

2.2.7.3   Completeness of observation

Surprisingly, the number of observations in the database for Istanbul is much smaller than for Izmir (Figure 2.7). Consequently, we assume that the database for Istanbul is probably missing some information.

For Istanbul, as was done for Greek cities, the completeness is set to 1850 for all the intensities. For Izmir, due to the quantity of information back to 1653, completeness years for intensity VII and VIII are set to 1800 and 1700 respectively, while 1850 is used for intensities V and VI.

FUGRO
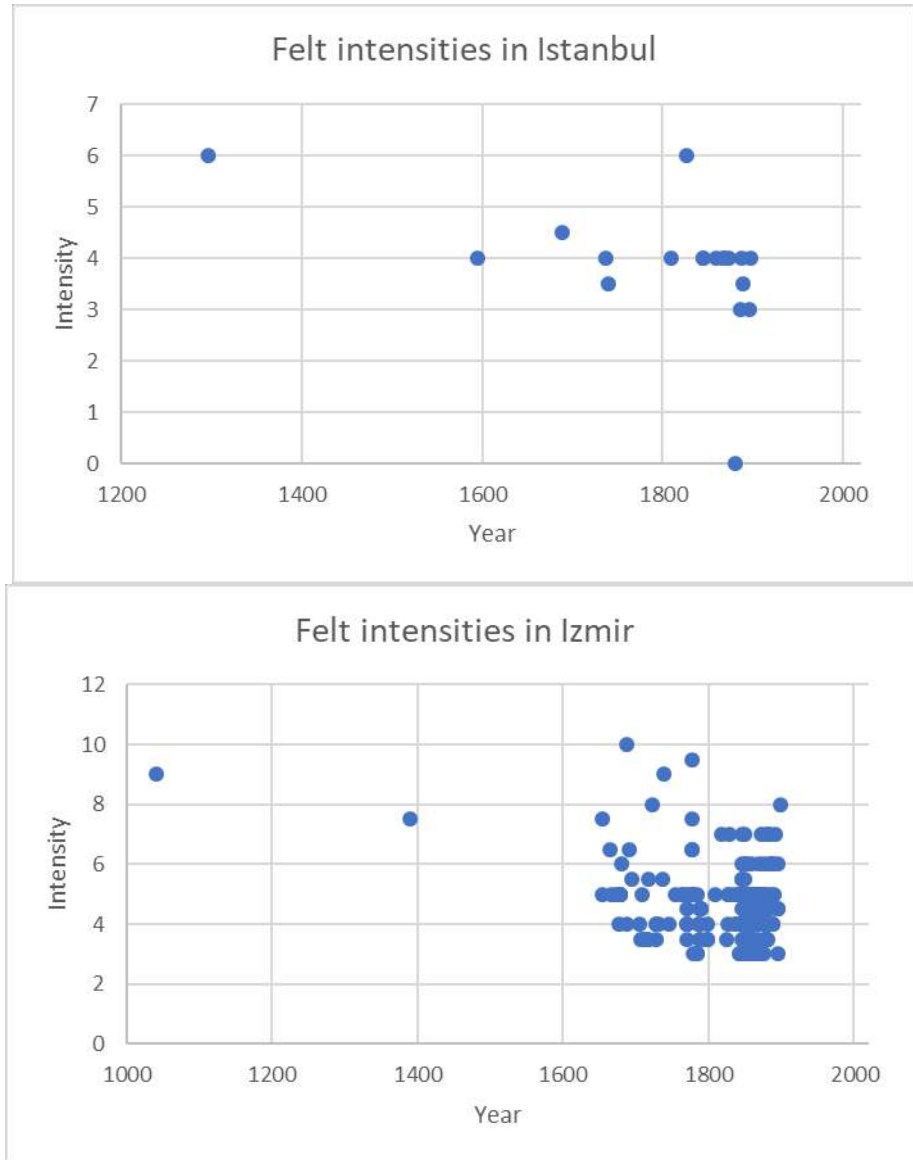
Figure 2.7: Felt intensities in Istanbul (top) and Izmir (bottom) versus time.

2.2.7.4 Analysis of the database

Table 2.12 indicates the number of occurrences for different intensity bins.

As already mentioned, the database for Istanbul is doubtful and leads to zero observations for this city. Consequently, it is not retained in the final database for the testing approach.

Table 2.12: Number of exceedances of intensity thresholds for sites located in Turkey.

Site	Intensity	Number of occurrences	Observation period (Years)	Completeness year (Year)
Istanbul	[V-VI[	0	49	1850
	[VI-VII[	0	49	1850
	[VII-VIII[	0	49	1850

Site	Intensity	Number of occurrences	Observation period (Years)	Completeness year (Year)
	[VIII-XI[	0	49	1850
Izmir	[V-VI[	9	49	1850
	[VI-VII[	5	49	1850
	[VII-VIII[	7	99	1800
	[VIII-XI[	2	199	1700

2.3 Sensitivity analyses for the macroseismic database

2.3.1 France

The number of exceedances observed in the different cities were compared with the number of exceedances defined in the report GTR_EDF_0907_396 (PSHA performed in terms of intensity in 2007 for France). The number of observations is coherent. Small differences are observed mainly due to the present consideration of a minimum magnitude in the selection criteria (this minimum magnitude was not considered in 2007) and due to small changes in the SISFRANCE database (from 2007 to 2017).

In order to verify that the built database for France is consistent, synthetic number of occurrences for intensity ranges [V-VI[, [VI-VII[, [VII-VIII[and [VIII-XI[have been computed. Using the FCAT-17 catalogue complemented by the LDG bulletins for the period 2010-2019, and the IPE (IPE) from Baumont et al. (2017) (metropolitan France coefficients), intensities produced by events within 200 km from each city have been computed. Moment magnitudes provided in the catalogues and distances computed from earthquake location in the catalogue are used as input to the IPE. The mean intensity for each event is computed from the different sets of coefficients for metropolitan France (see Baumont et al., 2017).

Figure 2.8 compares the observed and synthetic occurrences. Globally, observed and synthetic data are consistent. For intensity bin [V-VI[, however, relatively large differences between observations and synthetics are obtained for Grenoble (7 observations vs. 3 synthetics), and La Rochelle (1 observations vs. 4 synthetics), Mulhouse (3 observations vs. 0 synthetics), and Nice (5 observations vs. 2 synthetics). For intensity bin [VI-VII[, there is a tendency to compute lower synthetics than observations. For higher intensities ([VII-VIII[and [VIII-IX[), almost all sites are characterized by zero observation and zero synthetic. For Lourdes, however, no observation of intensity [VII-VIII[is recorded while 2 synthetics are computed. For Nice, 1 observation of intensity [VIII-IX[is recorded while zero synthetic are computed.

In order to assess the impact of the completeness levels on the database, the number of observations is also computed after modification of the completeness by -50 to +50%. For intensity bins [V-VI[and [VI-VII[, the impact is relatively large for Lourdes, Nice and Grenoble. For most of the sites, taking into account an uncertainty in the completeness years make the

observations and synthetics more compatible. But there are still some sites showing discrepancy between observations and synthetics. Table 2.13 gives the cumulated number of occurrences and observation period over the 15 sites when completeness is perturbed by + or – 50%.

Table 2.13: Influence of completeness on cumulated number of occurrences of intensity thresholds in 15 cities considered in France. Number of occurrences and global observations periods when completeness years are increased and reduced by 50 years.

Intensity	Completeness +50%		Completeness -50%	
	Number of occurrences	Observation period (Years)	Number of occurrences	Observation period (Years)
Total [V-VI[	38	3008	10	1003
Total [VI-VII[	13	4763	4	1588
Total [VII-VIII[	2	6038	0	2013
Total [VIII-XI[	2	11408	1	3803

Globally, the agreement is acceptable, giving more confidence in the observation database created. To go further in the comparison, an analysis comparing, one by one, earthquakes that produced observed and synthetic occurrences could be performed but this is beyond the scope of the present study.
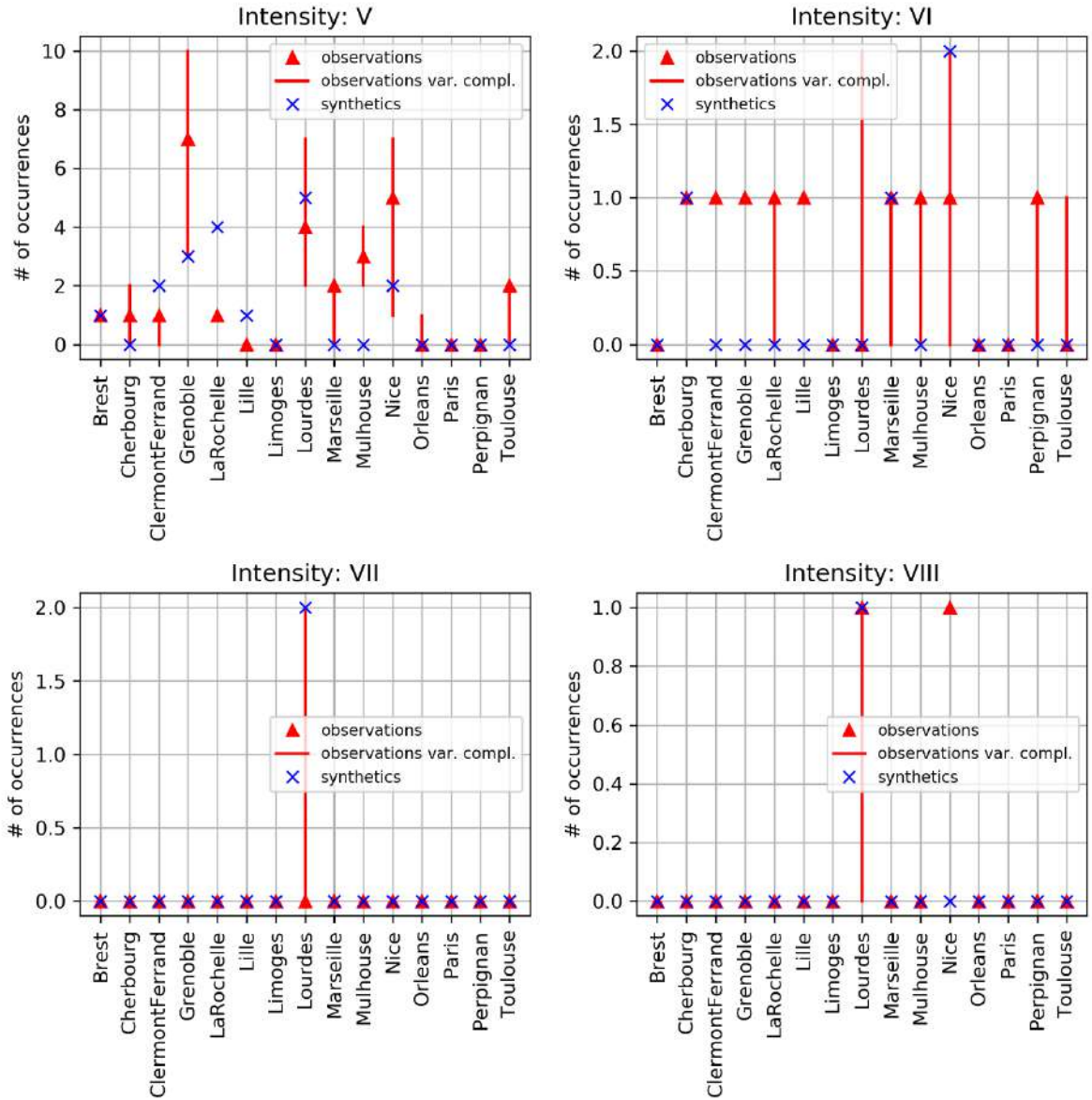
Figure 2.8: Comparison of observed (red triangles) and synthetic (blue crosses) number of occurrences at each selected cities for different intensity bins (top left: [V-VI[; top right: [VI-VII[; bottom left: [VII-VIII[; bottom right: [VIII-XI[). The impact of a variation of 50 years in the completeness years on the observations is also shown (red lines).

2.3.2   Europe

As was done for the data in France, completeness years have been perturbated to assess the impact on the collected observations. Completeness years for all the intensity bins are simultaneously modified by a factor from -80%to +80% using a 10% step. The number of observations is computed for these 10 new sets of completeness years. Figure 2.11 presents the resulting rates of occurrence observed with the modified completeness. When completeness is increased (Figure 2.11 top), the number of observations remains almost unchanged (not many events in the older part of the catalogue) while the completeness

period increases such that the rate of occurrence decreases. On the other hand, when completeness is decreased (Figure 2.11 top), one can note that the computed rates increase when completeness modification of -10 to -50% is applied; then for larger modifications, above 50%, the computed rates decrease significantly. We explain this last observation by the fact that macroseismic observations are not abundant in the most recent part of the catalogue, most probably because this information is not systematically compiled for the most recent years. Nevertheless, if we exclude those case with reduction of the completeness by more than -50% (which are extreme cases), we observe an increase of the computed rates when completeness is reduces while one would expect a constant rate. The increase in computed rates is more pronounced for intensities V and VII while it is limited for intensity VII and negligible for intensity VIII. However, those results may suggest that completeness years are relatively conservative or selected close to the oldest entries in the databases.

Table 2.14 and Table 2.15 give the number of observations and cumulated observation period using the original completeness years as well as taking into account + and – 50% perturbations. Table 2.14 presents the results when all the sites included in the macroseismic data compilation (France, Spain, Italy, Switzerland, Belgium, Greece, Turkey are considered) and Table 2.15 without Bern and Istanbul (which are not selected in the final data set, see 2.2.4 and 2.2.7).
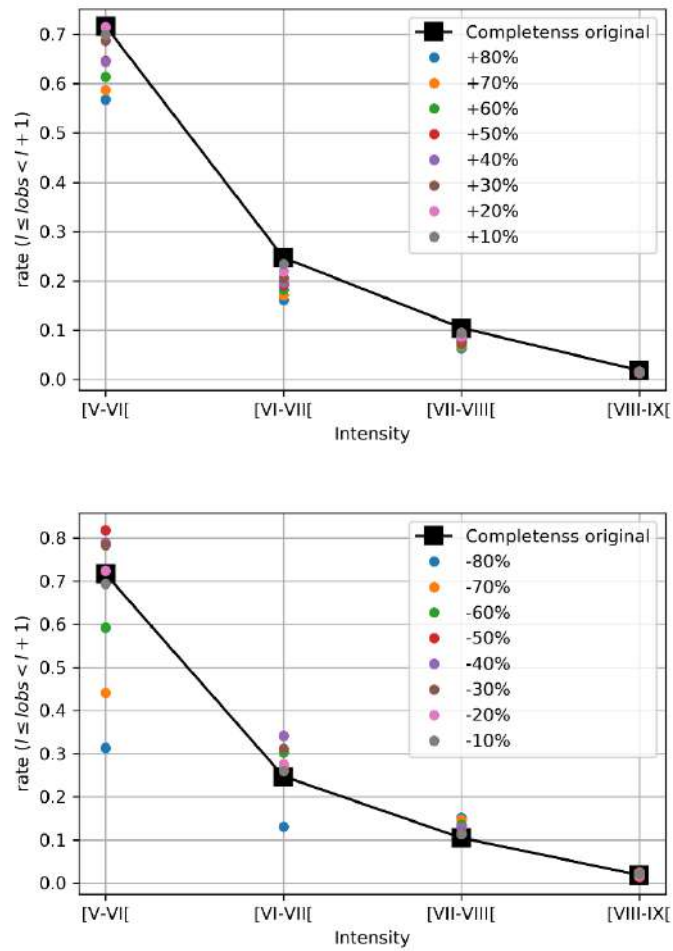
Figure 2.9: Number of occurrences in the database for different intensities (5 for [V-VI[intensity bin, 6 for [VI-VII[intensity bin, 7 for [VII-VIII[intensity bin and 8 for [VIII-IX[intensity bin). Occurrences computed using original completeness years are shown (black squares) as well as occurrences computed after application of a constant number of years (from -50 to +50 years with a 10 years step) perturbation to all completeness years.

Table 2.14: Influence of completeness on cumulated number of occurrences of intensity thresholds in all the sites with compiled macroseismic information. Number of occurrences and global observations periods when completeness years are increased and reduced by 50 %.

Intensity	Completeness original		Completeness +50%		Completeness -50%	
	Number of occurrences	Observation period (Years)	Number of occurrences	Observation period (Years)	Number of occurrences	Observation period (Years)
Total [V-VI[	99	3990	125	5985	64	1995
Total [VI-VII[	45	6050	53	9075	25	3025
Total [VII-VIII[	21	9008	24	13512	11	4504
Total [VIII-XI[	7	14023	8	21035	2	7012

Table 2.15: Influence of completeness on cumulated number of occurrences of intensity thresholds in all the sites with compiled macroseismic information except Bern and Istanbul. Number of occurrences and global observations periods when completeness years are increased and reduced by 50 %.

Intensity	Completeness original		Completeness +50%		Completeness -50%	
	Number of occurrences	Observation period (Years)	Number of occurrences	Observation period (Years)	Number of occurrences	Observation period (Years)
Total [V-VI[	87	3812	108	5718	58	1906
Total [VI-VII[	41	5745	49	8618	24	2873
Total [VII-VIII[	20	8632	23	12948	10	4316
Total [VIII-XI[	7	13647	8	20471	2	6824

2.4 Instrumental database

The instrumental database is built from three sources:

- Database from European NPP instrumentation from OCDE/NEA report OECD/NEA/CSNI/R(2019)1;
- RAP-RLBP flatfile (Traversa et al., 2020) ;
- European strong-motion database (ESM, https://esm.mi.ingv.it/) developed in the framework of the NERIES project.

2.4.1 European NPP accelerometric data

In the framework of the Organisation for Economic Co-operation and Development (OECD), Nuclear Energy Agency (NEA) is currently aiming at publishing a report gathering data (more specifically number of exceedances of a number of ground-motion threshold) recorded by the seismological instrumentation installed in European NPPs (OECD/NEA/CSNI/R(2019)1 and OECD/NEA/CSNI/WGIAGE, 2019).

Figure 2.10 shows the European NPPs which seismological instrumentation system contributed to the compilation of observations from the OECD/NEA.
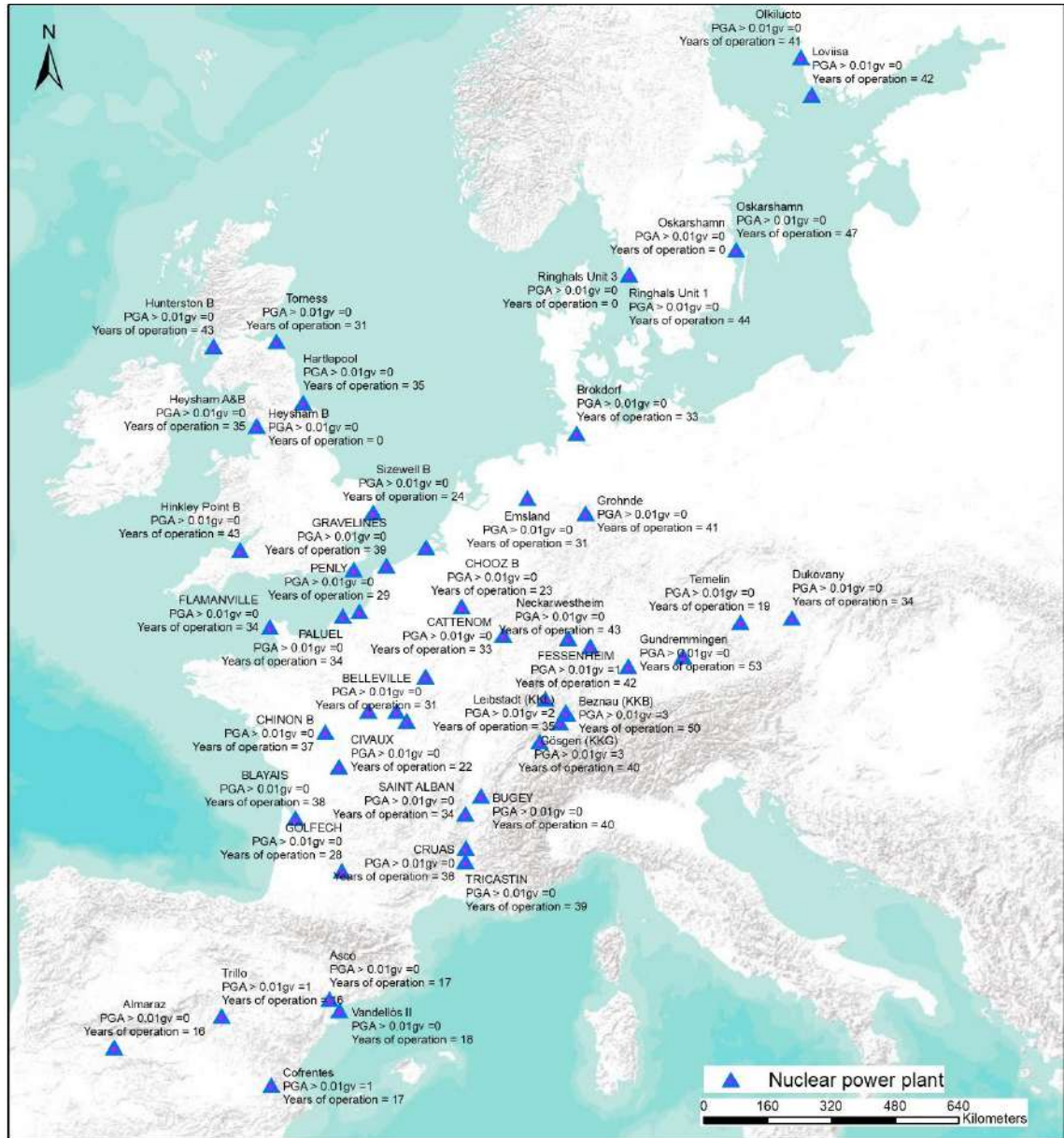
Figure 2.10: European NPPs which seismological instrumentation system contributed to the compilation of observations from the OECD/NEA.

A subset of sites was selected in order to cover a wide area but also considering a minimum distance between sites to avoid correlations. The number of observed exceedances for the subset of sites is provided in Table 2.16.

Table 2.16: Number of observed exceedances for different acceleration thresholds recorded by seismological instrumentation of European NPPs.

NPP	Number of exceedances for acceleration threshold				Installation date	End of observation
	0.1 m/s^2	0.2 m/s^2	0.5 m/s^2	1.0 m/s^2		
Dukovany	0	0	0	0	1985	2017
Blayais	0	0	0	0	1982	2017
Cattenom	0	0	0	0	1987	2017

| NPP | Number of exceedances for acceleration threshold | | | | Installation date | End of observation |
	0.1 m/s²	0.2 m/s²	0.5 m/s²	1.0 m/s²		
ChoozB	0	0	0	0	1997	2017
Civaux	0	0	0	0	1998	2017
Flamanville	0	0	0	0	1986	2017
Golfech	0	0	0	0	1992	2017
Gravelines	0	0	0	0	1981	2017
Nogent	0	0	0	0	1989	2017
Paluel	0	0	0	0	1986	2017
SaintAlban	0	0	0	0	1986	2017
SaintLaurentB	0	0	0	0	1984	2017
Grohnde	0	0	0	0	1979	2017
Isar	0	0	0	0	1979	2017
Neckarwestheim	0	0	0	0	1977	2017
Almaraz	0	0	0	0	1980	2017
Cofrentes	1	1	0	0	2002	2017
Trillo	1	0	0	0	2003	2017
Vandellos	0	0	0	0	2002	2017
Ringhals_Unit_3	0	0	0	0	1982	2017
Hartlepool	0	0	0	0	1985	2017
Heysham_B	0	0	0	0	1989	2017
Hinkley_Point_B	0	0	0	0	1977	2017
Hunterston_B	0	0	0	0	1977	2017
Sizewell_B	0	0	0	0	1996	2017
Torness	0	0	0	0	1989	2017

2.4.2   RAP-RLBP data

Traversa et al. (2020) published a flatfile (RAP-RLBP) of all records from the French RESIF network for events with local magnitude above 3.5. The complete dataset includes 6500 quality-checked records from 468 earthquakes recorded at 379 stations (Figure 2.11). Figure 2.12 presents the moment magnitude Mw – epicentral distance scatter plot for the global dataset.
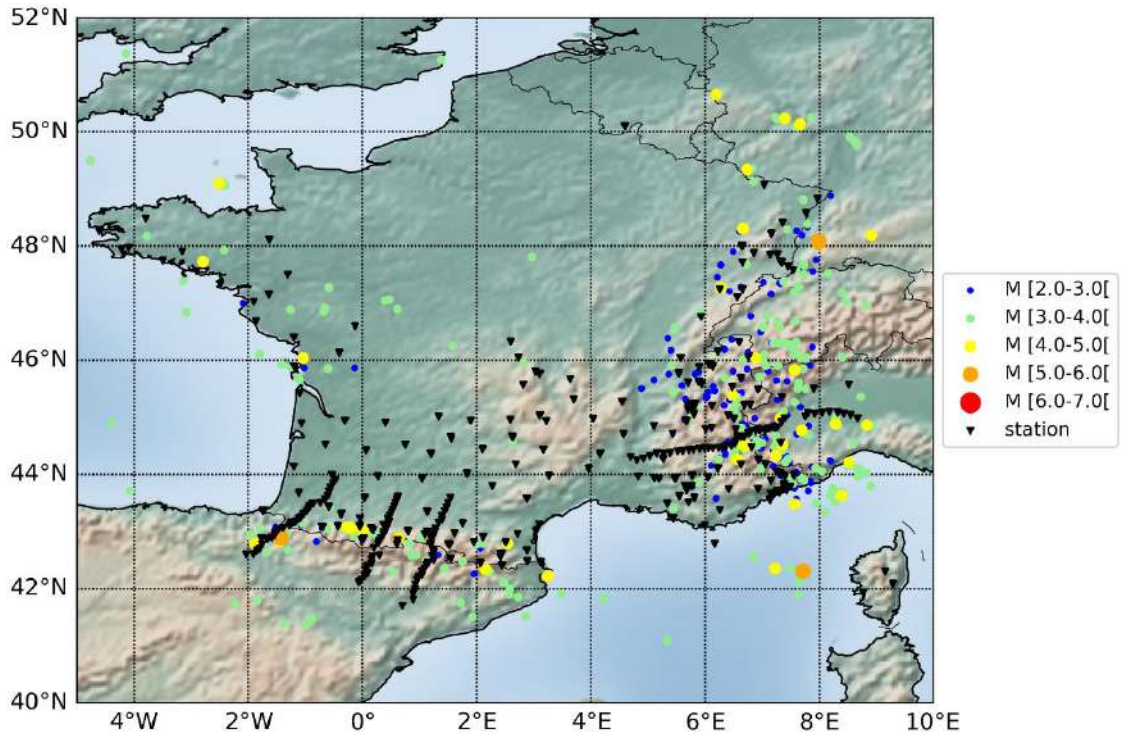
Figure 2.11: Earthquakes and stations included in the RAP-RLBP flatfile (Traversa et al., 2020).
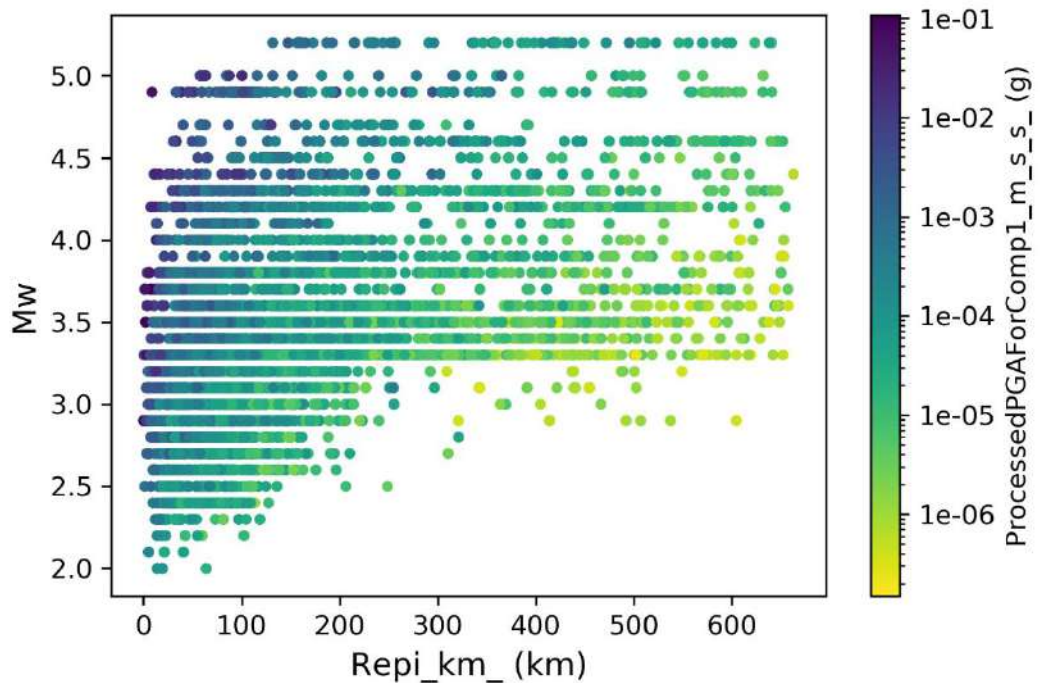
Figure 2.12: Magnitude-distance scatter plot for the data included in the RAP-RLBP flatfile (Traversa et al., 2020).

From the global dataset, events with moment magnitude Mw larger than 4.5 are extracted and recordings at less than 200 km and for rock sites only are selected. These filters are

applied for consistency of the hazard calculation parameters. The map of events and stations and the magnitude distance scatter plot for the "filtered" dataset are shown in Figure 2.13 and Figure 2.14, respectively.
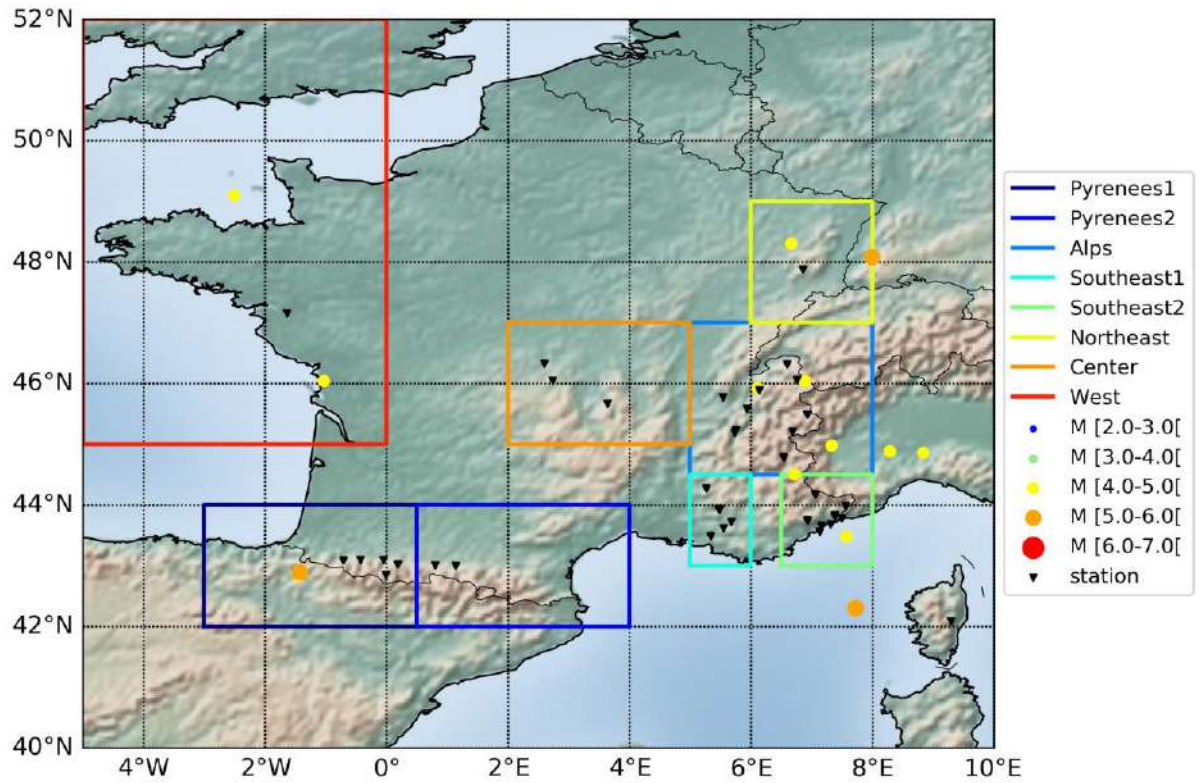
Figure 2.13: Earthquakes and stations included in the RAP-RLBP flatfile (Traversa et al., 2020) for events with Mw≥4.5 recorded at distances lower than 200 km on rock sites. The colour coded boxes represent sub-regions used for the final selection of the sites.
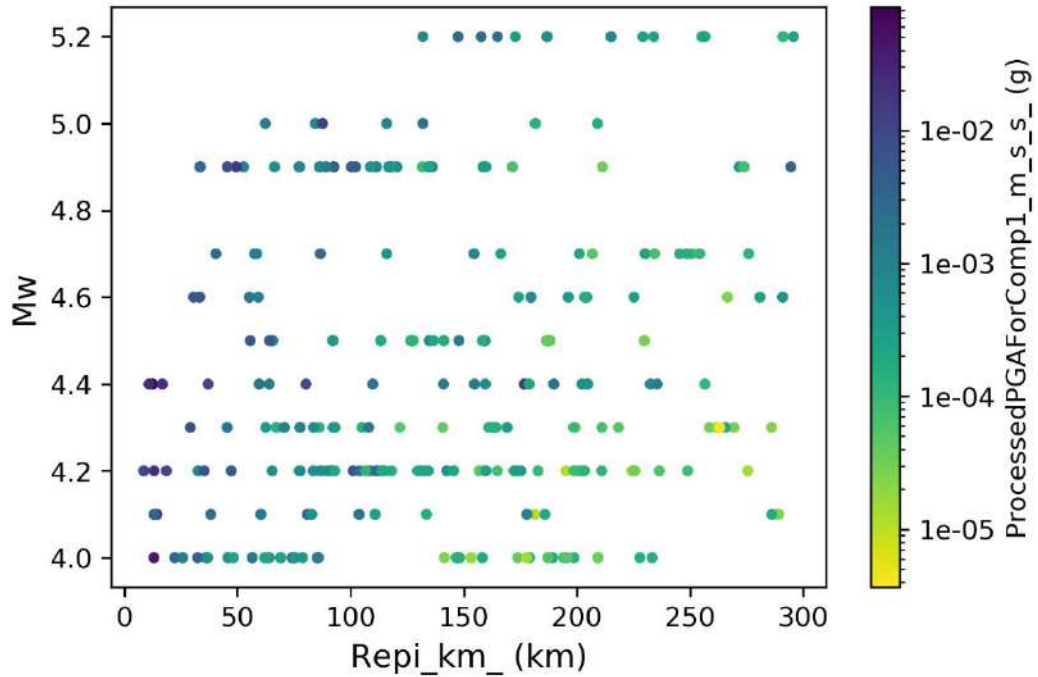
Figure 2.14: Magnitude-distance scatter plot for the data included in the RAP-RLBP flatfile (Traversa et al., 2020) for events with Mw≥4.5 recorded at distances lower than 300 km on rock sites.

Information about the observation period are retrieved from the RESIF FDSN webservices which provide an easy access to station information. The station metadata include the history of the instrumentation at the different sites. Any change in the instrumentation is reported and the time span with active instrumentation is available. During intervention on the site, short periods of interruption can occur, and the analysis of the station metadata allows also to retrieve that information. For all the stations the complete observation period is computed from which the small interruptions are removed. Consequently, the observation periods provided in the following table should be close to actual operation period.

The reference date to compute observation periods is the date of the last event included in the flatfile: May 17, 2016 at 4:50 AM.

Using the "filtered" flatfile, number of exceedances for 4 acceleration thresholds (0.1, 0.2, 0.5 and 1.0 m/s²) are computed for each component at each station (Table 2.18).

The selection of the sites for the testing procedure is based on sub-regions. To avoid correlation between observations, distant stations are selected. The sub-regions are shown in Figure 2.13.

Due to the low level of seismic activity in France, only one of the stations recorded exceedances of the defined acceleration thresholds, station STBU located in Northeast France. This station is selected in the final set. For the other sub-regions, we selected the stations with the longest observation period. The final selected set of stations is shown in Figure 2.15, and their geographical coordinates given in Table 2.17 with information related to site classification.
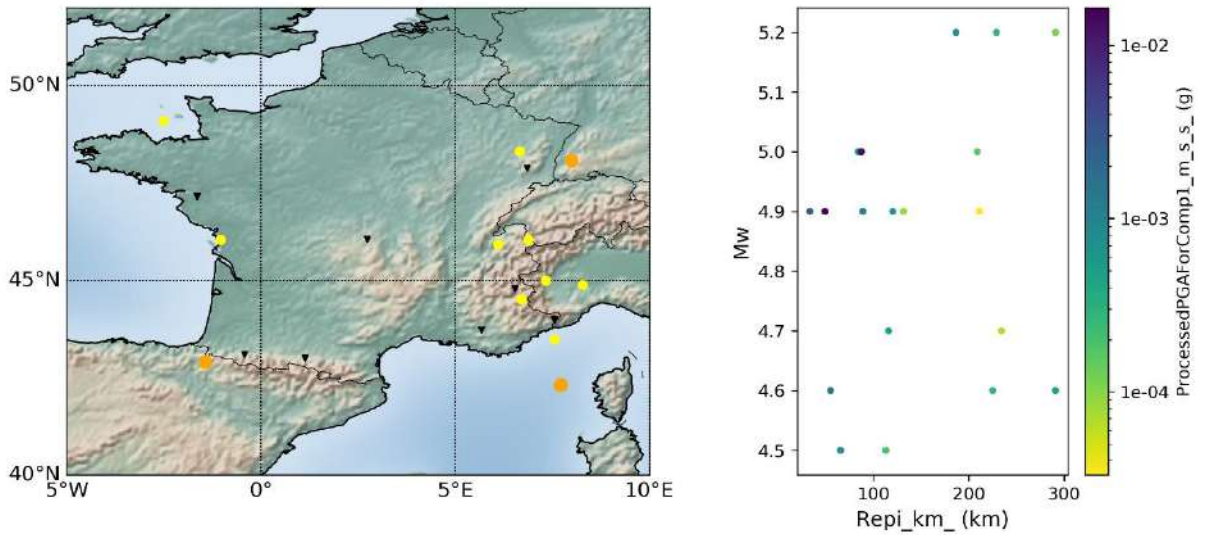
Figure 2.15: Final selected set of selected stations from the RAP-RLBP flatfile.

Table 2.17: Geographical coordinates (WGS84) and site classification information of the selected RAP-RLBP stations.

station	Longitude (°)	Latitude (°)	Site class (EC8)	V_{S30} (m/s)
OCSJ	2.733	46.051	A	1042
OGAG	6.54	44.788	A	972
OGCA	5.672	43.732	A	1383
PYAD	-0.428	43.097	A	2500
PYLI	1.136	43.002	A	1257
SAOF	7.553	43.986	A	2025
STBU	6.851	47.885	A	981
UBNA	-1.637	47.156	A	880

Table 2.18: Number of observed exceedances for different thresholds of acceleration for instrumental data in France. Selected stations are highlighted in green.

sta	Number of observations		Observation period	max PGA m/s²		Number of exceedances							
	comp1	comp2		comp1	comp2	comp1				Comp 2			
						0.1 m/s²	0.2 m/s²	0.5 m/s²	1.0 m/s²	0.1 m/s²	0.2 m/s²	0.5 m/s²	1.0 m/s²
Pyrenees1													
PYAD-00-HN	1	1	15.051284	0.006754	0.006677	0	0	0	0	0	0	0	0
PYAT-00-HN	2	2	13.586176	0.011598	0.009388	0	0	0	0	0	0	0	0
PYCA-00-HN	2	2	12.750064	0.017992	0.020831	0	0	0	0	0	0	0	0
PYLO-00-HN	1	1	14.824027	0.000596	0.000699	0	0	0	0	0	0	0	0
PYLS-00-HN	1	1	14.807553	0.010129	0.011587	0	0	0	0	0	0	0	0
Pyrenees2													
PYAS-00-HN	1	1	13.919939	0.001388	0.002452	0	0	0	0	0	0	0	0
PYLI-00-HN	2	2	14.095253	0.001674	0.001969	0	0	0	0	0	0	0	0
Alps													
GRN-00-HH	1	1	2.886845	0.023256	0.028163	0	0	0	0	0	0	0	0
GRN-00-HN	1	1	2.886855	0.008934	0.010916	0	0	0	0	0	0	0	0
OGAG-00-HH	3	3	10.024269	0.022398	0.039121	0	0	0	0	0	0	0	0
OGAG-00-HN	4	4	20.347229	0.026980	0.048442	0	0	0	0	0	0	0	0
OGAN-00-HN	5	5	19.254048	0.007730	0.006863	0	0	0	0	0	0	0	0
OGCH-00-HN	4	4	18.886926	0.024317	0.013410	0	0	0	0	0	0	0	0
OGMA-00-HN	1	1	11.482108	0.032039	0.024291	0	0	0	0	0	0	0	0
OGMO-00-HH	1	1	2.813110	0.021884	0.018646	0	0	0	0	0	0	0	0
OGMO-00-HN	3	3	16.808097	0.053145	0.070206	0	0	0	0	0	0	0	0
OGMU-00-HN	2	2	19.327381	0.004186	0.006217	0	0	0	0	0	0	0	0

| sta | Number of observations | | Observation period | max PGA m/s² | | Number of exceedances | | | | | | | |
| | comp1 | comp2 | | comp1 | comp2 | comp1 | | | | Comp 2 | | | |
						0.1 m/s²	0.2 m/s²	0.5 m/s²	1.0 m/s²	0.1 m/s²	0.2 m/s²	0.5 m/s²	1.0 m/s²
OGSI-00-HN	3	3	16.971003	0.009252	0.006383	0	0	0	0	0	0	0	0
OGTB-00-HN	2	2	12.838326	0.026373	0.031951	0	0	0	0	0	0	0	0
OGTI-00-HN	2	2	13.687588	0.053003	0.071410	0	0	0	0	0	0	0	0
Southeast1													
ARBF-00-HH	4	4	17.262891	0.006098	0.003809	0	0	0	0	0	0	0	0
ARBF-00-HN	1	1	16.377115	0.006232	0.002834	0	0	0	0	0	0	0	0
IRVG-00-HN	1	1	12.454063	0.006959	0.008142	0	0	0	0	0	0	0	0
OGBB-00-HN	3	3	15.889760	0.003988	0.004927	0	0	0	0	0	0	0	0
OGCA-00-HN	2	2	19.842907	0.006732	0.005134	0	0	0	0	0	0	0	0
RUSF-00-HN	3	3	4.298917	0.002695	0.002752	0	0	0	0	0	0	0	0
RUSF-01-HH	3	3	11.149590	0.002158	0.002932	0	0	0	0	0	0	0	0
RUSF-02-HN	1	1	10.951250	0.002167	0.003351	0	0	0	0	0	0	0	0
RUSF-03-HH	3	3	10.774450	0.004638	0.004467	0	0	0	0	0	0	0	0
RUSF-04-HH	3	3	10.058068	0.003982	0.002441	0	0	0	0	0	0	0	0
RUSF-05-HH	3	3	11.112918	0.002078	0.001884	0	0	0	0	0	0	0	0
RUSF-06-HH	2	2	10.795224	0.000972	0.001565	0	0	0	0	0	0	0	0
RUSF-07-HH	3	3	10.265747	0.004694	0.005194	0	0	0	0	0	0	0	0
Southeast2													
ANTF-00-HH	3	3	8.830112	0.012563	0.015047	0	0	0	0	0	0	0	0
ANTF-00-HN	3	3	9.434914	0.024545	0.027809	0	0	0	0	0	0	0	0
CAGN-00-HN	3	3	12.756809	0.043032	0.041397	0	0	0	0	0	0	0	0
CALF-00-HH	5	5	19.642498	0.007493	0.012042	0	0	0	0	0	0	0	0

sta	Number of observations		Observation period	max PGA m/s²		Number of exceedances								
	comp1	comp2		comp1	comp2	comp1				Comp 2				
						0.1 m/s²	0.2 m/s²	0.5 m/s²	1.0 m/s²	0.1 m/s²	0.2 m/s²	0.5 m/s²	1.0 m/s²
CALF-00-HN	5	5	20.095091	0.009935	0.012619	0	0	0	0	0	0	0	0
ESCA-00-HH	1	1	7.334064	0.001588	0.001065	0	0	0	0	0	0	0	0
ESCA-00-HN	1	1	8.239020	0.001600	0.001064	0	0	0	0	0	0	0	0
ESCA-01-HH	1	1	4.024775	0.038734	0.032114	0	0	0	0	0	0	0	0
ESCA-01-HN	1	1	4.080743	0.034666	0.030790	0	0	0	0	0	0	0	0
ISO-00-HH	3	3	7.768396	0.060322	0.066955	0	0	0	0	0	0	0	0
ISO-00-HN	4	4	12.672794	0.075003	0.085939	0	0	0	0	0	0	0	0
MENA-00-HN	4	4	17.278171	0.066458	0.087453	0	0	0	0	0	0	0	0
NBOR-00-HN	2	2	10.591623	0.051509	0.027941	0	0	0	0	0	0	0	0
SAOF-00-HH	4	4	20.121936	0.014446	0.015252	0	0	0	0	0	0	0	0
SAOF-00-HN	6	6	21.068944	0.015203	0.017636	0	0	0	0	0	0	0	0
Northeast													
STBU-00-HN	2	2	14.645544	0.161512	0.211619	2	0	0	0	1	1	0	0
Center													
OCMN-00-HN	1	1	10.484341	0.002824	0.003130	0	0	0	0	0	0	0	0
OCOL-00-HN	1	1	10.810077	0.000726	0.000743	0	0	0	0	0	0	0	0
OCSJ-00-HN	1	1	12.707162	0.004495	0.003681	0	0	0	0	0	0	0	0
West													
UBNA-00-HN	1	1	7.585713	0.002720	0.004047	0	0	0	0	0	0	0	0

2.4.3 European Strong-Motion

In the framework of the European Project NERA (Network of European Research Infrastructures for Earthquake Risk Assessment and Mitigation), the INGV releases online a European strong-motion database (ESM, https://esm.mi.ingv.it/). One of the associated products is the ESM strong motion flatfile 2018 which is a parametric table which contains metadata and intensity measures of manually processed waveforms recorded by accelerometers. The complete dataset includes 23014 quality-checked records from 2179 earthquakes recorded at 2027 stations (Figure 2.16). Figure 2.17 presents the moment magnitude Mw – epicentral distance scatter plot for the global dataset.
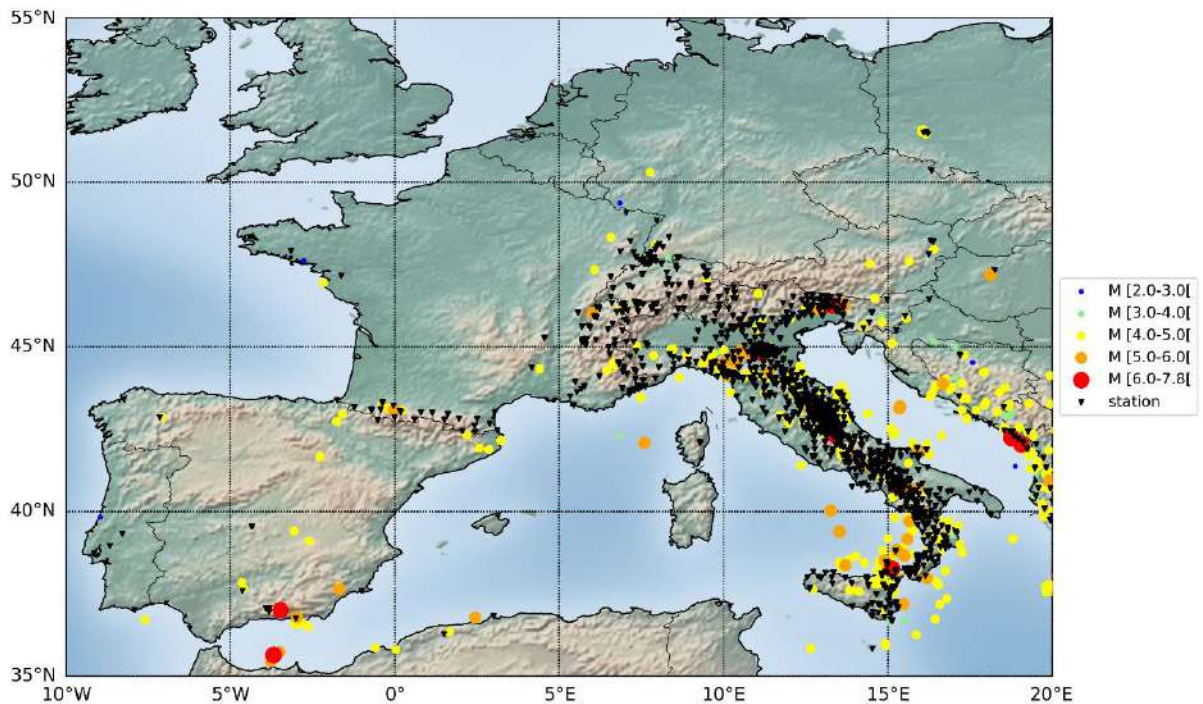

Figure 2.16: Earthquakes and stations included in the ESM flatfile (https://esm.mi.ingv.it/).
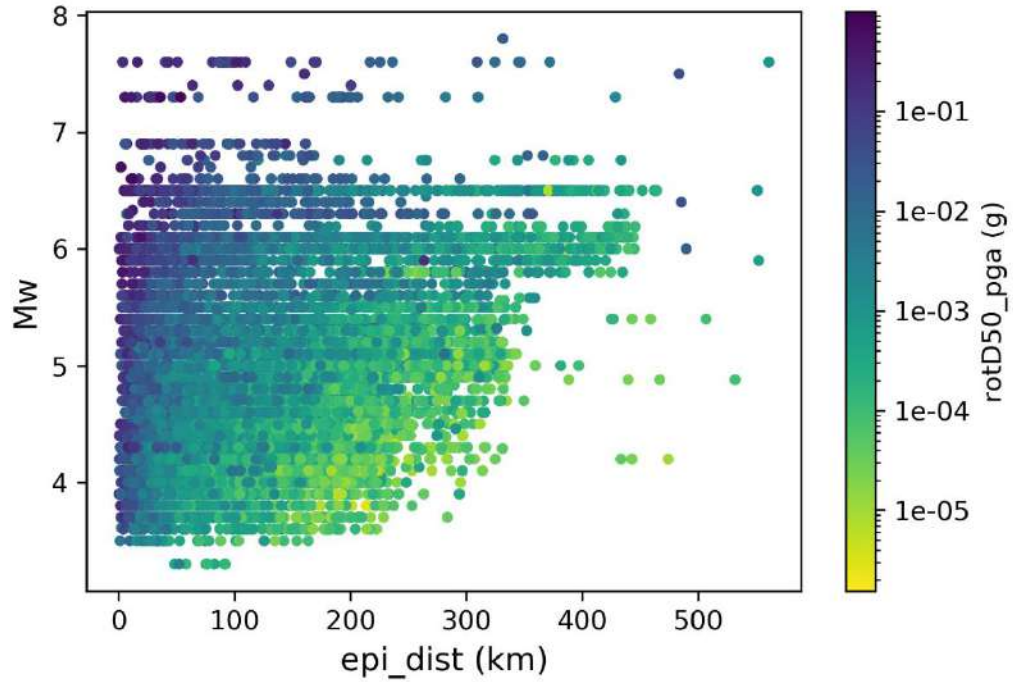
Figure 2.17: Magnitude-distance scatter plot for the data included in the ESM flatfile (https://esm.mi.ingv.it/).

From the global dataset, events with moment magnitude Mw larger than 4.5 are extracted and recordings at less than 200 km and for rock sites only are selected. These filters are applied for consistency of the hazard calculation parameters. The map of events and stations and the magnitude distance scatter plot for the "filtered" dataset are shown in Figure 2.18 and Figure 2.19, respectively.
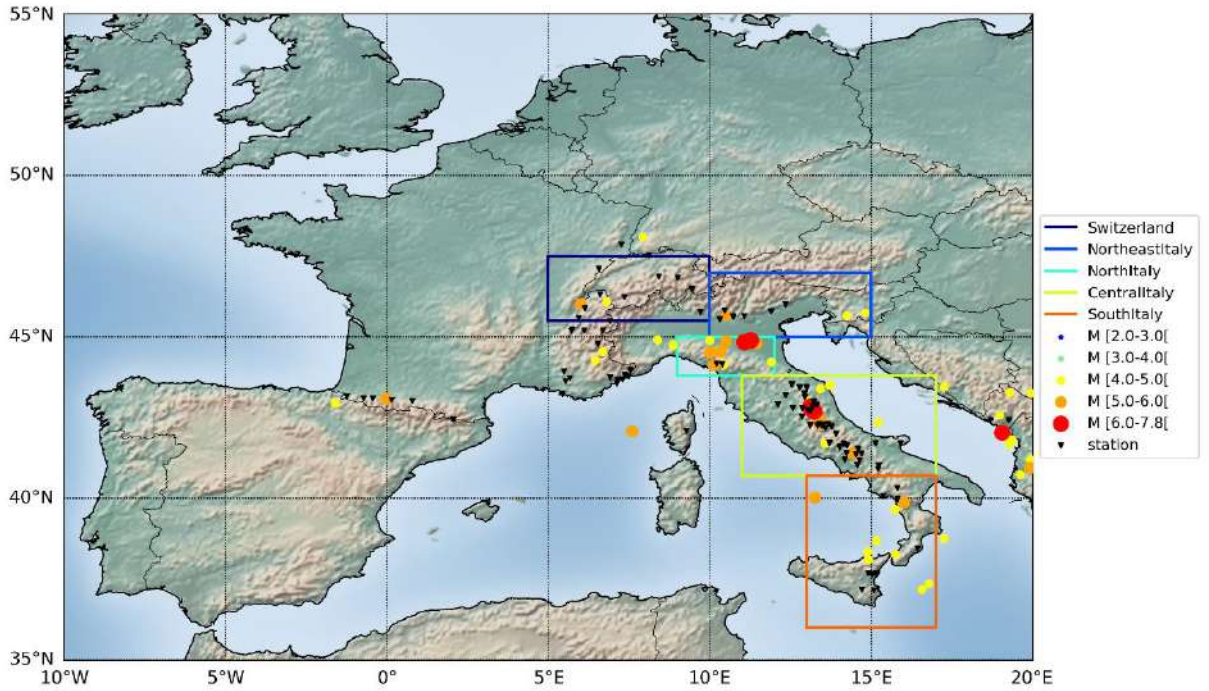
Figure 2.18: Earthquakes and stations included in the ESM flatfile (https://esm.mi.ingv.it/) for events with Mw≥4.5 recorded at distances lower than 200 km on rock sites. The colour-coded boxes represent sub-regions used for the final selection of the sites.
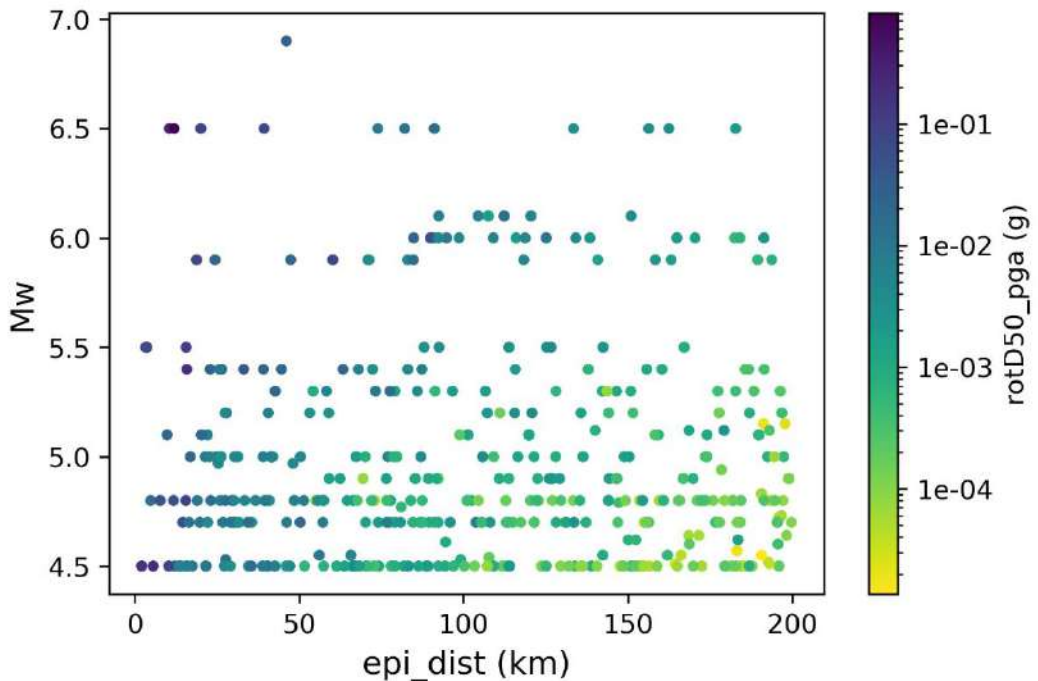

Figure 2.19: Magnitude-distance scatter plot for the data included in the ESM flatfile (https://esm.mi.ingv.it/) for events with Mw≥4.5 recorded at distances lower than 200 km on rock sites.

Information about the observation period are retrieved from the INGV and ETH FDSN webservices which provide an easy access to station information. The station metadata

include the history of the instrumentation at the different sites. The level of available information is lower than for the stations of the RAP-RLBP flatfile and only start and eventually end date of the station are available. The full history indicating eventual down time of the stations is not available. The operation period is then simply computed based on the start date of the stations.

The reference date to compute observation periods is the date of the last event included in the flatfile: December 27, 2016 at 11:20 PM.

Using the "filtered" flatfile, number of exceedances for 4 acceleration thresholds (0.1, 0.2, 0.5 and 1.0 m/s^2) are computed for each component at each station (Table 2.20).

The selection of the sites for the testing procedure is based on sub-regions. To avoid correlation between observations, distant stations are selected. The sub-regions are shown in Figure 2.18.

For the sub-regions Switzerland and Southern Italy, no exceedances have been recorded and we selected the stations with the longest observation period. For Northeast Italy, a single station recorded exceedances. Its observation period is of the same order as for the other stations, and the number of data in the flatfile (recorded data including those below exceedance thresholds) are also similar to the other stations. We consequently decide to select the station with observations above the exceedance thresholds. For Northern Italy, the two stations detected exceedances of the thresholds but the observation periods are very different 0.3 years versus 16 years. We selected the station with the longest observation period. For Central Italy, the situation is more complex. Due to the 2016 seismic crises stations from temporary network are included in the flatfile with a high number of exceedances. Figure 2.20 maps the stations with a colour-code indicating the number of exceedances of the 0.1 m/s^2 threshold and shows that most of the stations with a high number of exceedances are located in the region of the 2016 crises. To select the station in central Italy, we compared the station exceedance rates with regional exceedance rates. The regional rates are computed using different criteria: all the stations, only stations with at least one exceedance, only stations with an observation period greater than 1, 5 or 10 years. These tests highlighted that regional rates vary largely depending on these criteria. The exclusion of the stations with an observation period lower than 1 year (temporary stations) is the dominant factor. Hence, we selected a station showing a rate close the regional rate computed with only stations with an observation period greater than 1 year, and with a relatively long observation period. The final selected set of stations is shown in Figure 2.21, and there geographical coordinates given in Table 2.19.
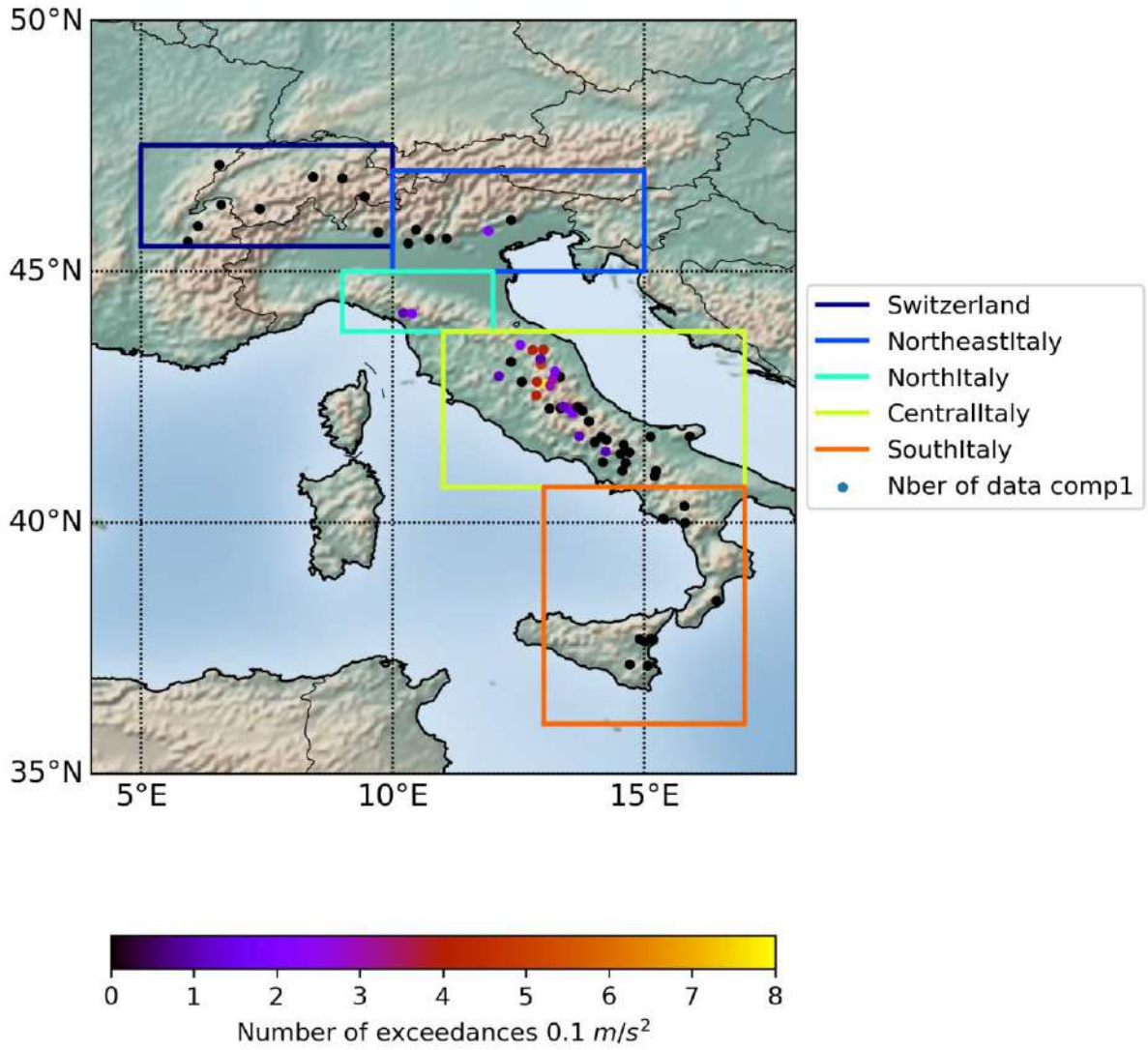
Figure 2.20: Stations included in the ESM flatfile (https://esm.mi.ingv.it/) for events with Mw≥4.5 recorded at distances lower than 200 km on rock sites. The station locations are shown as color-coded dots indicating the number of exceedances of the 0.1 m/s² threshold. The color coded boxes represent sub-regions used for the final selection of the sites.
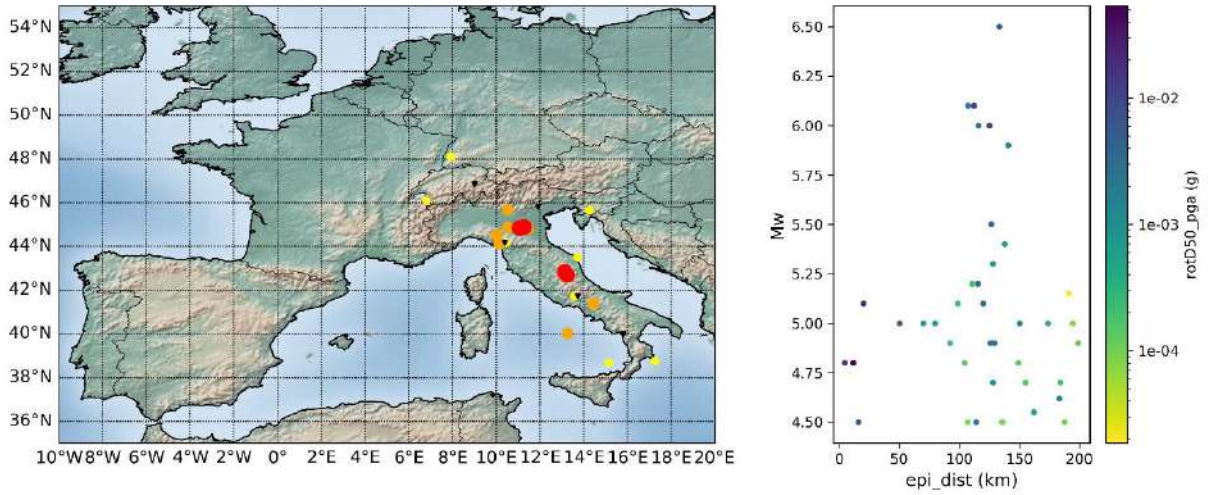
FUGRO

Figure 2.21: Final set of selected stations from the ESM flatfile (black triangles).

Table 2.19: Geographical coordinates (WGS84) of the selected ESM stations.

sta	Longitude (°)	Latitude (°)	Site class (EC8)	V_{S30} (m/s)
ASOL	11.9023	45.8003	A	-
CUC	15.8155	39.9938	A	-
LLS	9.00825	46.84676	A	2925
POFI	13.71202	41.71743	A	-
VLC	10.3864	44.1594	A	-

Table 2.20: Number of observed exceedances for different thresholds of acceleration for instrumental data in Europe. Selected stations are highlighted in green.

Station	Number of observations		Observation period	max PGA m/s²		Number of exceedances							
	comp1	comp2		comp1	comp2	comp1				comp2			
						0.1 m/s²	0.2 m/s²	0.5 m/s²	1.0 m/s²	0.1 m/s²	0.2 m/s²	0.5 m/s²	1.0 m/s²
Switzerland													
BNALP	1	1	18.720474	0.013541	0.006381	0	0	0	0	0	0	0	0
LLS	3	3	41.991706	0.005955	0.005638	0	0	0	0	0	0	0	0
SIOV	1	1	14.588967	0.000941	0.000914	0	0	0	0	0	0	0	0
VDL	3	3	33.504035	0.009464	0.011037	0	0	0	0	0	0	0	0
MDI	1	1	12.076638	0.002309	0.001570	0	0	0	0	0	0	0	0
Northeast Italy													
ASOL	12	12	5.116519	0.191816	0.146319	2	0	0	0	2	0	0	0
BAG8	17	17	6.844560	0.066852	0.056423	0	0	0	0	0	0	0	0
BOTT	14	14	4.967920	0.076410	0.058414	0	0	0	0	0	0	0	0
FRE8	12	12	5.748670	0.039712	0.029175	0	0	0	0	0	0	0	0
ROVR	1	1	8.227323	0.001410	0.003092	0	0	0	0	0	0	0	0
ZEN8	17	17	6.825263	0.069278	0.074298	0	0	0	0	0	0	0	0
North Italy													
T0912	1	1	0.392806	1.227177	2.250567	1	1	1	1	1	1	1	1
VLC	10	10	15.999926	0.173740	0.216654	2	0	0	0	2	1	0	0
Central Italy													
MI05	5	5	0.056564	6.515090	3.041034	5	3	2	1	5	4	2	1
ATTE	10	10	7.098556	0.074345	0.088838	0	0	0	0	0	0	0	0
BSSO	9	9	11.953350	0.093487	0.098108	0	0	0	0	0	0	0	0
CAFE	3	3	11.476638	0.007401	0.004759	0	0	0	0	0	0	0	0
CERA	13	13	10.449241	0.063845	0.082629	0	0	0	0	0	0	0	0

Station	Number of observations		Observation period	max PGA m/s²		Number of exceedances							
						comp1				comp2			
	comp1	comp2		comp1	comp2	0.1 m/s²	0.2 m/s²	0.5 m/s²	1.0 m/s²	0.1 m/s²	0.2 m/s²	0.5 m/s²	1.0 m/s²
FIAM	11	11	12.470017	0.075118	0.054224	0	0	0	0	0	0	0	0
INTR	3	3	13.328693	0.033699	0.052110	0	0	0	0	0	0	0	0
MELA	4	4	8.685770	0.024296	0.024493	0	0	0	0	0	0	0	0
MGAB	13	13	8.743761	0.131859	0.135736	1	0	0	0	1	0	0	0
MIDA	9	9	12.064480	0.051040	0.040276	0	0	0	0	0	0	0	0
MMO1	1	1	4.141560	0.082356	0.119660	0	0	0	0	1	0	0	0
MMUR	12	12	8.174121	0.708861	1.025177	4	2	1	0	4	3	1	1
MOMA	1	1	5.392848	0.006993	0.008819	0	0	0	0	0	0	0	0
MSAG	3	3	10.600725	0.007543	0.010917	0	0	0	0	0	0	0	0
PAOL	4	4	6.839423	0.030022	0.034355	0	0	0	0	0	0	0	0
PIEI	11	11	13.838282	0.203964	0.118449	2	1	0	0	1	0	0	0
PIGN	5	5	5.179387	0.065351	0.041900	0	0	0	0	0	0	0	0
POFI	14	14	9.759857	0.697999	0.290031	1	1	1	0	1	1	0	0
PTRJ	2	2	9.950611	0.001583	0.000982	0	0	0	0	0	0	0	0
RM01	2	2	0.405478	0.067305	0.138306	0	0	0	0	2	0	0	0
RM03	8	8	0.405478	0.908977	0.708648	2	2	1	0	2	2	1	0
RM13	6	6	0.408217	0.880281	1.309172	2	1	1	0	2	2	1	1
RM27	1	1	0.205478	0.031224	0.039848	0	0	0	0	0	0	0	0
RNI2	13	13	13.838282	0.077791	0.058715	0	0	0	0	0	0	0	0
SACR	2	2	12.558830	0.068183	0.046484	0	0	0	0	0	0	0	0
SEF1	7	7	5.143830	0.435271	0.442785	5	2	0	0	5	2	0	0
SNAL	1	1	12.349241	0.000483	0.000459	0	0	0	0	0	0	0	0
SNTG	8	8	13.838282	0.116172	0.079845	1	0	0	0	0	0	0	0
SSFR	6	6	6.483202	0.571087	0.495548	4	2	1	0	4	2	0	0
T0106	2	2	1.883128	0.108265	0.116336	1	0	0	0	1	0	0	0

Station	Number of observations		Observation period	max PGA m/s²		Number of exceedances								
	comp1	comp2		comp1	comp2	comp1				comp2			
						0.1 m/s²	0.2 m/s²	0.5 m/s²	1.0 m/s²	0.1 m/s²	0.2 m/s²	0.5 m/s²	1.0 m/s²
T0110	1	1	7.324127	0.002802	0.002986	0	0	0	0	0	0	0	0
T1211	9	9	0.344674	0.592732	0.741560	4	2	1	0	4	3	1	0
T1212	9	9	0.344674	2.744297	2.731541	8	7	4	2	8	7	4	3
T1213	4	4	0.344674	7.792716	8.499660	3	3	2	2	4	3	2	1
T1215	8	8	0.341250	0.734584	0.872416	4	3	1	0	6	3	1	0
T1245	3	3	0.234229	2.295734	1.889173	3	3	2	2	3	3	2	1
T1256	2	2	0.170093	0.470772	0.676761	2	2	0	0	2	2	2	0
VAGA	12	12	11.806775	0.239555	0.268995	1	1	0	0	1	1	0	0
VITU	1	1	2.995203	0.000187	0.000500	0	0	0	0	0	0	0	0
SouthItaly													
BULG	2	2	10.399012	0.028623	0.036668	0	0	0	0	0	0	0	0
ECHR	1	1	8.571159	0.038727	0.045725	0	0	0	0	0	0	0	0
ENIC	1	1	3.790015	0.026357	0.024276	0	0	0	0	0	0	0	0
EPOZ	2	2	3.790031	0.010194	0.010147	0	0	0	0	0	0	0	0
EVRN	4	4	6.941181	0.054191	0.074319	0	0	0	0	0	0	0	0
HVZN	2	2	11.476638	0.011718	0.013077	0	0	0	0	0	0	0	0
MCEL	2	2	10.399926	0.029663	0.025382	0	0	0	0	0	0	0	0
PLAC	4	4	11.202665	0.012286	0.015783	0	0	0	0	0	0	0	0
SSY	1	1	12.471159	0.025187	0.029381	0	0	0	0	0	0	0	0
CUC	3	3	13.462939	0.002297	0.001856	0	0	0	0	0	0	0	0

2.5   Synthesis of observation sites used in this study

Based on the previous sections, observation stations that are used in the following part of the study are plotted in the next figures.

The Figure 2.22 shows:

- The 15 sites located in France with macroseismic intensity observations
- The 19 sites located in France with instrumental observations

The number of cumulated observations for both historical and instrumental data are given in Table 2.21 and Table 2.22, respectively.
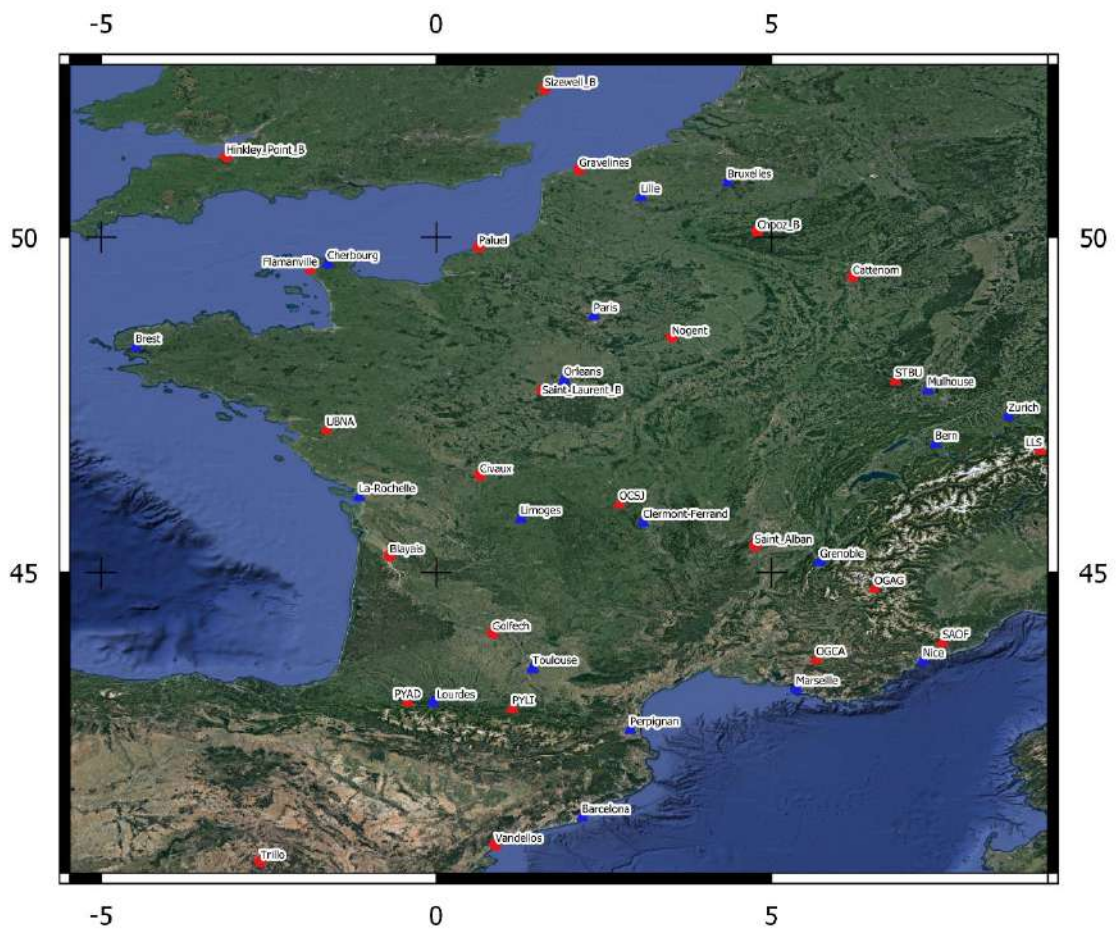
Figure 2.22: Selected sites for the Bayesian update for France (blue triangles: macroseismic observation points; red triangles: instrumental observation points).

Table 2.21: Number of intensity observations for the 15 sites located in France.

Intensity bin	Number of occurrences	Intensity threshold	Number of exceedances	Cumulated observation period (years)
[VI-VII[	9	I≥VI	11	3095
[VII-VIII[	0	I≥VII	2	3855
[VIII-IX[	2	I≥VIII	2	7605

Table 2.22: Number of acceleration exceedances for the 19 sites located in France.

Number of exceedances for acceleration threshold				Cumulated observation period (years)
0.1 m/s²	0.2 m/s²	0.5 m/s²	1.0 m/s²	
2	0	0	0	443

Figure 2.23 shows:

- The 28 sites located in Europe with macroseismic intensity observations
- The 39 sites with instrumental observations.

The number of observations for both historical and instrumental data are given in Table 2.23 and Table 2.24, respectively.
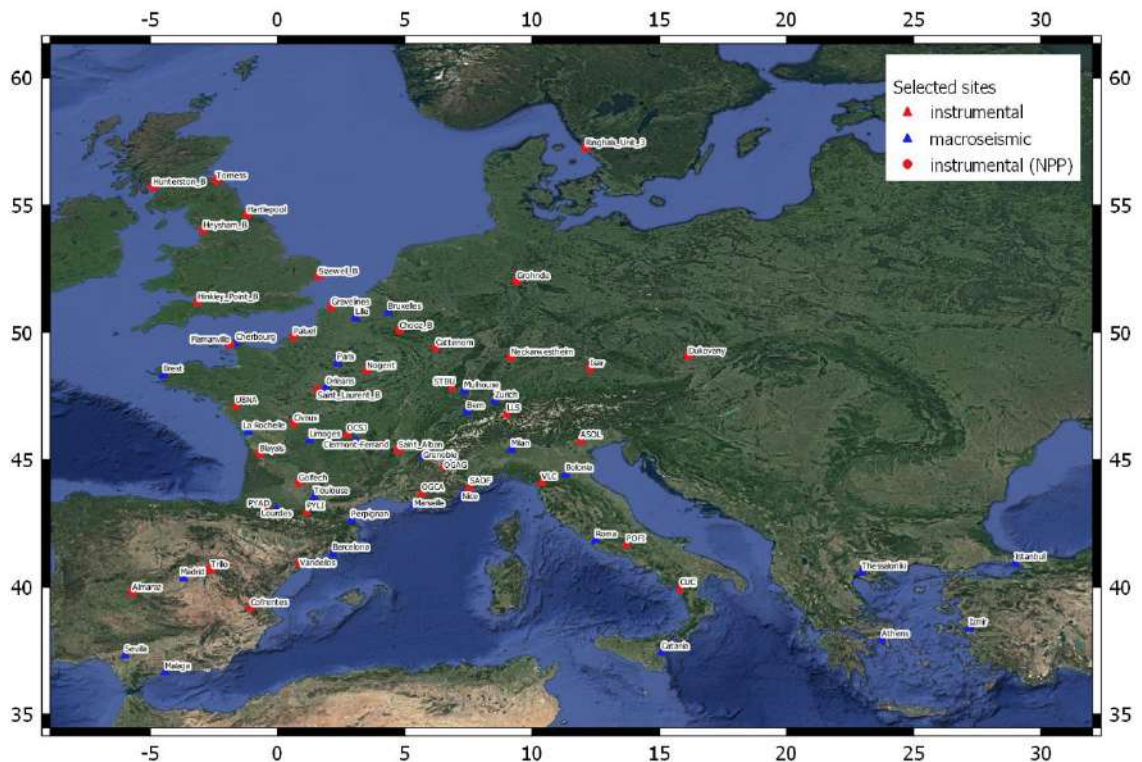
Figure 2.23: Selected sites for the Bayesian update for Europe (red triangles: macroseismic observation points; blue triangles: instrumental observation points).

Table 2.23: Number of intensity observations for the 28 sites located in Europe.

Intensity bin	Number of occurrences	Intensity threshold	Number of exceedances	Cumulated observation period (years)
[VI-VII[	41	I≥VI	68	5745
[VII-VIII[	20	I≥VII	27	8632
[VIII-IX[	7	I≥VIII	7	13647

Table 2.24: Number of acceleration exceedances for the 39 sites located in Europe.

Number of exceedances for acceleration threshold				Cumulated observation period (years)
0.1 m/s²	0.2 m/s²	0.5 m/s²	1.0 m/s²	
9	2	1	0	983

2.6 Seismic hazard results

The observed number of exceedances will be compared with seismic hazard predictions (hazard curves). The ultimate objective is to compare observations with the most recent version of the European hazard model ESHM20 developed in the framework of the SERA project. At the beginning of the project, the ESHM20 results were not available and preliminary tests were performed using the prediction of the previous European hazard model ESHM13 developed in the framework of SHARE.

Two different sets of hazard curves are considered initially with the ESHM13 model:

▪ a set including all the hazard curves of all the branches of the logic-tree, and
▪ a set of hazard curves corresponding to the various quantiles of the hazard results.

Using the first set in the Bayesian testing methodology allows one to evaluate each branch of the logic-tree and its likelihood with respect to observed data. Those results could help refining models or parameters or simply adjust their weights to make the hazard model more compatible with observations. However, different sites might be sensitive to different parts of the hazard model and due to the limited individual observation period at each site, the evaluation process usually combines observations form different sites.

The second set allows a more global assessment of the hazard model by evaluation of the ground-motion distribution (center body and range) with respect to observed data. In this case no direct correlation with individual branch of the logic-tree can be made, but the testing methodology can help updating the weight to adjust the ground-motion distribution in the direction suggested by the data.

For the ESMH13 model, the testing methodology has been applied to the dataset for France only.

The ESHM13 model has then been used to compute hazard curves for all the sites of interest (sites with macroseismic observation and those with instrumental observations). The hazard model is available from the European Facilities for Earthquake Hazard and Risk website (EFEHR, http://www.efehr.org/en/Documentation/specific-hazard-models/europe/overview/). Using the ESHM13 model, hazard curves for all the branches are computed as well as 99 hazard curves corresponding to 99 quantiles (1, 2, ..., 99).

Hazard curves provide probabilities (p) of exceedances for different acceleration threshold. Probabilities over a time period (t) are related to rates (λ) following:

$$p = 1 - exp(-\lambda \times t)$$

For the ESHM20 model, Laurentiu Danciu provided a set of hazard curves corresponding to 5 quantiles (5, 16, 50, 84 and 95) for all the sites considered in SERA (covering the whole Europe with a 10 km spacing). The closest point to the selected cities for the Bayesian evaluation were identified and the corresponding hazard curves extracted. The ESHM20 results were provided early April by L. Danciu (preliminary tests were also performed with a beta version of ESHM20 provided in September 2020 but are not shown in this report).

For the ESMH13 model, the testing methodology has been applied to the dataset for France only. For the ESHM20, both the dataset for France and the complete dataset have been used.

Both ESHM13 and ESHM20 models are developed for standard rock site conditions. Preliminary tests of the Bayesian update method suggested a discrepancy between instrumental and macroseismic observation sites which is probably linked with the site conditions. Indeed, in these preliminary tests rock site conditions are also assumed for the observation sites which is true for the instrumental ones selected based on their site conditions but is clearly not true for the macroseismic observation sites. Those are relatively important cities usually located in or close to fluvial basins. Sites conditions are difficult to assess in these cases but are most probably stiff to soft soils conditions. We used the EC8 parameters given in Table 2.25 to estimate a site coefficient which could be applied to take into account the site effects at the macroseismic observation sites.

Table 2.25: EC8 parameters to compute response spectra (Type 1 and Type 2, respectively). From Eurocode 8 (EN 1998-1).

Table 3.2: Values of the parameters describing the recommended Type 1 elastic response spectra

Ground type	S	T_B (s)	T_C (s)	T_D (s)
A	1,0	0,15	0,4	2,0
B	1,2	0,15	0,5	2,0
C	1,15	0,20	0,6	2,0
D	1,35	0,20	0,8	2,0
E	1,4	0,15	0,5	2,0

Table 3.3: Values of the parameters describing the recommended Type 2 elastic response spectra

Ground type	S	T_B (s)	T_C (s)	T_D (s)
A	1,0	0,05	0,25	1,2
B	1,35	0,05	0,25	1,2
C	1,5	0,10	0,25	1,2
D	1,8	0,10	0,30	1,2
E	1,6	0,05	0,25	1,2

The use of EC8 Type 1 or Type 2 spectra depends on the level of hazard at the site of interest. Type 2 applies where the magnitude dominating the hazard does not exceed Ms=5.5. In our case most of the sites are Type 1 but at the limit between Type 1 and Type 2 (sites from North West Europe). The sites in the more active regions (Southern and Eastern Europe) are more Type 1. In addition, the site class to take into account may vary a lot between each site but on average we assume that our macroseismic observation sites can be associated to classes C or D. Consequently, the site terms S to take into account in our study would range between 1.15 and 1.8. We selected 1.35 as a representative value.

To test this value, we made an additional test with the ESHM13 model. Hazard curves for our sites of interest have been computed assuming a v_{S30}=270 m/s (center of class C). We then compared hazard curves computed with v_{S30}=800 m/s but adjusted to "stiff/soft" site conditions by application of a multiplication factor (1.35 and 1.8 have been tested) and the hazard curves computed with v_{S30}=270 m/s. Figure 2.24 shows the results obtained for the cities of Cherbourg and Lourdes. Based on the results at all the sites, the site factor 1.35 seems a good approximation of the site amplification.
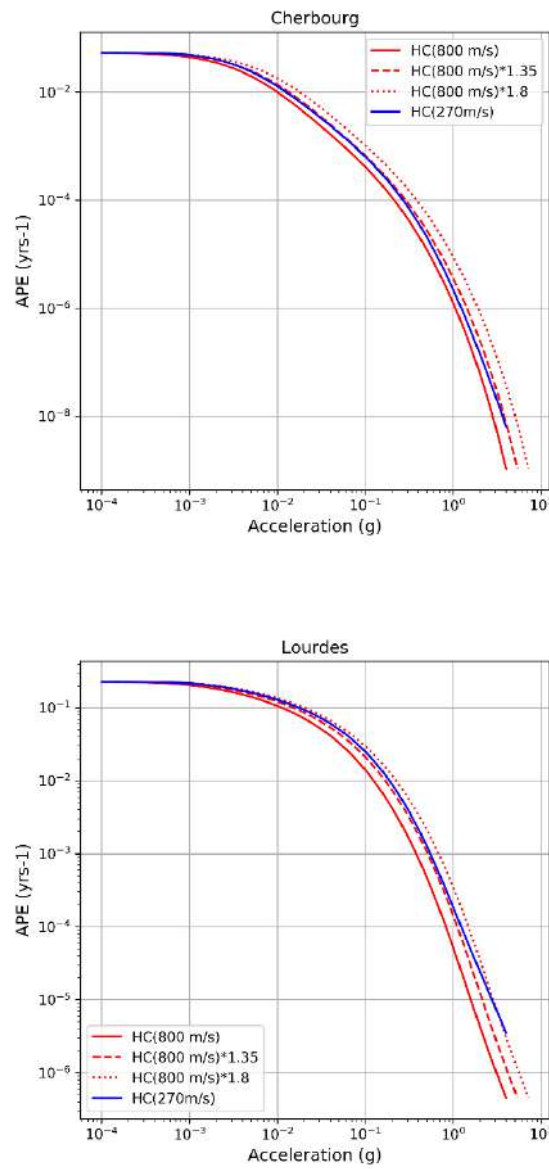
Figure 2.24: Hazard curves computed with the ESHM13 model for Cherbourg (top) and Lourdes (bottom) for rock site conditions (red curve) and soft site conditions (blue curve). Conversion of the rock site condition hazard curve to soft site conditions by multiplication by a factor 1.35 and 1.8 are also shown (dashed and dotted red curves, respectively).

Based on those results, the hazard curves computed for all the macroseismic sites are multiplied by a factor 1.35 (shift of the acceleration thresholds keeping the probabilities unmodified) to simulate site effects in the hazard prediction.

3. Methodology

The evaluation consists in the comparison of predictions and observations. Two main publications Viallet et al. (2019) and Secanell et al. (2018) applied Bayesian method to evaluate PSHA models in France in addition to the work of Tasan et al. (2014). A larger panel of existing methodologies and applications is given in OECD/NEA/CSNI workshop, 2015. We refer the reader to these publications for more details on the methodological aspects.

For instrumental data, acceleration data is compared to seismic hazard curves defined in terms of acceleration, both methodologies are equivalent since no specific treatment of the data is applied.

For historical data, the methods are slightly different. The Viallet et al. (2019) method converts the seismic hazard curves in acceleration into seismic hazard curves in intensity. Then, the historical observations (in intensity) are compared to the predictions. The Viallet et al. (2019) method includes the propagation of the uncertainties taking into account the standard deviation of the acceleration-intensity model during the conversion. Epistemic uncertainty can also be accounted for through the possibility to use alternative conversion models.

The Secanell et al. (2018) method converts the intensity observations into acceleration. Only epistemic uncertainty is taken into account in this method by using alternative intensity-acceleration conversion models.

In this study, the evaluation is performed using the Viallet et al. (2019) method since uncertainties of the intensity-acceleration conversion are better accounted for, which fulfills OECD/NEA workshop conclusions and recommendations.

We note that an alternative approach could be to improve the rationale presented in Secanell et al. (2018). This would require converting intensity observations into accelerations, accounting for the full range of uncertainties associated with the intensity-acceleration conversion step. Comparison of observation with predictions would then imply to use a more complex distribution-to-distribution comparison approach.

3.1 Bayes theorem

The methodology used to compare observations, both instrumental and macroseismic, to PSHA prediction is based on Viallet et al. (2019) who used a Bayesian inference technique to compute the likelihood of a PSHA prediction to explain observed data.

The method is based on the Bayes theorem of conditional probabilities:

$$P(A|B) = \frac{P(B|A).P(A)}{P(B)}$$

Where:

- P(A) is the prior estimation;
- P(B|A) is conditional probability of the observed event B according to the prior assessment;
- P(B) is the total probability of the observed event B;
- P(A|B) is the expected updated (posterior) estimation.

3.2 Instrumental data

For a given acceleration threshold, we can count over the observation period (t) the number of exceedances (n) at the sites of interest (assuming that observations at several sites are combined).

Assuming that ground-motion occurrence follows a Poisson distribution, with a PSHA model predicting an annual rate of exceedance $\lambda(PGA_{threshold})$, the probability of observing n exceedances of $PGA_{threshold}$ over a period of time t is:

$$P(n,t) = \frac{e^{-\lambda_{threshold} \times t}(\lambda_{threshold} \times t)^n}{n!}$$

P(n,t) gives us the term P(B|A) in section 3.1 and can be computed for each hazard curve considered. P(A) is simply the weight of the hazard curve leading to the annual rate of exceedance $\lambda_{threshold}$. P(B) is computed as the sum over all hazard curves of the P(B|A)=P(n,t).

Figure 3.1 illustrates the calculation of the likelihood of the observation for a given hazard curve P(B|A)=P(n,t).
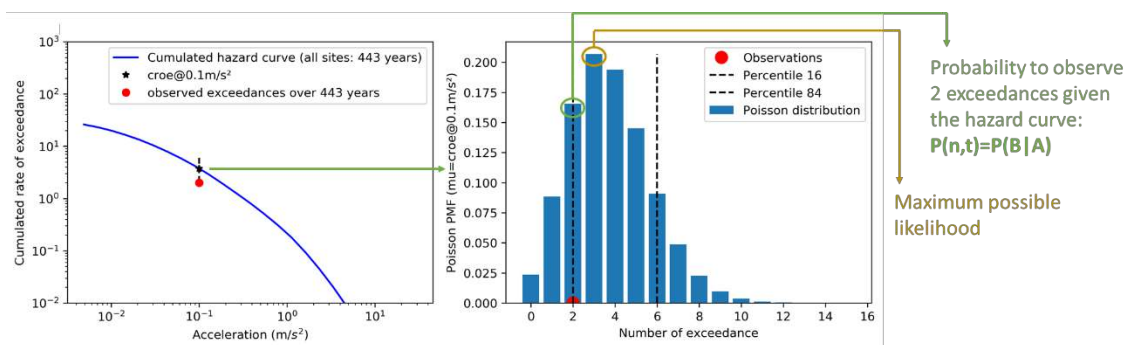
Figure 3.1: Illustration of the process to compute P(B|A) for instrumental observations. Left: Hazard curve (cumulated rate of exceedances over all the sites) (blue curve), number of observed exceedances for acceleration threshold 0.1 m/s² (red dot) and predicted rate of exceedance (black star), the range of number of predicted exceedances assuming a Poisson distribution (+/- 1σ) is also shown (dashed black line). Right: Poisson distribution with mean equal to the predicted rate of exceedance acceleration threshold 0.1 m/s² (blue bars), +/- 1σ interval is presented (dashed black lines) as well as the number of observations (red dot).

3.3 Macroseismic intensity data

Hazard curves used in this project give the probability of exceedance of various levels of ground-motion (PGA in the present case). In order to include macroseismic observation in the analysis, PGA-to-intensity relationships need to be used. In Secanell (2017), observed

intensities were converted to PGA using intensity-to-PGA relationships and these converted PGAs used in the analysis as are instrumental data. In Viallet et al. (2019), the approach is different, hazard curves are converted from PGA to intensity, taking into account uncertainties in the PGA-to-intensity relationships. Then intensity predictions are compared to observations.

The conversion of hazard curves from PGA to intensity is performed as follows:

$$N_{I_i} = \sum_{A_{min}}^{A_{max}} (N_{A+\Delta A} - N_A) . P_{I_i|A}$$

Where:

- N_{I_i} the annual rate of occurrence of a given Intensity I_i;
- N_A is the annual rate of exceedance of a given PGA A;
- $P_{I_i|A}$ is the probability of a given PGA A to produce the given intensity I_i according to the PGA-to-intensity relationship, including σ (i.e. percentage of the contribution of the given PGA level to the considered class of intensity);
- ΔA is a discretization step small enough in order to get stable results of N_{I_i} (in this study, PGA ranges from 0.001 to 40 m/s² discretized into 47 steps for ESHM13 and from 0.005 to 30 m/s² discretized into 25 steps for ESHM20).

A slight modification of the Viallet et al. (2019) method has been made to take into account different completeness periods at different sites. While Viallet et al. (2019) multiplied the annual rate of occurrence of a given Intensity I_i (N_{I_i}) by the total observation period of macroseismic data, we sum all the contributions from all the considered sites multiplied by individual completeness periods:

$$N_{I_i}^{all\ sites} = \sum_{j=1}^{j=N_{sites}} Completeness\_period_{I_i}^j \times N_{I_i}^j$$

Where:

- $Completeness\_period_{I_i}^j$ is the completeness period of intensity I_i at site j;
- $N_{I_i}^j$ is the annual rate of occurrence of a given Intensity I_i at site j.

The summation is actually performed at the level of the acceleration hazard curves:

$$N_{I_i}^{all\ sites} = \sum_{j=1}^{j=N_{sites}} Completeness_{period_{I_i}}^{j} \times \sum_{A_{min}}^{A_{max}} \left(N_{A+\Delta A}^{j} - N_{A}^{j}\right).P_{I_i|A}$$

$$= \sum_{A_{min}}^{A_{max}} P_{I_i|A} \sum_{j=1}^{j=N_{sites}} Completeness_{period_{I_i}}^{j} \times \left(N_{A+\Delta A}^{j} - N_{A}^{j}\right)$$

$$= \sum_{A_{min}}^{A_{max}} P_{I_i|A}\left(N_{A+\Delta A}^{all\_sites} - N_{A}^{all\ sites}\right)$$

Figure 3.2 illustrates the process of conversion of the hazard curve in acceleration into a hazard curve in intensity. Three steps are involved:

1. Compute the probability of acceleration A to produce intensity I (from an Intensity-PGA model) $P_{I_i|A}$;
2. Multiply this probability by the rate of occurrence of acceleration A $P_{I_i|A}\left(N_{A+\Delta A}^{all\_sites} - N_{A}^{all\ sites}\right)$;
3. For each intensity sum the contributions of the various acceleration thresholds to get the hazard curve in intensity (note that rates of occurrence are obtained, not rates of exceedance)

Note that in the conversion of hazard curves, resulting intensity hazard curves give the rates of occurrence of intensity I and not rates of exceedance. Hence the type of observation is different compared to the instrumental case where exceedances are considered.
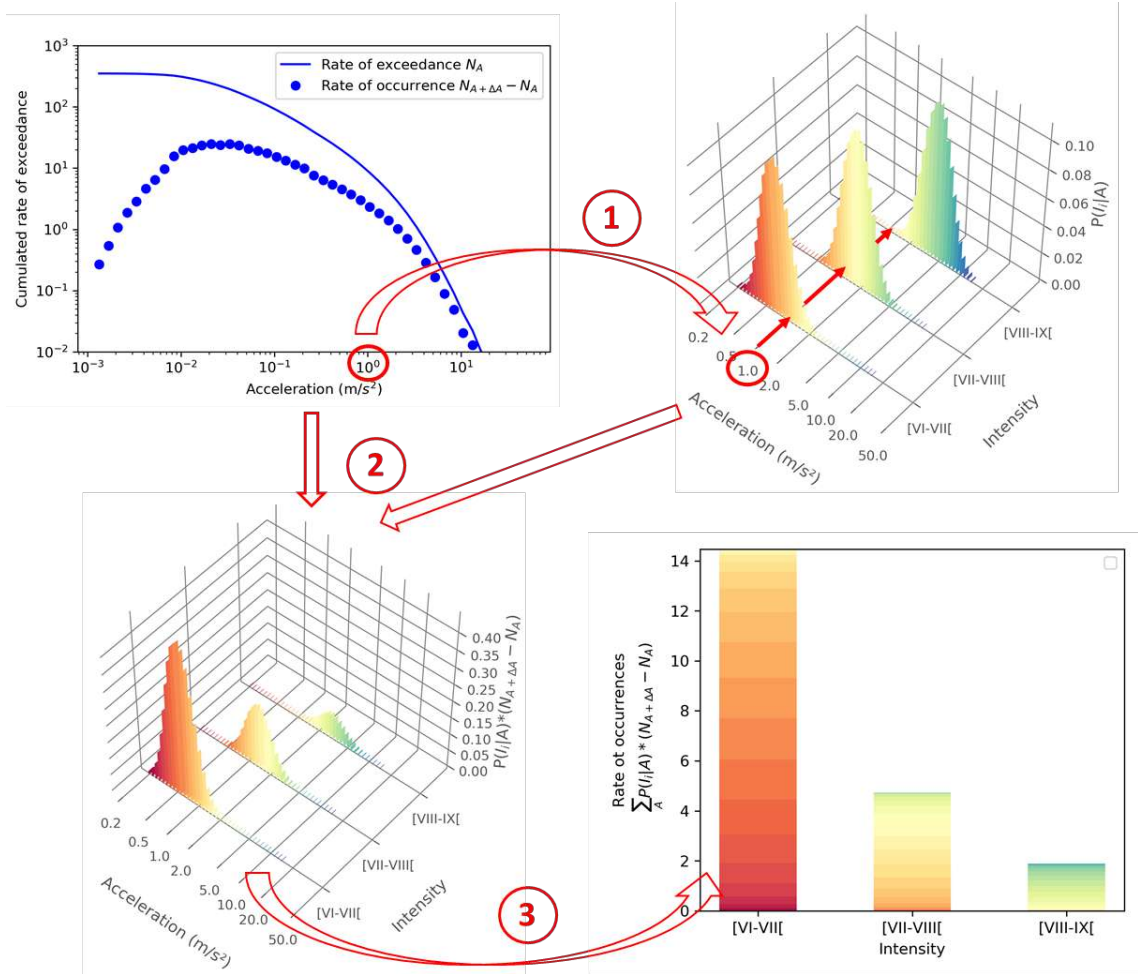
Figure 3.2: Illustration of the conversion of the hazard curve in acceleration into hazard curve in intensity. 1) Compute the probability of acceleration A to produce intensity I (from an Intensity-PGA model) $P(I_i|A)$; 2) Multiply this probability by the rate of occurrence of acceleration A $P(I_i|A) \times (N_{A+\Delta A} - N_A)$; 3) For each intensity sum the contributions of the various acceleration thresholds to get the hazard curve in intensity (note that rates of occurrence are obtained, not rates of exceedance).

Finally, from the hazard curve in intensity, one can compute the likelihood of the observation for a given hazard curve and Intensity-PGA model P(B|A) (Figure 3.3).
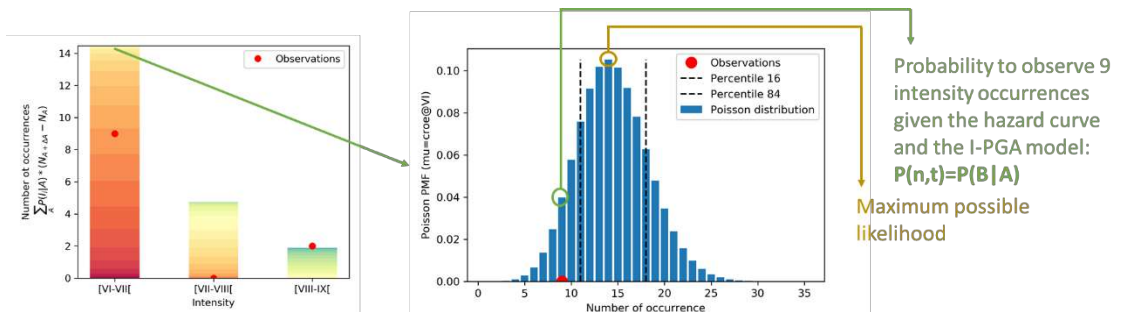
Figure 3.3: Illustration of the process to compute P(B|A) for macroseismic observations. Left: Hazard curve (cumulated rate of occurrence over all the sites) (coloured bars), number of observed occurrences for intensities [VI-VII[,[VII-VIII[and [VIII-IX[(red dot). Right: Poisson distribution with mean equal to the predicted rate of occurrences for intensity [VI-VII[(blue bars), +/- 1σ interval is presented (dashed black lines) as well as the number of observations (red dot).

In order to produce a plot which allows a very quick comparison between macroseismic intensity observations and hazard predictions, part of the approach presented previously is used. From the acceleration hazard curve and the Intensity-PGA model, an acceleration representative of the intensity level analysed can be computed (i.e. mean of the distribution $P_{I_i|A}\left(N_{A+\Delta A}^{all\_sites} - N_A^{all\ sites}\right)$ see Figure 3.2 bottom left). Figure 3.4 shows the median hazard curve for the ESHM13 model (cumulated over all the sites) with the observed number of exceedances (in that case we work with exceedances) which is plotted at the acceleration level obtained from the Intensity-PGA model (dotted and dashed curves in Figure 3.4).
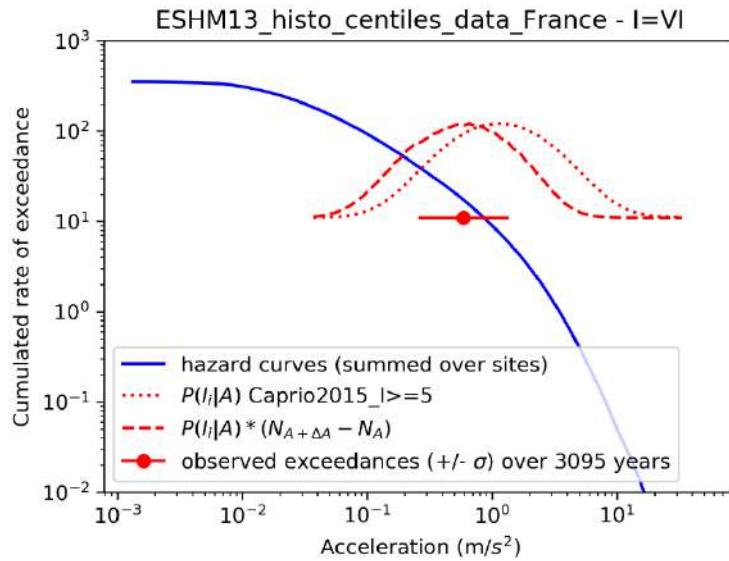
Figure 3.4: Illustration of the procedure used to obtain a quick comparison between macroseismic intensity observations and hazard predictions.

3.4   PGA-to-intensity relationships

Several PGA-to-intensity relationships are available in the literature, see for example Gomez Capera et al. (2020) for a compilation. Table 3.1 gives some characteristics of a set of representative PGA-to-intensity relationships.

As can be seen some of the models are calibrated over relatively low number of data. Also, the macroseismic scale may differ from one model to the other. Here for simplicity we assume equivalence between the different scales. The scale used in the SisFrance database is MSK which is very close to MCS (used in Italy) according to Marin et al. (2004).

The general form of the majority of the models is the following:

$$I = a + b \times log_{10}(PGA)$$

The Wald et al. (1999) and the Caprio et al. (2015) models have two sets of parameters (a and b) depending on the intensity considered. In the present work we used the coefficients for intensities ≥ V.

The other 2 exceptions are the Atkinson & Kaka (2007) model which introduces a quadratic term in $log_{10}(PGA)$ and Gomez Capera et al. (2015) model which uses the following form: $I = a \times exp^{b \times log_{10}(PGA)}$.

Table 3.1: Characteristics of a representative set of PGA-to-intensity relationships.

Equation	Region	Time window	# events	M range	PGA unit	I (scale)	# PGA-I pairs
Wald et al. (1999)	California	1971-1994	8	5.6-7.3	cm/s^2	(MM)	342
Gomez Capera et al. (2020)	Italy	1972-2016	?	?	?	(MCS)	?
Gomez Capera et al. (2015)	Italy	1976-2003	53	3.9-6.9	cm/s^2	(MCS)	118
Gomez Capera et al. (2018)	Italy	1976-2013	55	3.9-6.8	cm/s^2	(MCS)	127
Marin et al. (2004)	France	?	?	?	g	(MSK)	?
Atkinson & Kaka (2007)	?	?	?	?	cm/s^2	(MM)	?
Faenza & Michelini (2010)	Italy	1972-2004	66	3.9-6.9	cm/s^2	(MCS)	266
Tselentis & Danciu (2008)	Greece	1973-1999	89	4.0-6.9	cm/s^2	(MM)	310
Bilal & Askan (2014)	Turkey	1976-2011	14	5.7-7.4	cm/s^2	(MM)	92
Caprio et al. (2015)	Worldwide	1965-2005	?	2.5-7.3	cm/s^2	(Mixed)	2380
Zanini et al. (2019)	Italy	1983-2016	35	3.2-6.1	cm/s^2	(EMS-98)	220
Masi et al. (2020)	Italy	1980-2017	27	4.2-6.9	g	(MCS)	157

Figure 3.5 compares the PGA-to-intensity relationships indicated in Table 3.1. Figure 3.6 compares their uncertainty. Note that these uncertainties combine model uncertainty and data uncertainty (intensity data are binned prior to model fit).

Intensity
0
2
4
6
8
10
10^0
10^1
10^2
10^3
acceleration (cm.s^{-2})
Wald et al. (1999) (MM)
Marin et al. (2004) (MSK)
Atkinson & Kaka (2006) Phebus (MM)
Atkinson & Kaka (2007) (MM)
Tselentis & Danciu (2008) (MM)
Bilal & Askan (2014) (MM)
Caprio et al. (2015) (Mixed)
Gomez Capera et al. (2015) (MCS)
Gomez Capera et al. (2018) (MCS)
Faenza & Michelini (2010) (MCS)
Zanini et al. (2019) (EMS-98)
Masi et al. (2020) (MCS)
Gomez Capera et al. (2020) (MCS)
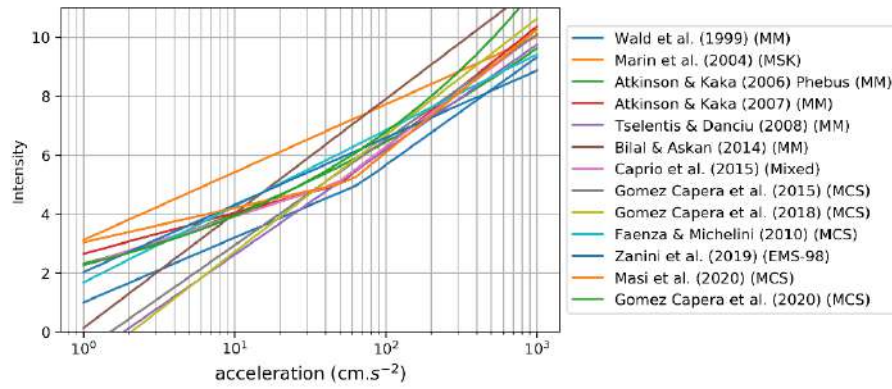
Figure 3.5: I-PGA conversion relationships from the literature.

sigma
0.2
0.4
0.6
0.8
1.0
1.2
1.4
Wald1999
Marin2004
Atkinson2006_Phebus
Atkinson2007
Tselentis2008
Bilal2014
Caprio2015
GomezCapera2015
GomezCapera2018
Faenza2010
Zanini2019
Masi2020
GomezCapera2020
I-PGA model
Wald et al. (1999) (MM)
Marin et al. (2004) (MSK)
Atkinson & Kaka (2006) Phebus (MM)
Atkinson & Kaka (2007) (MM)
Tselentis & Danciu (2008) (MM)
Bilal & Askan (2014) (MM)
Caprio et al. (2015) (Mixed)
Gomez Capera et al. (2015) (MCS)
Gomez Capera et al. (2018) (MCS)
Faenza & Michelini (2010) (MCS)
Zanini et al. (2019) (EMS-98)
Masi et al. (2020) (MCS)
Gomez Capera et al. (2020) (MCS)

Figure 3.6: Uncertainty in I-PGA conversion relationships from the literature.

From the different PGA-to-intensity relationships we computed the probability of a PGA generating an intensity I_i (term $P_{I_i|A}$ in section 3.3). Figure 3.7 shows these probabilities for intensity bins [VI-VII[, [VII-VIII[, and [VIII-IX[. A large variability is observed which will inevitably impact the testing results. Two relationships tend to predict large intensities even for small PGA values (Marin et al., 2004 and Bilal & Askan, 2014). Note that Marin et al. (2004) uses synthetic PGAs as input PGA data (and not observed ones as in the other relationships) computed using the PGA attenuation relationship as a function of magnitude and distance.
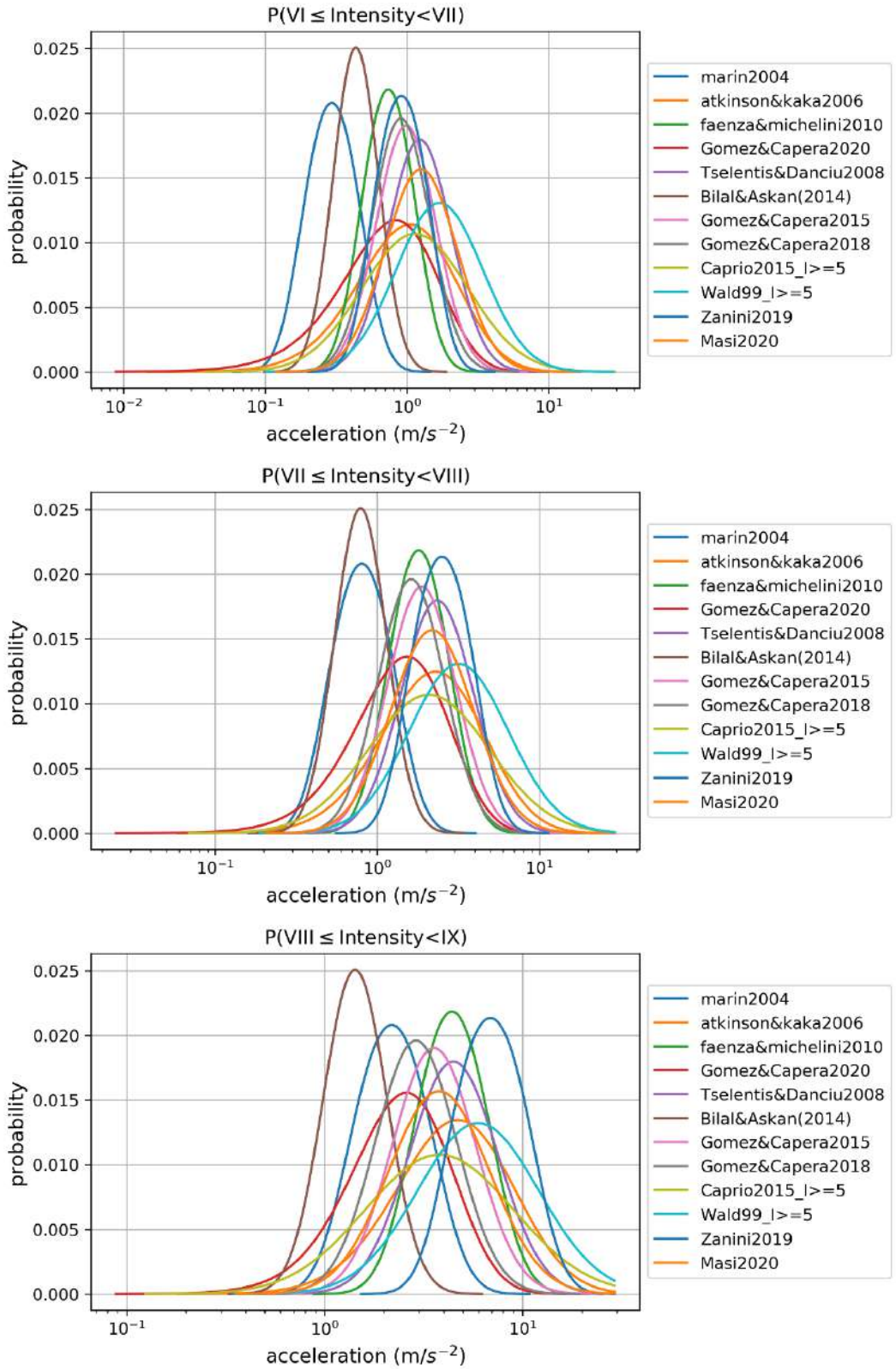
Figure 3.7: Probability of a PGA generating an intensity between VI and VII (top), VII and VIII (middle), VIII and IX (bottom) according to different Intensity-PGA relationships.

3.5   Tools

The evaluation process is performed through a program in Python called "Phebus" developed by Thomas Cousin-Dechenaud during an internship in EDF from May to December 2019.

A number of modifications and improvement have been performed in the course of the project:

- Update from Qt4 to Qt5 (application development framework: https://wiki.qt.io/About_Qt);
- Add OpenQuake hazard curve reader which converts Probabilities of Exceedance (POEs) into Annual Probabilities of Exceedance (APEs) taking into account the investigation time;
- Modify hazard curve interpolation tool such that log-interpolation is performed;
- Implement site-dependent completeness;
- Change intensity bins width from 0.5 to 1.0 intensity unit;
- Implement new form for Intensity-to-PGA relationships (exp(log10(PGA))) to accommodate the Gomez Capera et al. (2020) model.

4. Testing with data from France

Figure 2.22 shows the location of the 15 sites located in France with macroseismic intensity observations and the 19 sites with instrumental observations. The number of observations for both historical and instrumental data are given in Table 2.21 and Table 2.22, respectively.

4.1 Testing with the ESHM13 model

4.1.1 Historical data

As explained at the end of section 3.3 a quick visualisation of the observed intensity occurrences on top of the hazard curves predicted by the model is possible using the Intensity-PGA models.

All the hazard curves for the 15 sites are cumulated taking into account the observation periods at each site. The hazard curves corresponding to the median of the hazard models are used. Since the cumulated observation period varies with the considered intensity level, the cumulated hazard curves also depend on the intensity level. Consequently, one plot is produced for each intensity level.

From a given Intensity-PGA model, multiplied by the rate of occurrence of acceleration $((N_{A+\Delta A} - N_A).P_{I_i|A}$, see section 3.3) one can estimate the acceleration representative of the intensity level tested with an estimation of associated uncertainty. For the comparison figures, the Caprio et al. (2015) Intensity-PGA model is used since it is recent, calibrated on many data and has a large standard deviation such that it is representative of a large number of existing models.

Finally, the number of intensity exceedances (in that case exceedances are used as the hazard curves in acceleration provide rates of exceedance) are plotted at the acceleration level computed in the previous step.

Figure 4.1 shows the comparison of the median ESHM13 hazard curve (summed over all the sites) with the observed exceedances of intensity VI for France. The plot also shows the probability to produce an intensity VI for a given acceleration ($P_{I_i|A}$ from the Caprio et al., 2015 model) as well as the same probability multiplied by the rate of exceedance of acceleration $((N_{A+\Delta A} - N_A).P_{I_i|A})$. The figure indicates a rather good agreement between the median ESHM13 hazard curve and the number of exceedances of intensity VI and an overprediction for intensities VII and VIII. Again, this figure provides only a rapid visualisation of a given branch or centile of the hazard model and observations and it also depends on the Intensity-PGA model used.
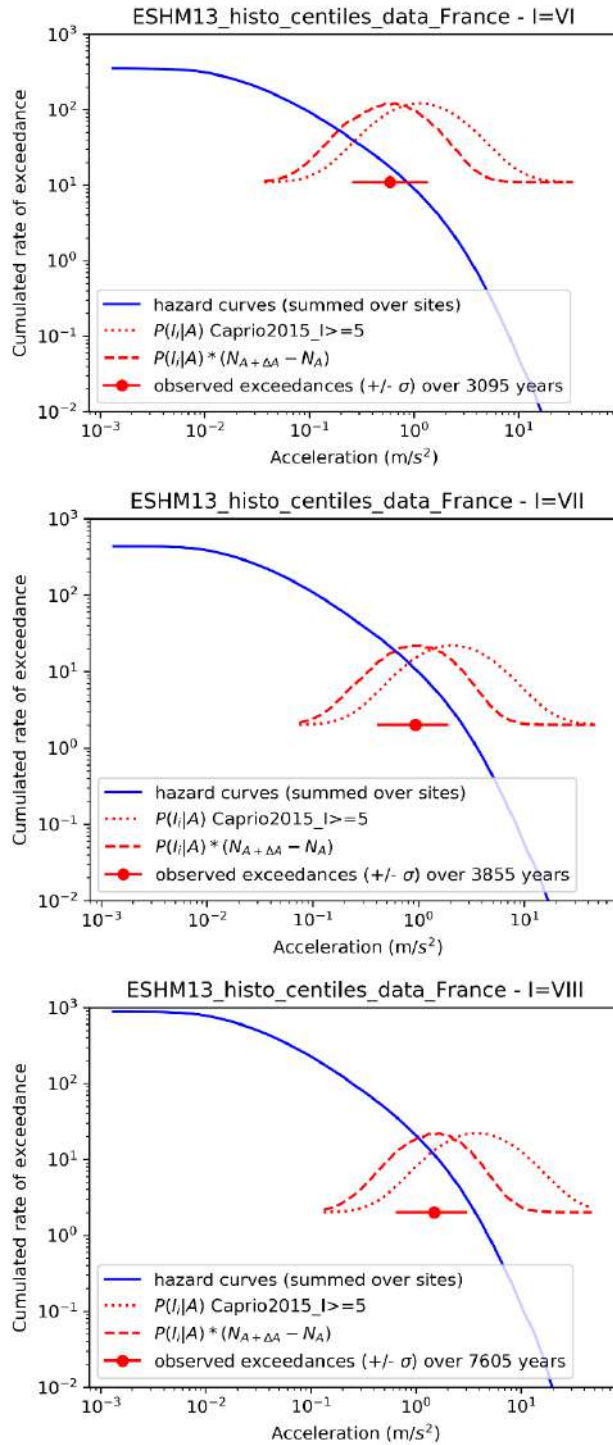
Figure 4.1: Sum over the sites of the median ESHM13 hazard curves taking into account completeness periods at each site (note that the curve differs for the different intensities due to varying completeness with intensity) for intensity VI (top), VII (middle) and VIII (bottom) for France. The probability of a given PGA producing an intensity VI, VII or VIII is also plotted on the figures based on Caprio et al. (2015) model (dotted red curves) as well as the same probability multiplied by the rate of occurrence of acceleration A: $(N_{A+\Delta A} - N_A).P_{I_i|A}$. From the $(N_{A+\Delta A} - N_A).P_{I_i|A}$ distribution a mean acceleration +/- σ is computed which is used to located the observed number of intensity exceedances (red dot and red line)..

Figure 4.2 shows the Bayesian update results following the complete methodology describe in section 3.3 for <u>all the branches of the ESHM13 model</u> and for intensity VI using 4 Intensity-

PGA models (Caprio et al., 2015; Faenza & Michelini, 2010; Gomez Capera, 2020; Wald et al., 1999). The figure shows the Poisson distributions corresponding to each branch of the logic tree (mean of the Poisson distribution is equal to the rate of exceedance predicted by the hazard curve) giving the predicted number of intensity exceedances. The likelihood of the actual observation (depicted as the vertical black arrow in the figure) is the value of the Poisson distribution for the observed number of exceedances. The left-hand side of the plots shows the likelihood values for all the hazard curves organized into 50 bins from 0.0 to the largest possible value (maximum of the Poisson distribution in case the model perfectly matches the observations) and Poisson distributions corresponding to each of the branches of the logic-tree.

Figure 4.2 clearly shows the impact of the Intensity-PGA model used to convert hazard curves in acceleration into intensity for the testing. For example, the Caprio et al. (2015) model leads to relatively high likelihoods for most of the branches of the logic-tree and the agreement between observations and predictions is good. On the opposite, the Wald et al. (1999) model which tend to predict higher acceleration for a given intensity compared to the other tested models (see Figure 3.5) the agreement between the hazard model and observations is decreased. The model seems to under-predict observations in that case. Since there is no mean to select the most appropriate Intensity-PGA model, several models are used, and the Bayesian testing results are combined at the end.
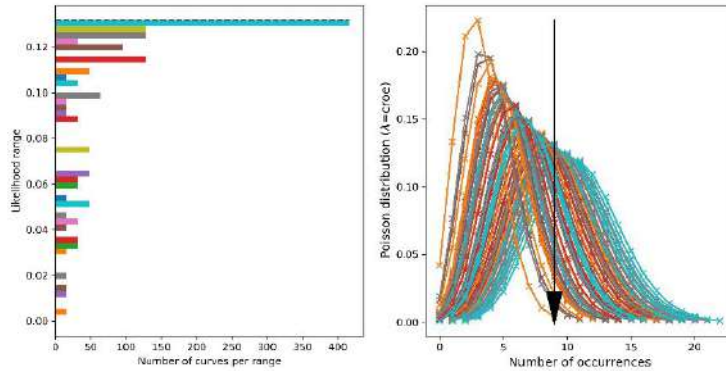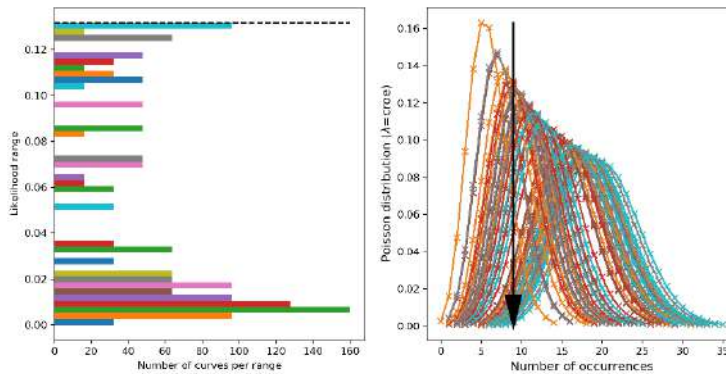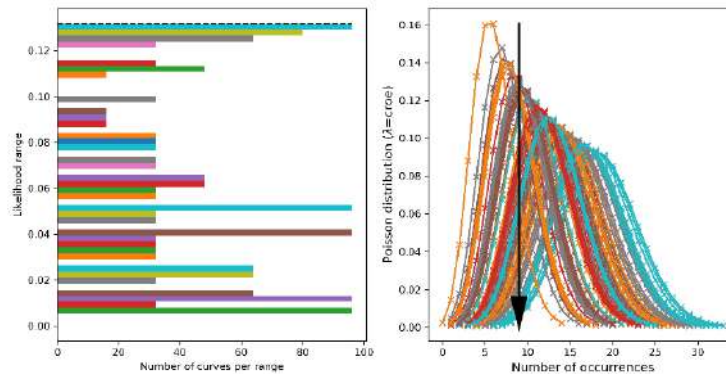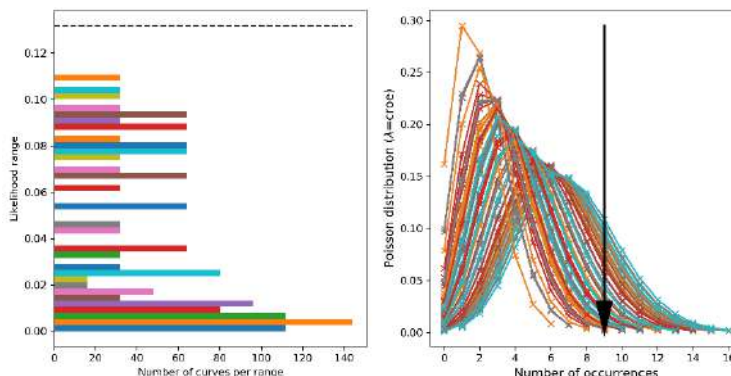
Figure 4.2: Left: Likelihood grouped by bins (coloured bars) and maximum theoretical likelihood (dashed line). Right: Poisson distributions generated from the cumulated rates of occurrences for the different branches of the logic-tree considered (coloured bars) and observed number of occurrences (black arrow). Results corresponding to the ESHM13 model (all branches) for intensity VI using data from France and 4 different PGA-to-intensity relationships (from top to bottom).

As explained earlier, for the ESHM13 model two sets of hazard curves have been considered: all the branches of the logic-tree and hazard curves corresponding to 99 fractiles of the distribution. Figure 4.3 is the same as Figure 4.2 but for the hazard curves corresponding to the 99 fractiles of the ground-motion distribution. As expected, the results are similar and show the same dependence to the Intensity-PGA models.

Caprio et al. (2015)
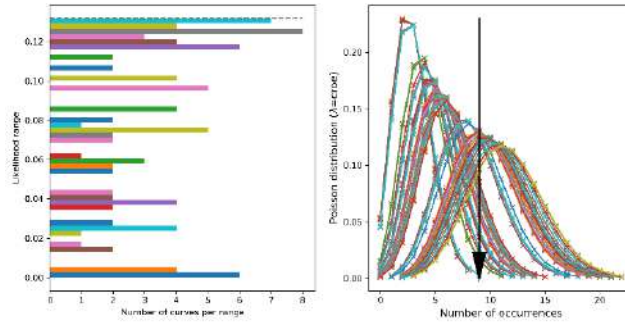
Faenza & Michelini (2010)
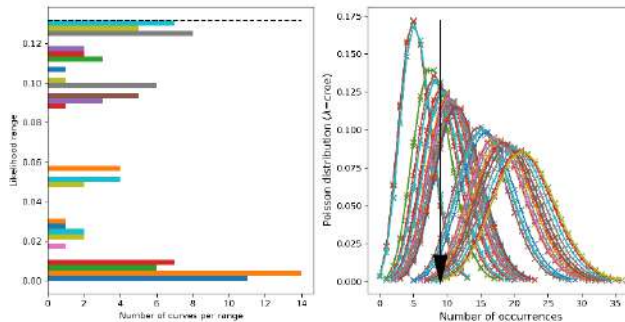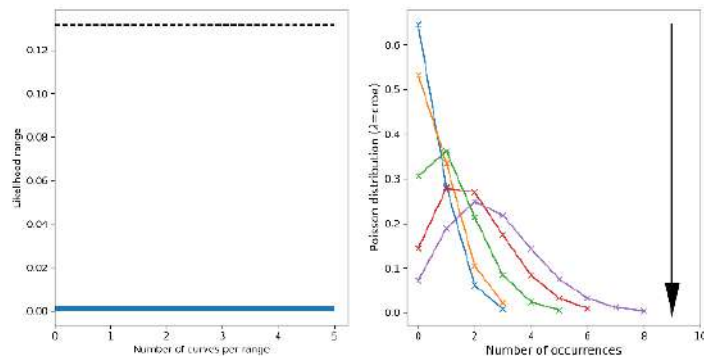
Gomez Capera (2020)
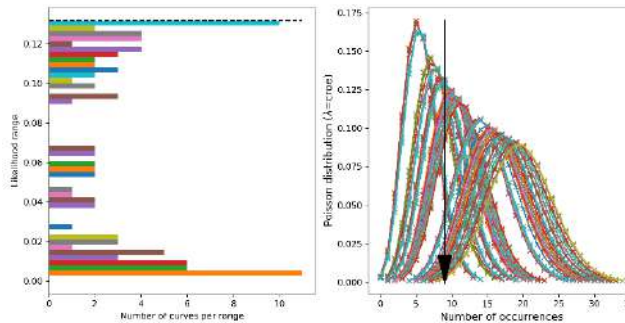
Wald et al. (1999)
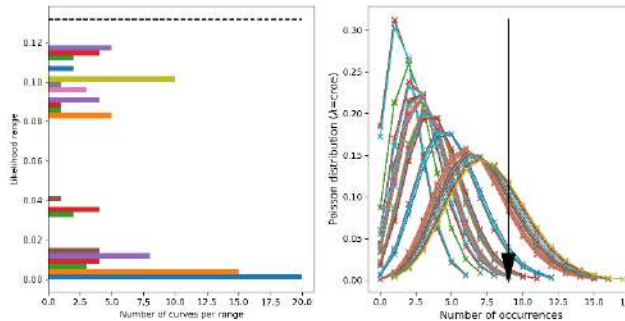
Figure 4.3: Left: Likelihood grouped by bins (coloured bars) and maximum theoretical likelihood (dashed line). Right: Poisson distributions generated from the cumulated rates of occurrences for the different branches of the logic-tree considered (coloured bars) and observed number of occurrences (black arrow). Results corresponding to the ESHM13 model (99 fractiles) for intensity VI using data from France and 4 different PGA-to-intensity relationships (from top to bottom).

The figures showing the likelihood analysis results for intensities VII and VIII are given in the Appendix B.

4.1.2   Instrumental data

All the hazard curves for the 19 sites are cumulated taking into account the observation periods at each site. As explained in section 3.2, for instrumental data, the predicted rate of exceedance for the acceleration threshold considered is directly read on the hazard curve. A Poisson distribution with mean equal to this rate of exceedance is built to predict the number of expected exceedances. The likelihood of the observation is then the Poisson distribution value for that number of exceedances. One can note that with instrumental data the number of exceedances is used in the analysis while for macroseismic intensity observation the conversion from PGA to intensity imposed the use of number of occurrences of intensities.

Figure 4.4 shows the median ESHM13 hazard curve (summed over all the sites) for the acceleration threshold 0.1 m/s². The 2 exceedances observed for the 0.1 m/s² threshold in France are plotted (red dot in Figure 4.4).The right-hand side of Figure 4.4 shows the Poisson distribution with mean equal to the rate of exceedance at 0.1 m/s² shown in the left-hand side of Figure 4.4. The +/- σ of the prediction is also indicated on both sides of Figure 4.4 (dashed black line).

Figure 4.4 shows that the ESHM13 model predicts much higher exceedances than observed at the 0.1 m/s² threshold.
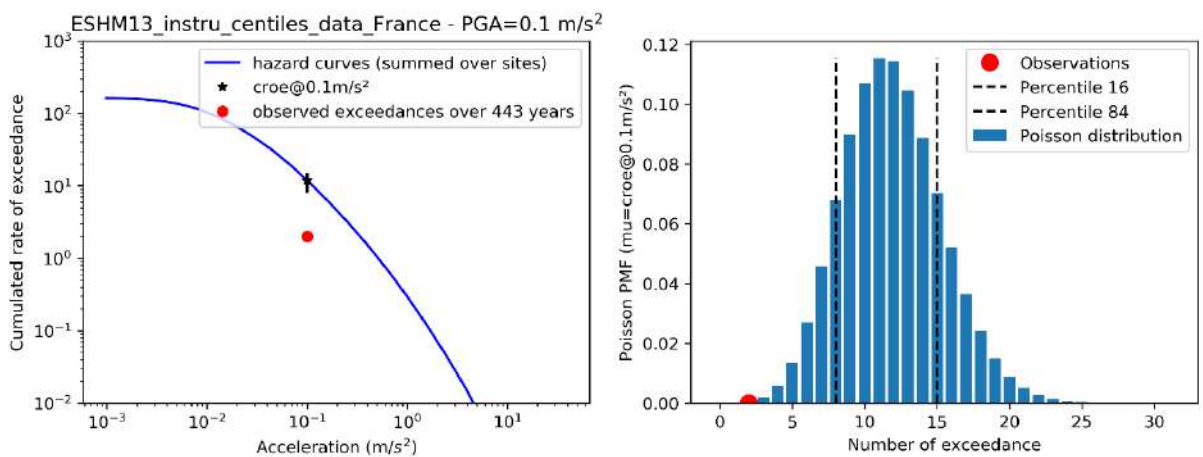
Figure 4.4: Observed exceedance rate for PGA 0.1 m/s² in France compared with the cumulated rates of exceedance for the 99 centiles computed with the ESM13 model (sum of the rates for all the 19 sites multiplied by individual observation periods).

The results in terms of likelihood are shown in Figure 4.5 and Figure 4.6 when all the hazard curves of the logic-tree or 99 fractiles are considered, respectively. The computed likelihoods are very low because while only 2 observations are collected, the model predicts several tens of observations.
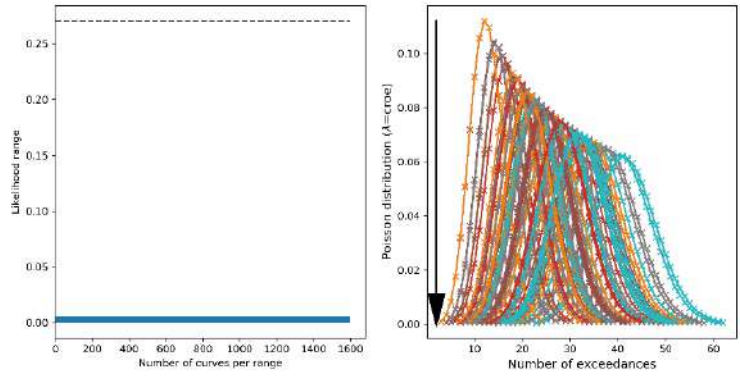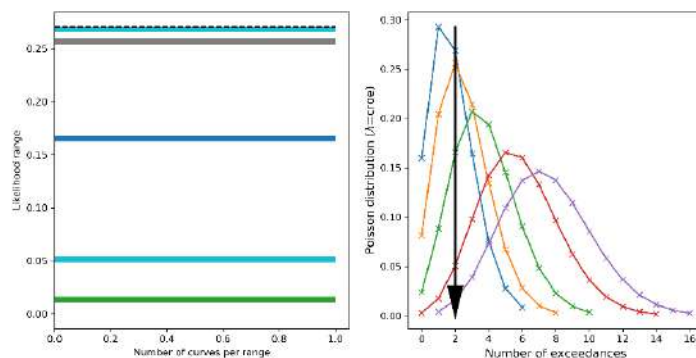
Figure 4.5: Left: Likelihood grouped by bins (coloured bars) and maximum theoretical likelihood (dashed line). Right: Poisson distributions generated from the cumulated rates of exceedance for the different branches of the logic-tree considered (coloured bars) and observed number of exceedances (black arrow). Results corresponding to the ESHM13 model (all branches) using data from France for the acceleration threshold 0.1 m/s^2.
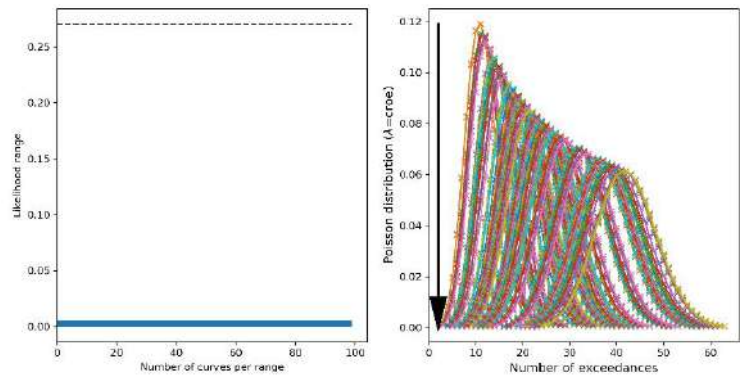
Figure 4.6: Left: Likelihood grouped by bins (coloured bars) and maximum theoretical likelihood (dashed line). Right: Poisson distributions generated from the cumulated rates of exceedance for the different branches of the logic-tree considered (coloured bars) and observed number of exceedances (black arrow). Results corresponding to the ESHM13 model (centiles) using data from France for the acceleration threshold 0.1 m/s^2.

Looking at higher acceleration threshold, even if the number of observations is zero, the likelihoods increase simply because at this level of acceleration the model predicts only a small number of exceedances (Figure 4.7).
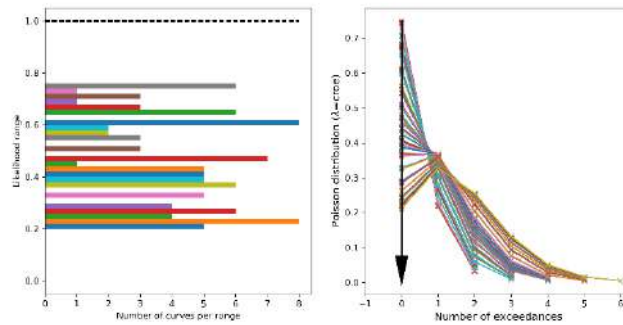
Figure 4.7: Left: Likelihood grouped by bins (coloured bars) and maximum theoretical likelihood (dashed line). Right: Poisson distributions generated from the cumulated rates of exceedance for the different branches of the logic-tree considered (coloured bars) and observed number of exceedances (black arrow). Results corresponding to the ESHM13 model (centiles) using data from France for the acceleration threshold 1.0 m/s².

The figures showing the likelihood resulting from the analysis at the other acceleration thresholds (0.2, 0.5 and 1.0 m/s²) are given in the Appendix B.

4.2 Testing with the ESHM20 model

In case of the ESHM20, only the hazard curves corresponding to the fractiles 5, 16, 50, 84 and 95 were provided. The results used are those provided by L. Danciu (pers. com.) in April 2021.

4.2.1 Historical data

Data and observations are first compared as was done previously. The individual sites hazard curves are cumulated taking into account the observation period at each site. Then the number of observations (see Table 2.21) are reported at the acceleration level resulting from the intensity-PGA model of Caprio et al. (2015). Figure 4.8 shows the comparison for intensity VI, VII and VIII with the median EASHM20 hazard curve (cumulated over all the sites).

Figure 4.8 suggests a relatively good agreement between observations and ESHM20 results. For intensities VI the model seems to predict rates slightly lower than observed ones while the opposite is observed for intensities VII and VIII. This result will be commented in section 6.
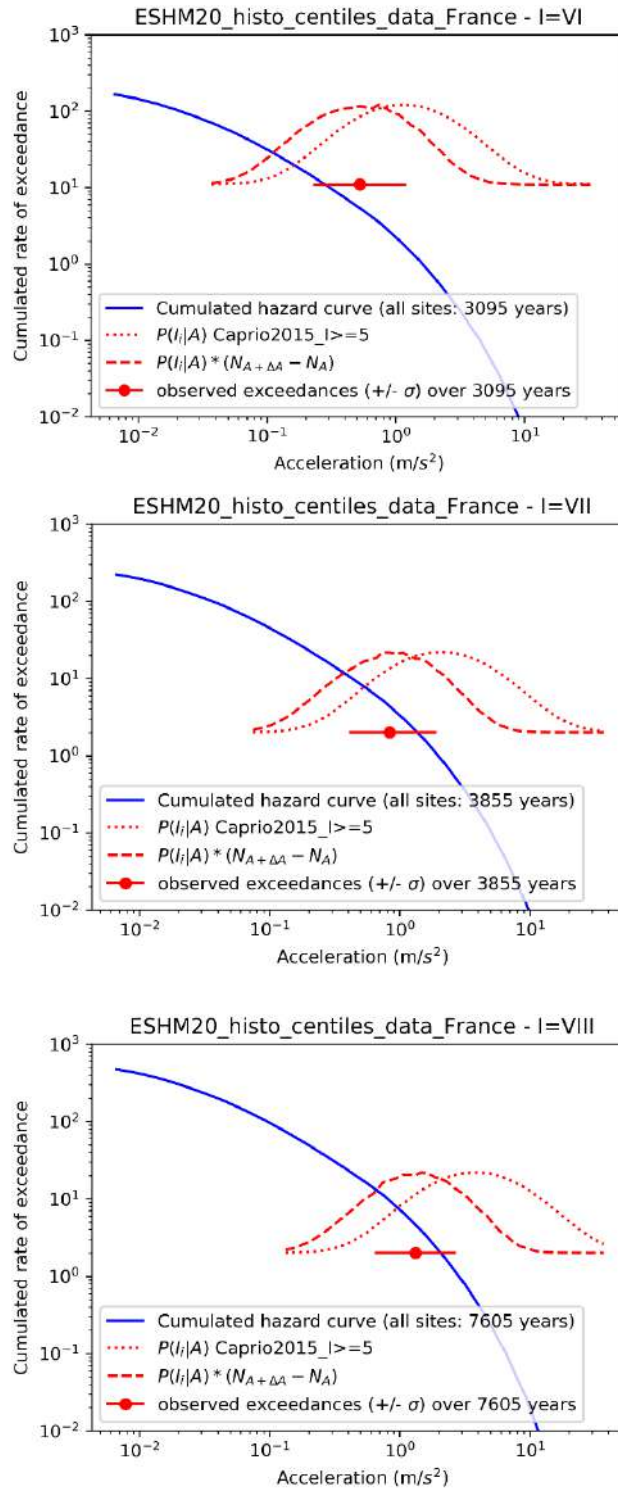
Figure 4.8: Sum over the sites of the median ESHM20 hazard curves taking into account completeness periods at each site (note that the curve differs for the different intensities due to varying completeness with intensity) for intensity VI (top), VII (middle) and VIII (bottom) for France. The probability of a given PGA producing an intensity VI, VII or VIII is also plotted on the figures based on Caprio et al. (2015) model (dotted red curves) as well as the same probability multiplied by the rate of occurrence of acceleration A: $(N_{A+\Delta A} - N_A).P_{I_i|A}$. From the $(N_{A+\Delta A} - N_A).P_{I_i|A}$ distribution a mean acceleration +/- σ is computed which is used to located the observed number of intensity exceedances (red dot and red line).

Figure 4.9 presents the likelihood results obtained for intensity VI. One can note that using the Caprio et al. (2015) and Wald et al. (1999) intensity-PGA models, the observations fall in the tail of the distribution corresponding to the 95 fractile (Figure 4.9 right plots). Using the Faenza & Michelini (2010) or the Gomez Capera (2020) intensity-PGA models, the ESHM20 95 fractile is compatible with observations.
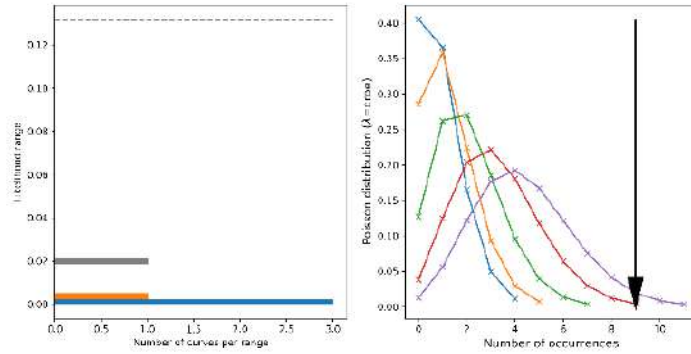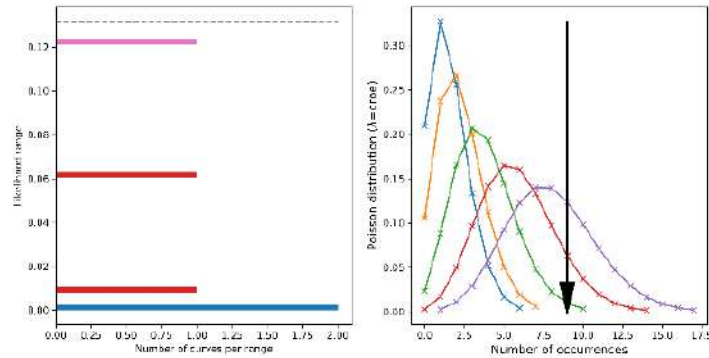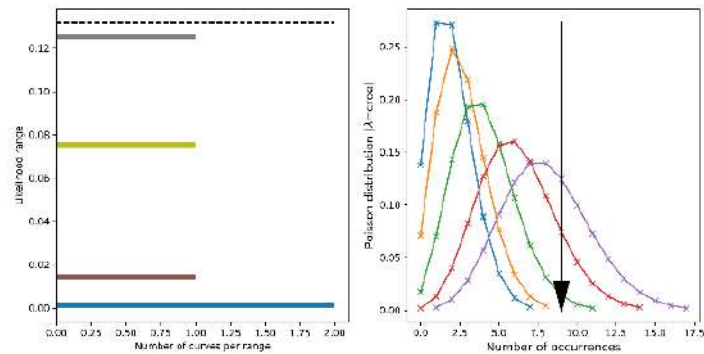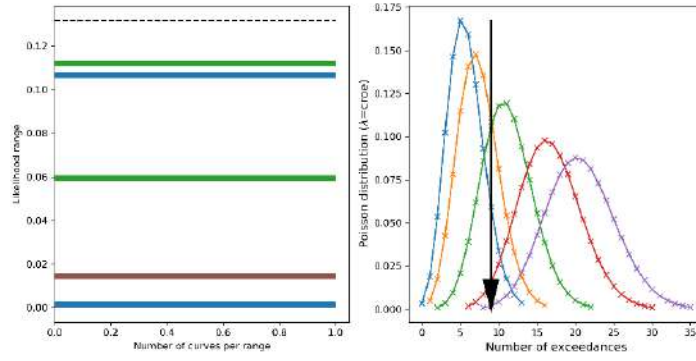
Figure 4.9: Left: Likelihood grouped by bins (coloured bars) and maximum theoretical likelihood (dashed line). Right: Poisson distributions generated from the cumulated rates of occurrences for the different branches of the logic-tree considered (coloured bars) and observed number of occurrences (black arrow). Results corresponding to the ESHM20 model (5 fractiles) for intensity VI using data from France and 4 different PGA-to-intensity relationships (from top to bottom).

Similar figures for intensities VII and VIII are included in the Appendix B.

4.2.2   Instrumental data

Figure 4.10 shows the median ESHM20 hazard curve (summed over all the sites) for the acceleration threshold 0.1 m/s². The 2 exceedances observed for the 0.1 m/s² threshold in France are plotted (red dot in Figure 4.10).The right-hand side of Figure 4.10 shows the Poisson distribution with mean equal to the rate of exceedance at 0.1 m/s² shown in the left-hand side of Figure 4.10. The +/- σ of the prediction is also indicated on both sides of Figure 4.10 (dashed black line).

Figure 4.10 shows that the ESHM20 seems consistent with the observations. Actually, the observations are slightly lower than the predictions but within the +/-1 σ interval.
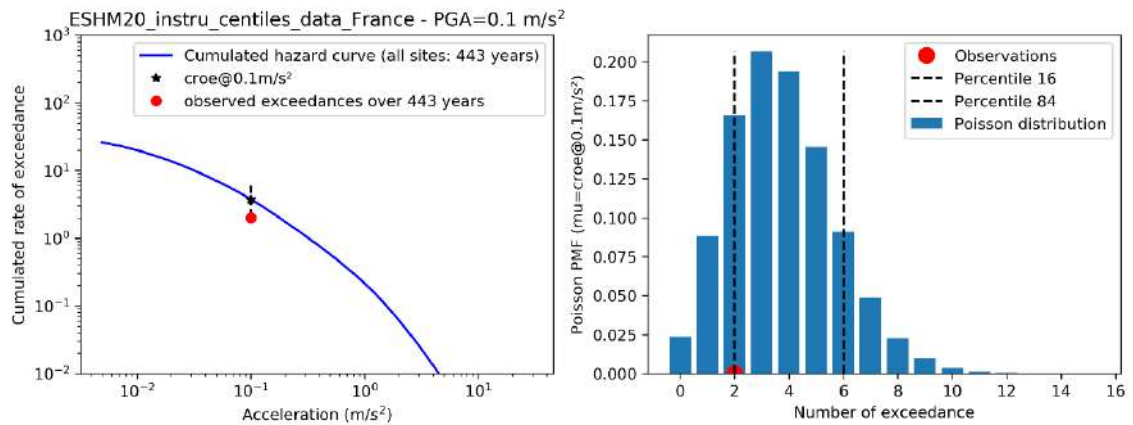
Figure 4.10: Observed exceedance rate for PGA 0.1 m/s² in France compared with the cumulated rates of exceedance for the 5 centiles computed with the ESM20 model (sum of the rates for all the 19 sites multiplied by individual observation periods).

Figure 4.11 shows the likelihoods obtained for the same acceleration threshold 0.1 m/s². The hazard curve corresponding to the 16th fractile is the more consistent with observations in that case. This result confirms the previous one indicating that the ESHM20 model is consistent with observations although a slight overestimation is possible.

Figure 4.11: Left: Likelihood grouped by bins (coloured bars) and maximum theoretical likelihood (dashed line). Right: Poisson distributions generated from the cumulated rates of exceedance for the different branches of the logic-tree considered (coloured bars) and observed number of exceedances (black arrow). Results corresponding to the ESHM20 model (5 centiles) using data from France for the acceleration threshold 0.1 m/s².

The figures showing the likelihood resulting from the analysis at the other acceleration thresholds (0.2, 0.5 and 1.0 m/s²) are given in the Appendix B.

5. Testing with data from Europe

The 28 sites located in Europe with macroseismic intensity observations are shown in Figure 2.23 together with the 39 sites with instrumental observations. The number of observations for both historical and instrumental data are given in Table 2.23 and Table 2.24, respectively.

5.1.1 Historical data

Data and observations are first compared as was done previously. The individual sites hazard curves are cumulated taking into account the observation period at each site. Then the number of observations (see Table 2.23) are reported at the acceleration level resulting from the intensity-PGA model of Caprio et al. (2015). Figure 5.1 shows the comparison for intensity VI, VII and VIII with the median EASHM20 hazard curve (cumulated over all the sites).

Figure 5.1 suggests a relatively good agreement between observations and ESHM20 results. For intensities VI and VII the model seems to predict rates very close to observed ones while for intensity VIII the model seems to lead to high predictions compared to observations. This result will be commented in section 6.

Figure 5.2 shows the likelihoods obtained for the intensity level VI. Again, the results depend on the intensity-PGA model used. At this intensity level, the Faenza & Michelini (2010) and Gomez Capera (2020) models lead to a better agreement between observations and ESHM20 model, while the Caprio et al. (2015) and Wald et al. (1999) models lead to ESHM20 model overpredicting observations.
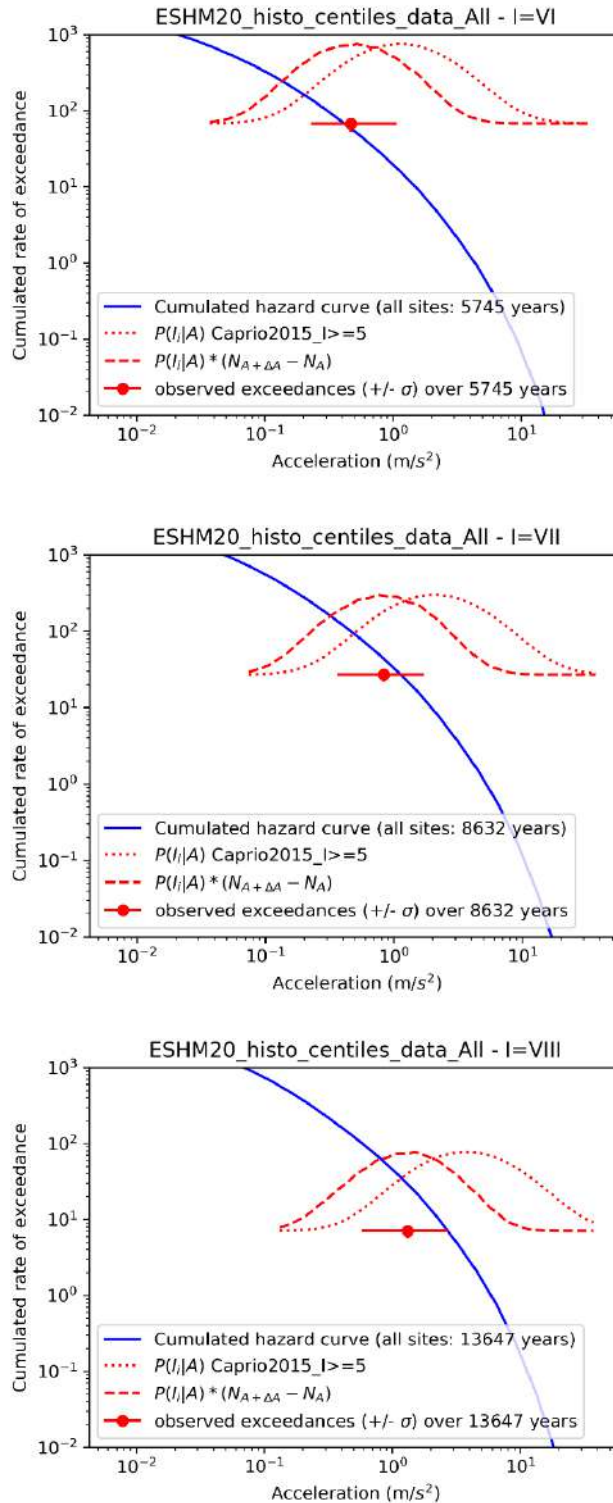
Figure 5.1: Sum over the sites of the median ESHM20 hazard curves taking into account completeness periods at each site (note that the curve differs for the different intensities due to varying completeness with intensity) for intensity VI (top), VII (middle) and VIII (bottom) for Europe. The probability of a given PGA producing an intensity VI, VII or VIII is also plotted on the figures based on Caprio et al. (2015) model (dotted red curves) as well as the same probability multiplied by the rate of occurrence of acceleration A: $(N_{A+\Delta A} - N_A).P_{I_i|A}$. From the $(N_{A+\Delta A} - N_A).P_{I_i|A}$ distribution a mean acceleration +/- σ is computed which is used to located the observed number of intensity exceedances (red dot and red line).
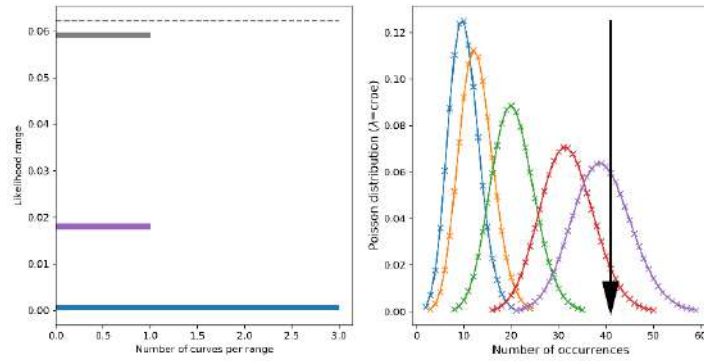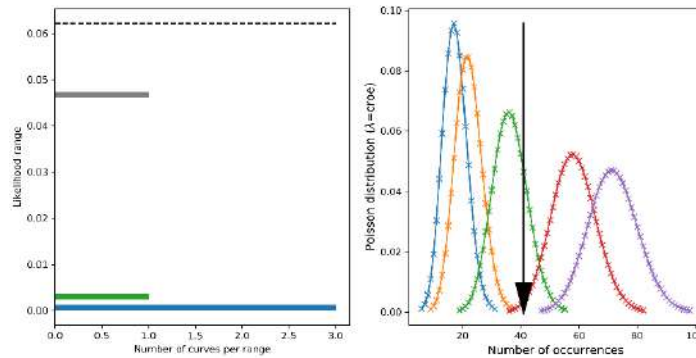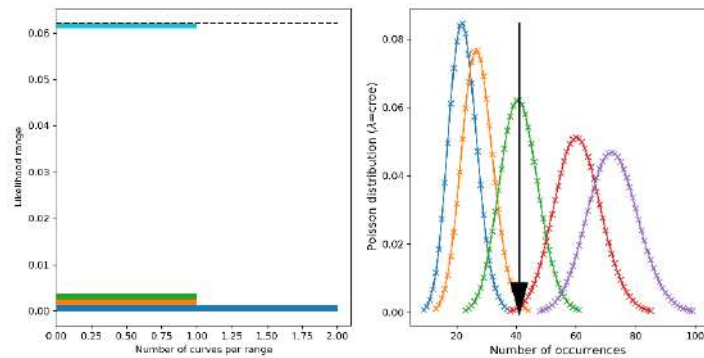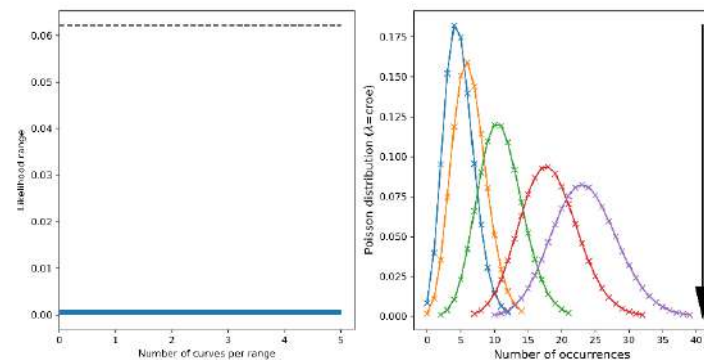
Figure 5.2: Left: Likelihood grouped by bins (coloured bars) and maximum theoretical likelihood (dashed line). Right: Poisson distributions generated from the cumulated rates of occurrences for the different branches of the logic-tree considered (coloured bars) and observed number of occurrences (black arrow). Results corresponding to the ESHM20 model (5 fractiles) for intensity VI using data from Europe and 4 different PGA-to-intensity relationships (from top to bottom).

Similar figures for intensities VII and VIII are included in the Appendix B.

FUGRO

5.1.2 Instrumental data

Figure 5.4 shows the median ESHM20 hazard curve (summed over all the sites) for the acceleration thresholds 0.1, 0.2 and 0.5 m/s². The corresponding number of observed exceedances (9, 2, and 1) for the three thresholds in Europe are plotted (red dot in Figure 5.4). The right-hand side of Figure 5.4 shows the Poisson distributions with mean equal to the rate of exceedance at 0.1, 0.2 and 0.5 m/s² shown in the left-hand side of Figure 5.4. The +/- σ of the prediction is also indicated on both sides of Figure 5.4 (dashed black line).

Figure 5.4 shows that the ESHM20 seems consistent with the observations. Actually, the observations are slightly lower than the predictions but within or close to the +/-1 σ interval.
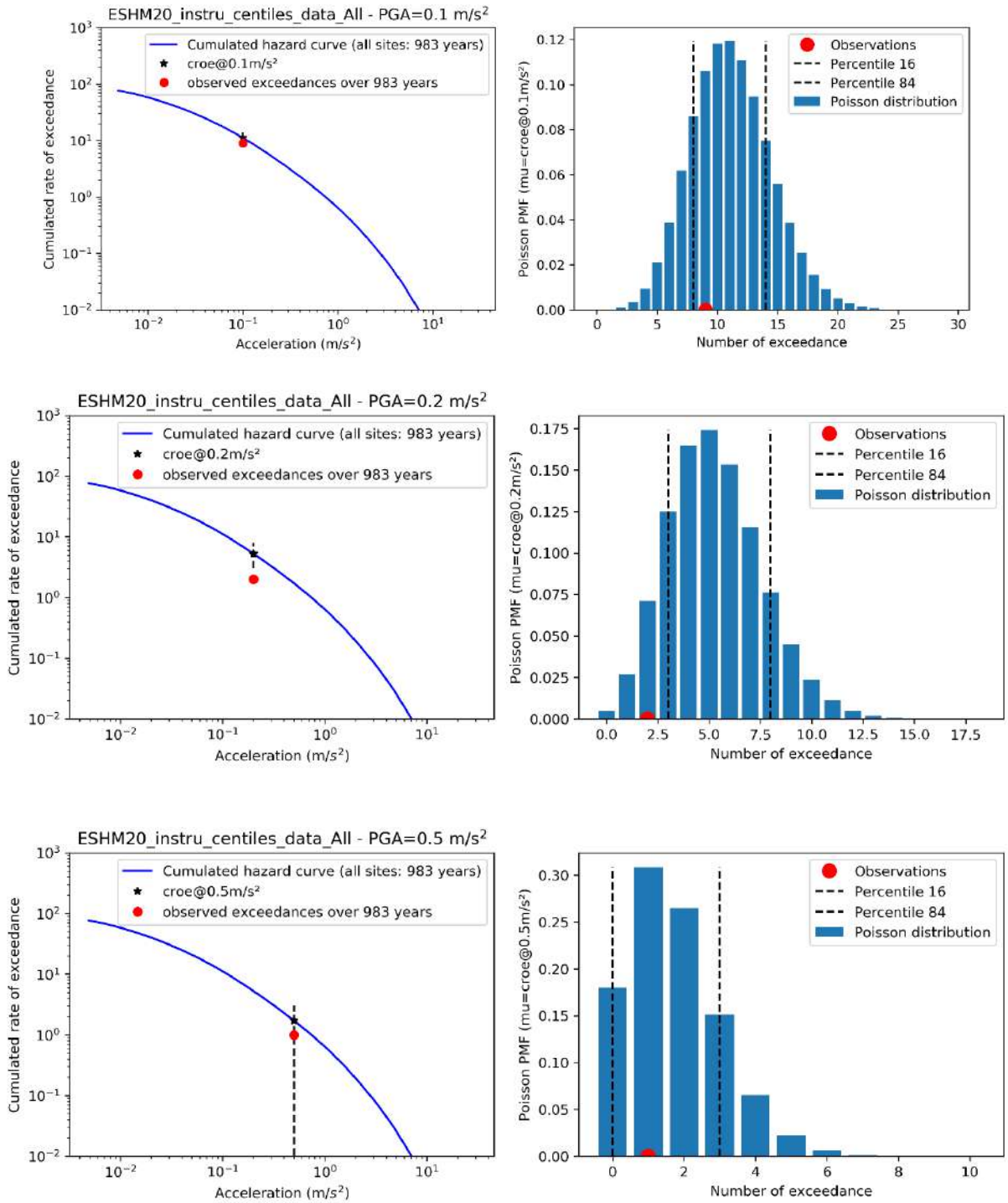
Figure 5.3: Observed exceedance rate for PGA 0.1 m/s² (top), 0.2 m/s² (middle) and 0.5 m/s² (bottom) in Europe compared with the cumulated rates of exceedance for the 5 centiles computed with the ESM20 model (sum of the rates for all the 39 sites multiplied by individual observation periods).

Figure 5.4 shows the likelihoods obtained for the 0.1 m/s² threshold and confirms that observations are compatible with predictions lying between centiles 14 and 50 of the ESHM20 model.

Similar figures for the other acceleration thresholds considered are given in the Appendix B

Figure 5.4: Left: Likelihood grouped by bins (coloured bars) and maximum theoretical likelihood (dashed line). Right: Poisson distributions generated from the cumulated rates of exceedance for the different branches of the logic-tree considered (coloured bars) and observed number of exceedances (black arrow). Results corresponding to the ESHM20 model (5 centiles) using data from Europe for the acceleration threshold 0.1 m/s^2.

6. Analysis of the evaluation results

Sections 4 and 5 described the calculation of the likelihoods of the different hazard curves considered given the observations (instrumental or macroseismic). Coming back to the Bayes theorem (see section 3.1) the term $\frac{P(B|A)}{P(B)}$ or the likelihood is now known.

The likelihood can then be used to update the weights of all the hazard curves. Comparing the original weights and updated ones allow us to evaluate how the distribution should be modified to achieve a better agreement with observed data.

When all the branches of the logic-tree are considered, the prior weights, $P(A)$ in the Bayes theorem are simply the weights of the hazard curves given in the logic-tree. When the hazard curves corresponding to the fractiles of the ground-motion distribution, the associated prior or "weights" are the values of the Gaussian probability mass function for the corresponding fractiles.

6.1 ESHM13

Figure 6.1 shows the effect of the evaluation on the original weights of 5 fractiles (5, 16, 50, 84 and 95) (i.e. Gaussian distribution). New weights are computed using results obtained with instrumental data and macroseismic data from France. We note that, in Figure 6.1, the addition of the weights of fractiles 5, 16, 50, 84 and 95 is not 1 because the ESHM13 model used contains 99 fractiles. For simplicity, the Figure 6.1 only shows the original and updated weights corresponding to 5 of the 99 fractiles used in the complete logic tree.

The analysis of the results shows that:

- *Instrumental data (*Figure 6.1 top)*:* These data are largely overpredicted by the ESHM13 model which would suggest a strong modification of the logic-tree giving a much higher weight to branches corresponding to low centiles (i.e. moving the distribution to lower values).
- *Macroseismic data (*Figure 6.1 bottom)*:* The same is true for macroseismic data when considering all the intensity levels (Figure 6.1 bottom). One can note however that results obtained with intensity VII largely contribute to the increase of the weights corresponding to the low centiles. This intensity level is characterized by no observed occurrences while the intensity level VIII includes 2 observations.
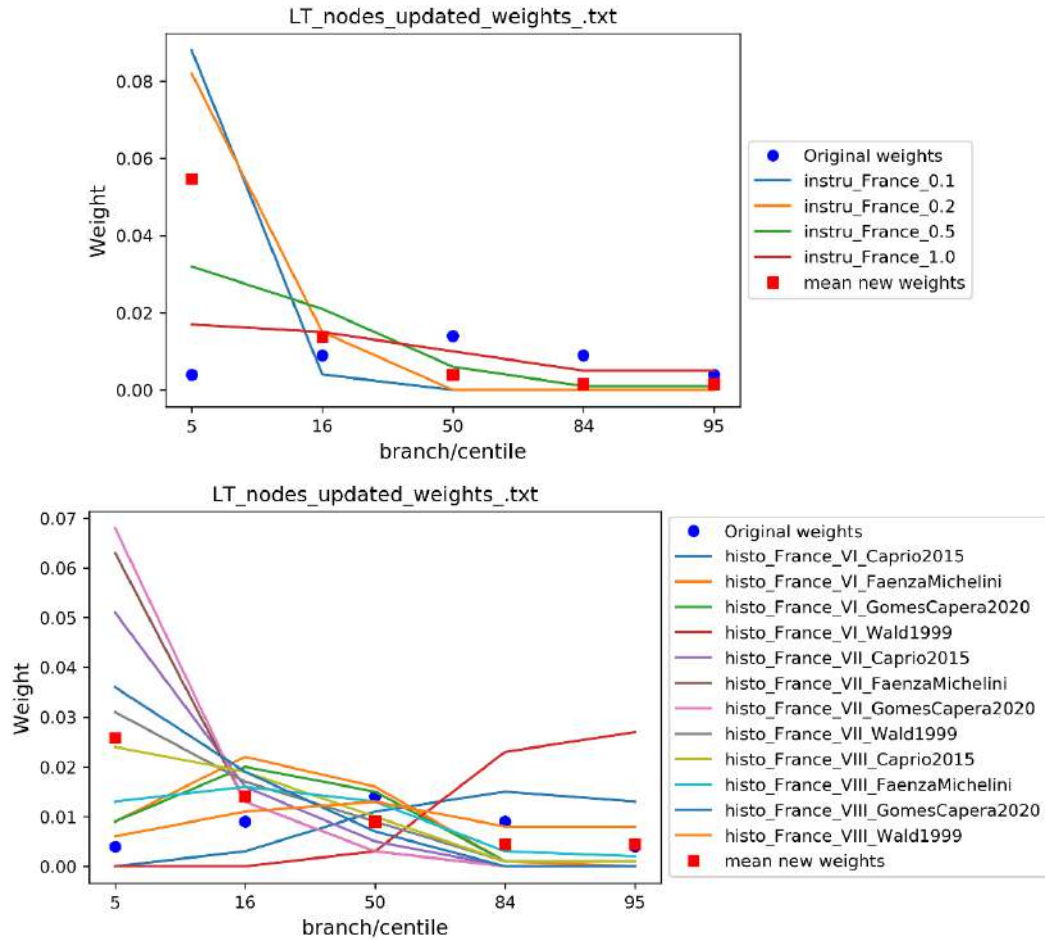
Figure 6.1: Effect of the evaluation of the ESHM13 model on the fractiles using instrumental data (top) and macroseismic data from France (bottom).

Using the hazard curves computed for all the branches of the logic-tree can help to identify how the weights of the different branches should be modified to make the model more compatible with observations. The main branches of the ESHM13 logic-tree are composed of:

- Source models:
    - b1: area source model (includes also Mmax uncertainty);
    - b2: faults and background model;
    - b3: smoothed seismicity model;
- GMPEs for active regions:
    - b1: Akkar & Bommer (2010);
    - b2: Cauzzi & Faccioli (2008);
    - b3: Chiou & Youngs (2008);
    - b4: Zhao et al. (2006) for active regions;
- GMPEs for stable regions (intermediate not Shield):
    - b21: Akkar & Bommer (2010);
    - b22: Cauzzi & Faccioli (2008);
    - b23: Chiou & Youngs (2008);

- b24: Toro (2002) adjusted for style-of-faulting and standard rock site conditions (v_{S30}=800 m/s);
- b25: Campbell (2003) adjusted for style-of-faulting and standard rock site conditions (v_{S30}=800 m/s);

The likelihood is used to update the weights of all the branches of the logic-tree. Grouping the different branches belonging to the same node with respect to source models or GMPEs for either active regions or global regions allows us to compute an updated weight for the different nodes. Figure 6.2 and Figure 6.3 present the original weights in the ESHM13 model, and the updated ones for each evaluation levels as well as the global updated weights combining all the evaluation levels for instrumental and macroseismic data, respectively.

The effect of the evaluation on the weights based on instrumental observation is very strong (Figure 6.2). This is because the ESHM13 predictions are much higher than observations and the update process puts as much weight as possible on the branches leading to the lowest predictions. This update is however not very relevant because even the lowest predictions are still much higher than observations. This means that a significant review of the underlying assumptions, models and corresponding weight should be performed.
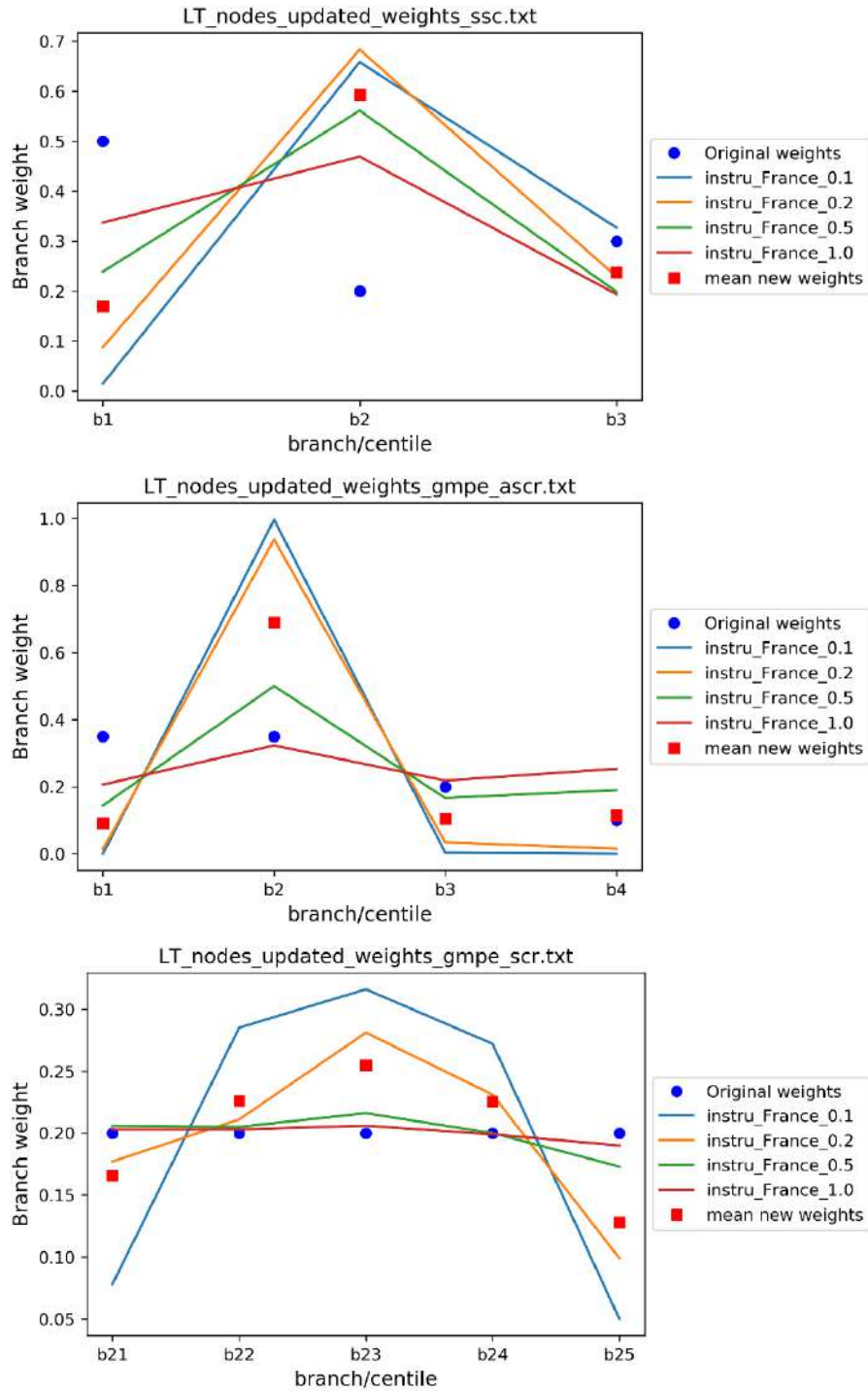
Figure 6.2: Effect of the evaluation of the ESHM13 model using instrumental data from France on the weights of the main logic-tree branches (top: source models weights; middle: GMPEs for active regions weights; bottom: GMPEs for stable regions weights).

Using macroseismic observations (Figure 6.3), the different evaluation cases (Intensity-to-PGA relationship, intensity level) lead to different sets of weights with quite strong contrasts with respect to the change of weight for the different branches.

The results suggest however large modifications of the weights for the source models with a decrease of the weight for the area source model (b1) and an increase of the weight for the

fault model (b2) and smoothed seismicity model (b3) although the increase is small in that case.

Regarding GMPEs for active regions, the evaluation suggests a decrease of the weights associated to the Akkar & Bommer (2010) and Chiou & Youngs (2008) models (b1 and b3) while increasing Cauzzi & Faccioli (2008) and Zhao et al. (2003)'s weights (b2 and b4).

For GMPEs for stable regions, the evaluation suggests a slight increase of the weights for the GMPEs of Akkar & Bommer (2010), Cauzzi & Faccioli (2008) and Chiou & Youngs (2008) (b21, b22 and b23) and a small decrease of the weights for Toro (2002) and Campbell (2003) GMPEs (b24 and b25).
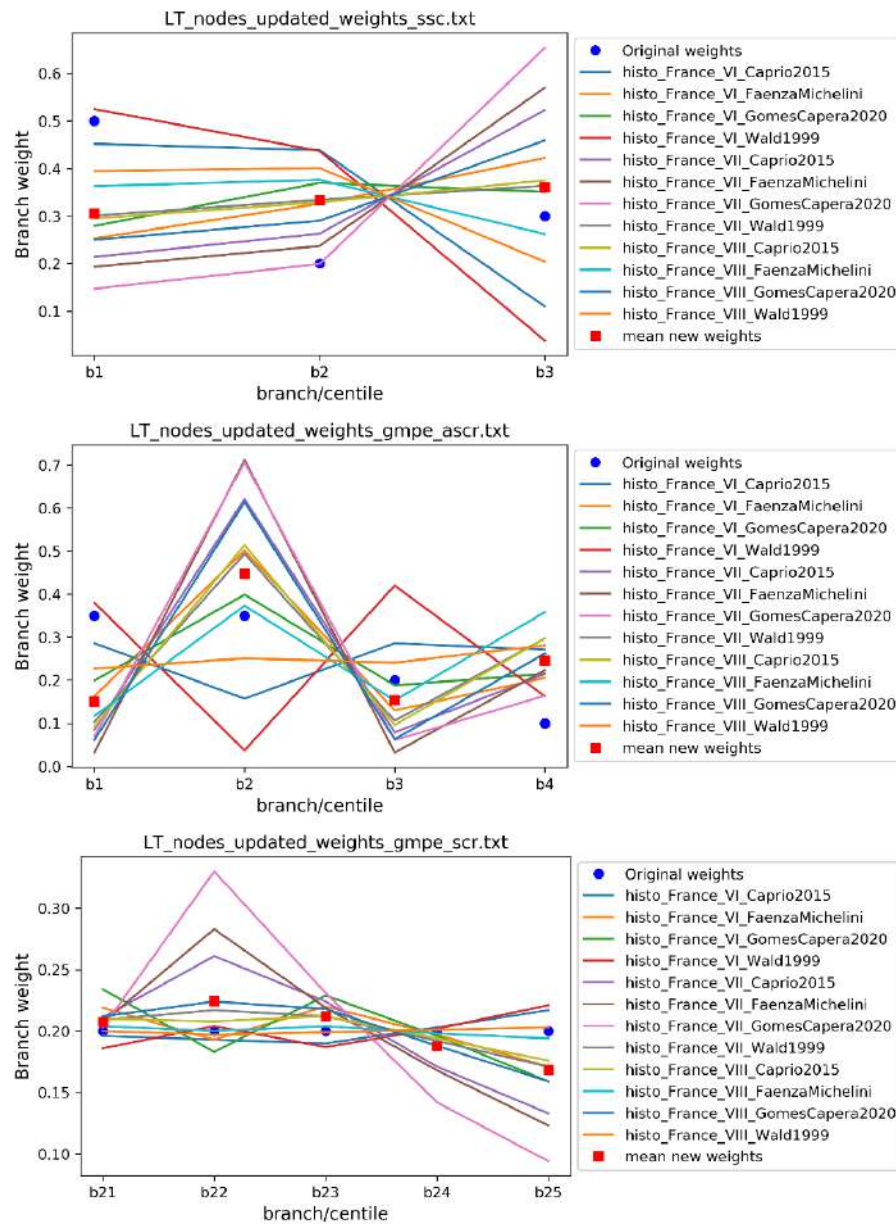
Figure 6.3: Effect of the evaluation of the ESHM13 model using macroseismic data from France on the weights of the main logic-tree branches (top: source models weights; middle: GMPEs for active regions weights; bottom: GMPEs for stable regions weights).

6.2   ESHM20

The same analysis as in the previous section for the hazard model fractiles is performed with the ESHM20 model using data for France and Europe.

The analysis of the results shows that:

- *France with instrumental data (*Figure 6.4, top)*:* The evaluation using instrumental data suggest that that the model overpredicts observations and the ground-motion distribution needs to be moved towards lower values by increasing weights of the lower centiles.
- *France with macroseismic data (*Figure 6.4, bottom)*:* French data suggest that the ESHM20 model could slightly underpredict the observations and weights of the upper centiles of the distribution would need to be increased to move the distributions to higher values. However, it seems that the results are not "balanced" and low intensity (VI) observation seems to be underestimated but high intensity (VII and VIII) observations seem to be overestimated (Figure 4.8 and Figure 6.4).
- *Europe with instrumental data (*Figure 6.5 top)*:* For Europe dataset, we observe the same than with the French dataset. The model seems to overpredict observations and the weights of the lower centiles would need to be increased to achieve a better agreement with the data.
- *Europe with macroseismic data (*Figure 6.5, bottom)*:* Using the whole set of sites for Europe suggests a balanced distribution and a good agreement between observations and the model. However, as per results obtained on French data, it seems that the results are not "balanced" and intensities VI and VII seem to be well estimated but high intensity (VIII) seems to be overestimated (Figure 5.1).
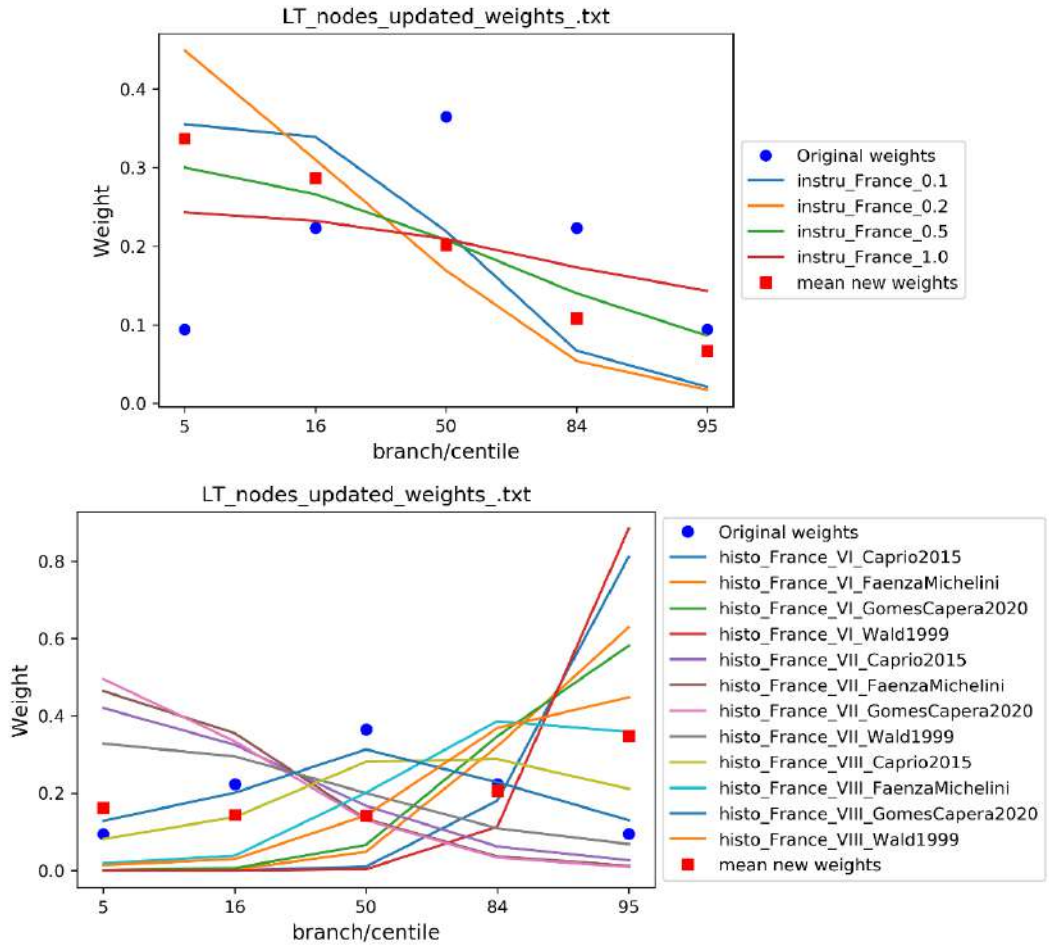
Figure 6.4: Effect of the evaluation of the ESHM20 model on the fractiles using instrumental data (top) and macroseismic data from France (bottom).
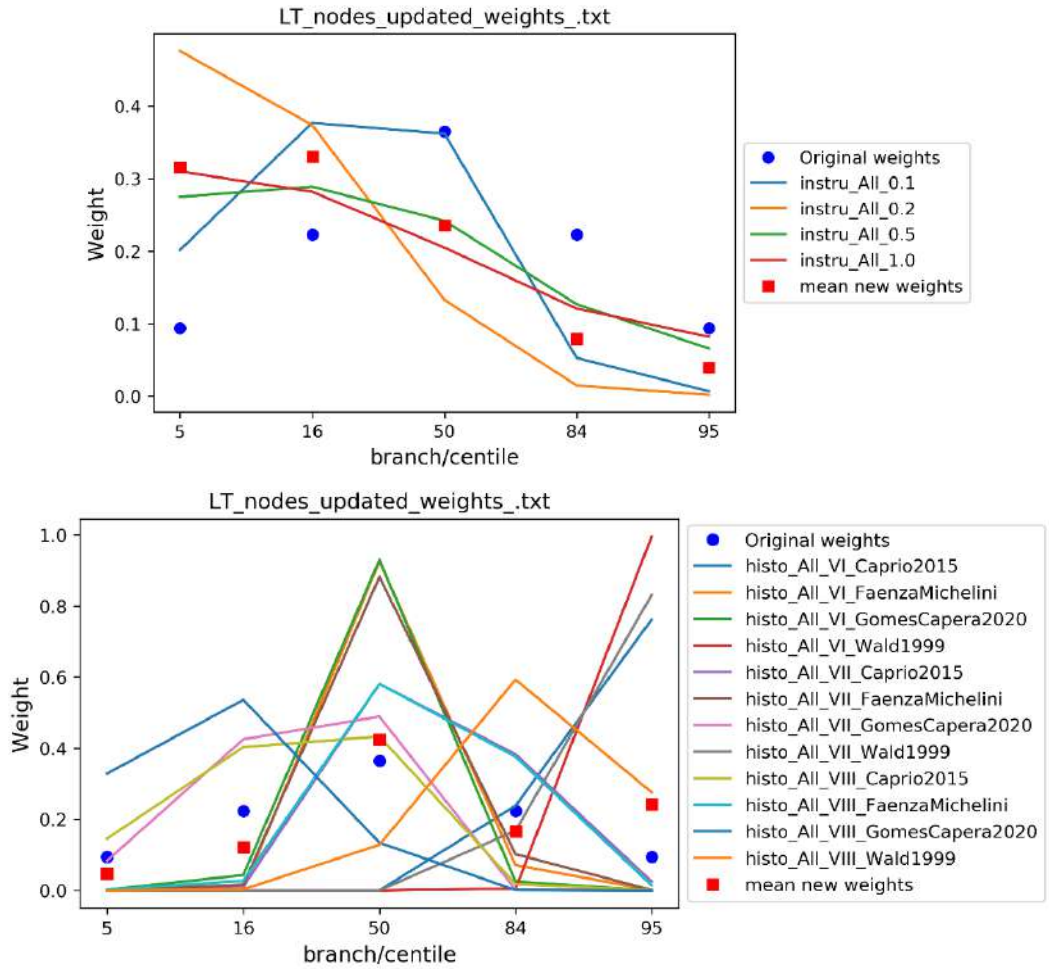
Figure 6.5: Effect of the evaluation of the ESHM20 model on the fractiles using instrumental data from Europe (top), macroseismic data from Europe (bottom).

7. Conclusions and perspectives

Two databases have been built in order to apply a testing procedure to PSHA model based on a Bayesian approach. Several sites with instrumental or macroseismic observations have been considered in Western Europe complemented by a couple of sites in more active regions (Italy, Greece, Turkey). Considering several sites is necessary in order to obtain a meaningful observation period. In order to avoid correlations between the different observations, a minimum inter-site distance of 200 km has been considered. For consistency with the PSHA calculations, only observations from events with magnitude above 4.5 (minimum magnitude used in the PSHA calculations) and located at distance lower than 200 km (consistent with the maximum integration distance used in the PSHA) are considered.

In addition to observations, i.e. exceedances of a given acceleration threshold or a given intensity level, the completeness period for the observations are also needed. Most of the information related to completeness is taken from the literature with exception of the completeness for Italian sites which have been computed by Pr. Albarello (pers. com.). For instrumental data the completeness is evaluated based on station metadata information downloaded from the FDSN webservices of RESIF, INGV and ETH.

The PSHA results from two versions of the European Seismic Hazard Model are considered: ESHM13 developed in the framework of the SHARE project, and ESHM20 being currently finalized in the framework of the SERA project. For the ESHM13 model, calculations have been performed at the sites of interest while for ESHM20, hazard curves have been provided by L. Danciu for points at a distance lower than 5 km from the points of interest.

The Viallet et al. (2019) Bayesian evaluation approach is applied. For instrumental data, the likelihoods of the various hazard curves are computed from Poisson distribution with mean equal to the cumulated rate of exceedance over all the sites (taking into account the completeness period). For macroseismic data a preliminary step is necessary to convert the hazard curve in acceleration into hazard curve in intensity. However, the likelihoods are then computed in a similar way considering the cumulated rate of occurrence of intensity.

The testing procedure is applied to a sub-set of data covering only France and to the complete set of data. Both ESHM13 and ESHM20 are tested. The results can be summarised as follows:

- Evaluation of the ESHM13 model with French data:
    - Based on macroseismic observations, the ESHM13 model seems to slightly over-estimate observations (see Figure 6.1) for intensities VII and VIII. For intensity VI, the model is relatively close to observations;
    - The evaluation based on macroseismic data is strongly dependent on the Intensity-to-PGA relationship. From the list of models compiled (see Table 3.1) we

selected a subset of 4 models representative of the uncertainty in the intensity-PGA conversion;

  o The evaluation at intensity VII also leads to different results compared to intensity VI and VIII due to the fact that no observations exist at I=VII, but this random occurrence process is taken into consideration in the evaluation;

  o Based on instrumental data (for 0.1 m/s² threshold), the ESHM13 seems to largely overestimate observations (overestimation of seismic hazard).

  o Since there are no observations for acceleration thresholds 0.2, 0.5, 1.0 m/s², the results of the Bayesian update must be used with caution, but predictions seem to slightly over-estimate observation because predictions lead to expect some occurrences;

- Evaluation of the ESHM20 model with French data:
  - Based on macroseismic observations, the ESHM20 model seems to slightly underpredict observations (underestimation of seismic hazard) (see Figure 6.4) but the agreement is better compared to that obtained with ESHM13;
  - The evaluation at intensity VII also leads to different results compared to intensity VI and VIII due to the fact that no observations exist at intensity VII, but this random occurrence process is taken into consideration in the evaluation;
  - The evaluation based on macroseismic data is again very dependent on the Intensity-to-PGA relationship;
  - Based on instrumental data, the ESHM20 seems to overpredict slightly observations (see Figure 6.4).

- Evaluation of the ESHM20 model with data from Europe:
  - Based on macroseismic observations, the ESHM20 model seems to be consistent with observations, for intensities VI and VII. For intensity VIII, the predictions of ESHM20 model overestimate the observations;
  - Based on instrumental data, the ESHM20 seems to overpredict slightly the observations but the agreement is rather good.

In addition to the previous analyses, some additional considerations are made in order to discuss the results and identify further development of this approach:

- In order to better evaluate PSHA results based the historical seismicity, site amplification at the macroseismic site may be improved. A single generic soil amplification factor has been used for all the sites;

- Further tests on the intensity-PGA relationships may also improve the results since these models have a strong impact on the results. A specific model for France may be developed, or a model selection and ranking based on the approach used for GMPEs (Scherbaum et al., 2009) can be used taking into account also potential discrepancies between the macroseismic intensity scales used in the models and for the data;

- The instrumental observations using the French database contains only few observations. To enlarge the number of observations and increase the confidence on the evaluation process, a larger set of observations would be needed. One way to increase the number

of observations would be to select all the seismic stations (a distance of 200 km between seismic stations was used as selection criteria in the present study). However, if close seismic stations are selected then the correlation between stations must be considered, it is possible in that case to use appropriate probability distributions (see Secanell et al, 2017). Increasing the number of data is also possible by relaxing the constraint on the site conditions imposed in the present study (rock sites) but would imply hazard calculation including the site condition for the sites of interest or application of site terms to convert hazard curves from rock to soft soil conditions.

- In addition to the previous point, it has to be pointed out that historical seismicity is based on observed damages, which can be sensitive to sites effects in the sense that number of observations can be increased in some cases because of high site amplification (which is rarely considered). This means that efforts should be made to improve the knowledge of historical seismicity (which is also part of input data for PSHA) in order to reduce uncertainties and improve confidence is PSHA analyses, and in the evaluation process based on observations;

- Also, to better evaluate PSHA results based on instrumental seismicity, the process should take into consideration the so-called SSI (soil-Structure Interaction) effect that could be of interest depending on the implementation of the accelerometric sensor (especially in the case of NPP sites). Of course, this could be neglected in case of light stations installed on rock, but could be of significance in other cases, as highlighted in OECD/NEA/CSNI workshop, 2015. This could lead to decrease the expected number of observations (in case of attenuation of ground motion due to SSI effects) and then could reduce the gap observed between predictions and observed instrumental seismicity;

- The testing process should be performed based on the results from the whole logic tree of the PSHA study (not only centiles) in order to provide PSHA actors with useful feedback in order to let them adjust weight of the whole logic tree (even reconsider some branches), as performed for ESHM13 in section 4.1. This was not done for ESHM20 due to time delay and organizational issues, but this could be tested in a future stage. If necessary, a subset of the whole logic tree representative of the PSHA calculation uncertainties could be used if the logic-tree includes too many branches.

- The evaluation process used in the present study considers independently instrumental and macroseismic data. One other way to improve the testing procedure would be to find an approach allowing to combine the datasets. In the present study, the results from both sources of data are combined a posteriori;

- The results obtained in this study have also to be crosschecked with the risk testing results obtained through a parallel study in order to identify common conclusions and axes of improvement either related to the evaluation of PSHA approach or dedicated to the actors of ESHM20.

Finally, it is expected to share the tools that were developed in the framework of this study with the largest scientific community in order to disseminate good practices, consolidate and develop its scientific background and finally improve confidence in seismic hazard assessment and seismic risk evaluations.

8. References

ATKINSON, G., S. KAKA (2007). Relationships between Felt Intensity and Instrumental Ground Motion in the Central United States and California. Bulletin of the Seismological Society of America, Vol. 97, No. 2, pp. 497–510, April 2007, doi: 10.1785/0120060154

ALBARELLO, D., R. CAMASSI and A. REBEZ (2001): Detection of space and time heterogeneity in the completeness level of a seismic catalogue by a «robust» statistical approach: an application to the Italian area, Bull. Seismol. Soc. Am., 91 (6) 1694-1703.

Bilal M, Askan A (2014) Relationships between felt intensity and recorded ground-motion parameters for Turkey. Bull Seismol Soc Am 104(1):484–496. https ://doi.org/10.1785/01201 30093

Caprio M, Tarigan B, Worden CB, Wiemer S, Wald DJ (2015) Ground motion to intensity conversion equations (GMICEs): a global relationships and evaluation of regional dependency. Bull Seismol Soc Am 105(3):1476–1490. https ://doi.org/10.1785/01201 40286

ECOS-02, Swiss Seismological Service (2002): ECOS - Earthquake Catalog of Switzerland. ECOS Report to PEGASOS, Version 31. 3. 2002. SED: Zürich.

Eurocode 8 (2004). Design of structures for earthquake resistance - Part 1: General rules, seismic actions and rules for buildings. Document EN 1998-1.

Faenza, L and A. Michelini (2010). Regression analysis of MCS intensity and ground mo-tion parameters in Italy and its application in ShakeMap. March 2010Geophysical Journal International 180(3):1138 – 1152. DOI: 10.1111/j.1365-246X.2009.04467.

Gomez Capera AA, Locati M, Fiorini E, Bazzurro P, Luzi L, Massa M, Puglia R, Santulin M (2015) D3.1 Macroseismic and ground motion: site specific conversion rules. DPC-INGV-S2 Project 2015, Deliverable 3.1, https ://sites .googl e.com/site/ingvd pc201 4prog ettos 2/deliv erabl es/. Accessed Dec 2019

Gomez Capera AA, Santulin M, D'Amico M, D'Amico V, Locati M, Luzi L, Massa M, Puglia R (2018) Macroseismic intensity to ground motion empirical relationships for Italy. Proceedings, 37° Convegno Nazionale GNGTS, Bologna (Italy) 19–21 Nov 2018, pp 289–291 http://www3.ogs.tries te.it/gngts /files /2018/S21/Riass unti/Gomez .pdf

Gomez-Capera AA, D'Amico M., Lanzano G., Locati M. and Santulin M. (2020). Relationships between ground motion parameters and macroseismic intensity for Italy. Bulletin of Earthquake Engineering (2020) 18:5143–5164, https://doi.org/10.1007/s10518-020-00905-0

Marin, S., Avouac, J.P., Nicolas, M., Schlupp, A., 2004. A probabilistic approach to seismic hazard in metropolitan France. BSSA 94(6), 2137–2163.

Masi A, Chiauzzi L, Nicodemo G, Manfredi V (2020) Correlations between macroseismic intensity estimations and ground motion measures of seismic events. Bull Earthq Eng. https ://doi.org/10.1007/s10518-019-00782 -2

OECD/NEA/CSNI/R(2019)1, "Comparison of PSHA in areas with different level of seismic activity", OECD/NEA Report, https://www.oecd-nea.org/jcms/pl_19896/comparison-of-psha-in-areas-with-different-level-of-seismic-activity?details=true

OECD/NEA/CSNI/WGIAGE (2019), "Activity of the OECD/NEA/CSNI/WGIAGE Seismic Engineering sub-Group in the Field of Seismic Hazard and Seismic Behaviour of Civil Structures and Mechanical Equipment: Findings, Recommendations and Perspectives", SMiRT-25, Charlotte, NC, USA, August 4-9, 2019

OECD/NEA/CSNI/R(2015)15, "Workshop on Testing Probabilistic Seismic Hazard Analysis Results and the Benefits of Bayesian Techniques", Workshop proceedings, Pavia, Italy 4-6 February 2015. https://www.oecd-nea.org/nsd/docs/2015/csni-r2015-15.pdf

Secanell, R., Martin, C., Viallet, E., Senfaute, G., 2017. A Bayesian methodology to updatethe probabilistic seismic hazard assessment. Bull. Earthq. Eng doi: 10.1007/s10518- 017-0137-3

Tasan H., Beauval C., Helmstetter A., Sandikkaya A., and Guéguen P. (2014). Testing probabilistic seismic hazard estimates against accelerometric data in two countries: France and Turkey. Geophysical Journal International, Volume 198, Issue 3, September, 2014, Pages 1554–1571, https://doi.org/10.1093/gji/ggu191

Tselentis G, Danciu L (2008) Empirical relationships between modified Mercalli intensity and engineering ground-motion parameters in Greece. Bull Seismol Soc Am 98(4):1863–1875. https ://doi.org/10.1785/01200 70172

Viallet et al. (2019): "Updating a probabilistic seismic hazard assessment with instrumental and historical observations based on a Bayesian inference", Nuclear Engineering and Design 350 (2019) 98–106

Wald DJ, Quitoriano V, Heaton TH, Kanamori H (1999) Relations between peak ground acceleration, peak ground velocity, and modified Mercalli intensity in California. Earthq Spectra 15(3):557–564. https ://doi.org/10.1193/1.15860 58

Zanini MA, Hofer L, Faleschini F (2019) Reversible ground motion-to-intensity conversion equations based on the EMS-98 scale. Eng Struct 180:310–320. https ://doi.org/10.1016/j.engst ruct.2018.11.032

Appendix A

Data compilation

Maps of observed intensities and figures of the distribution of observations over time are presented for each selected site with macroseismic observations.

The maps show the epicenters of the events felt in the cities:

- With observed intensity in the city lower than VI (grey dots);
- With observed intensity in the city VI or higher (coloured dots);
- In addition, for events with felt intensity in the city VI or higher and which are within the completeness period, labels indicate the magnitude (Mw), year of occurrence (Y) and intensity observed in the city (IOBS).

Plots of observed intensities over time are also shown. The years of completeness for intensity levels V, VI, VII and VIII are also indicated on the figures.

A.1   France

A.1.1   Brest
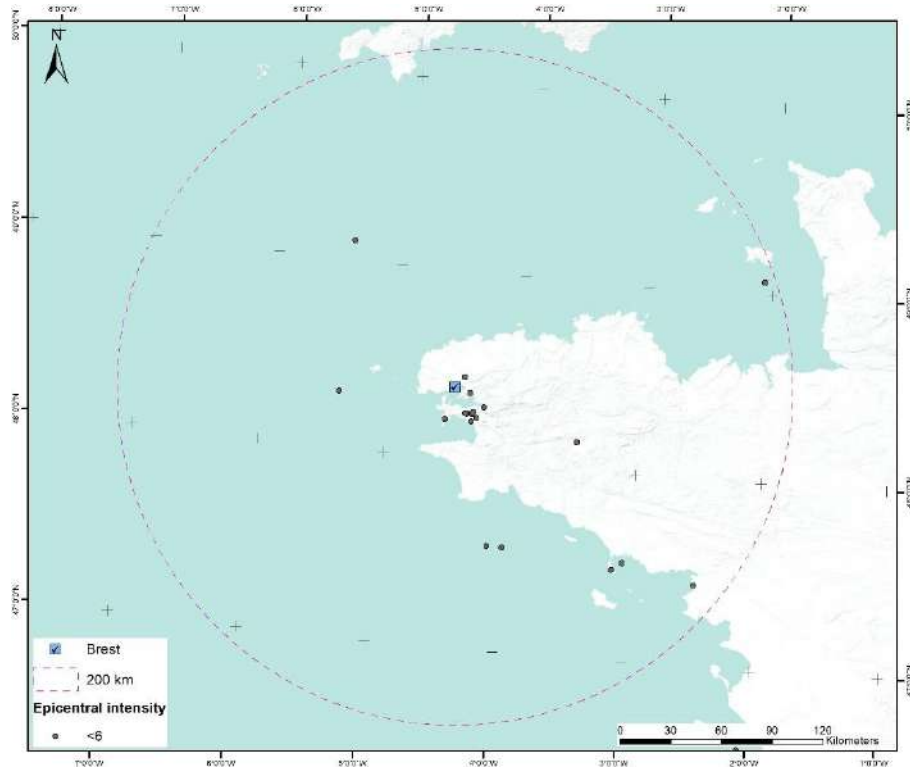
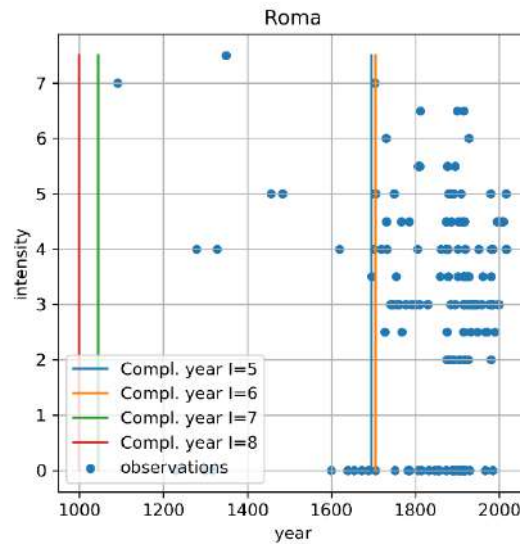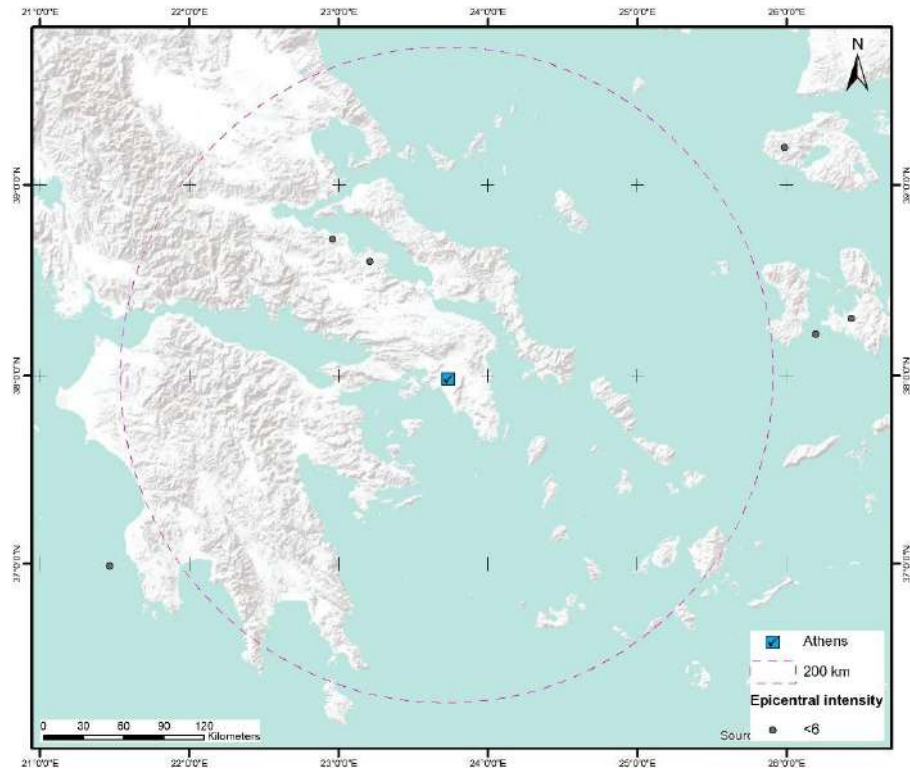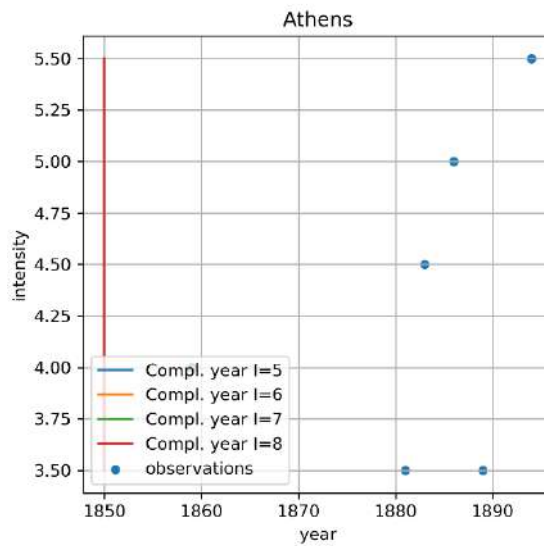
Figure A.1: Map of observed intensities for Brest.
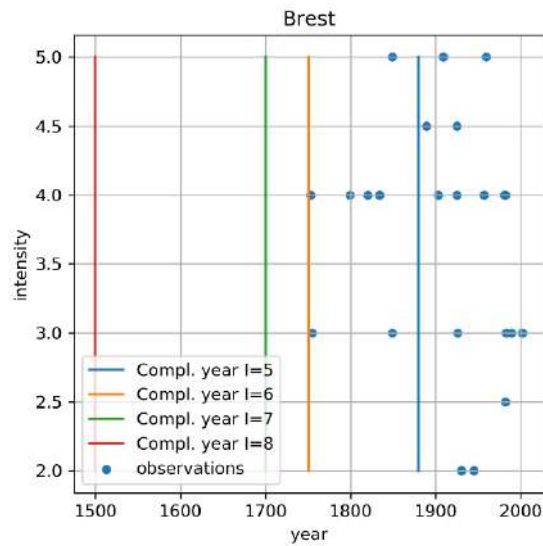
Figure A.2: Observed intensities versus time (blue dots) for Brest. Completeness years for intensities V, VI, VII and VIII are also plotted (coloured lines).
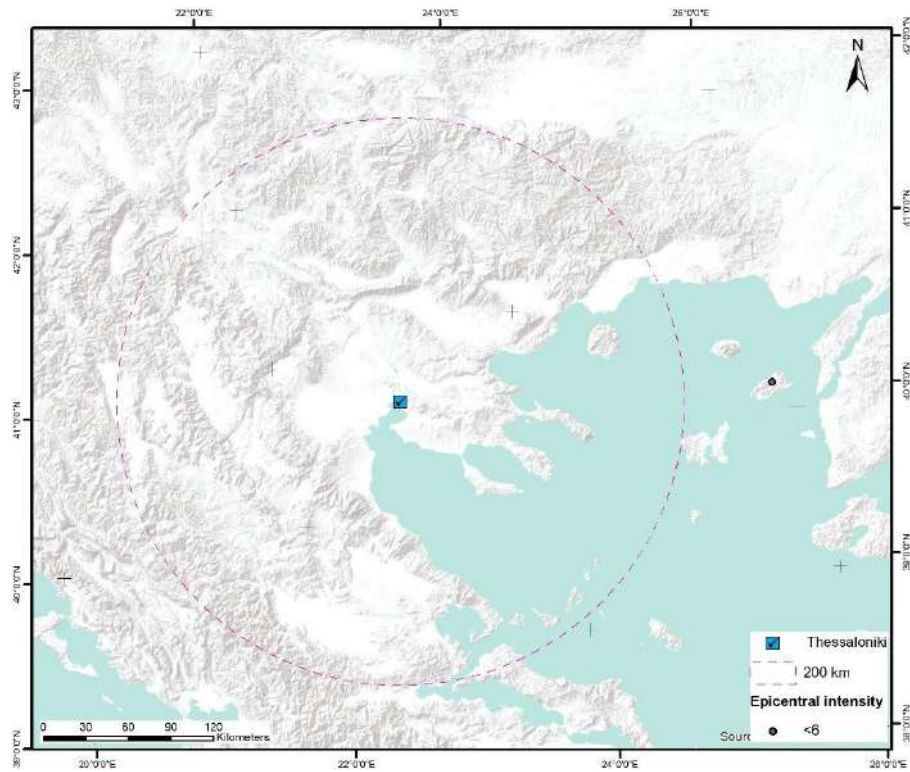
A.1.2 Cherbourg
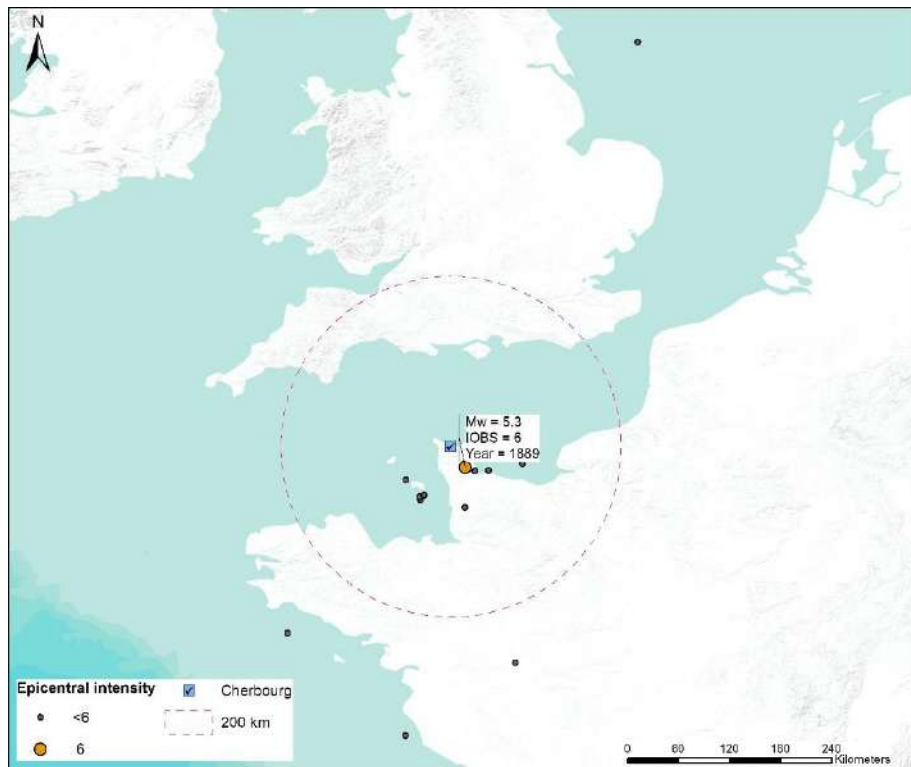
Figure A.3: Map of observed intensities for Cherbourg.
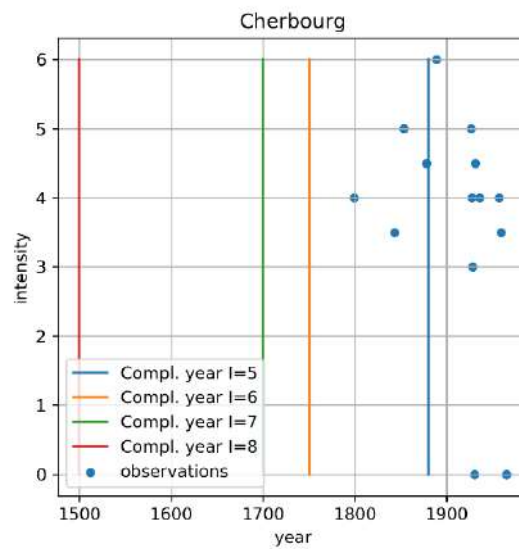
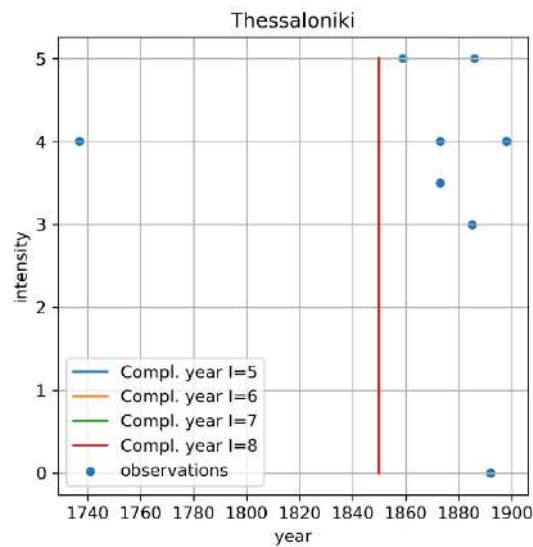Figure A.4: Observed intensities versus time (blue dots) for Cherbourg. Completeness years for intensities V, VI, VII and VIII are also plotted (coloured lines).

A.1.3   Clermont-Ferrand
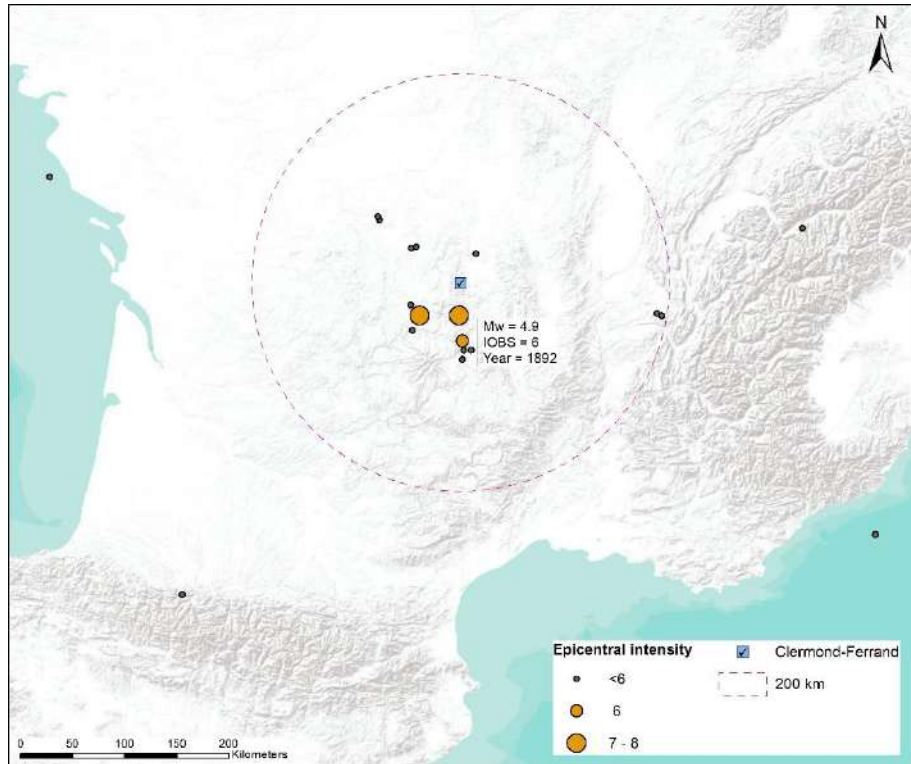
Figure A.5: Map of observed intensities for Clermont-Ferrand.
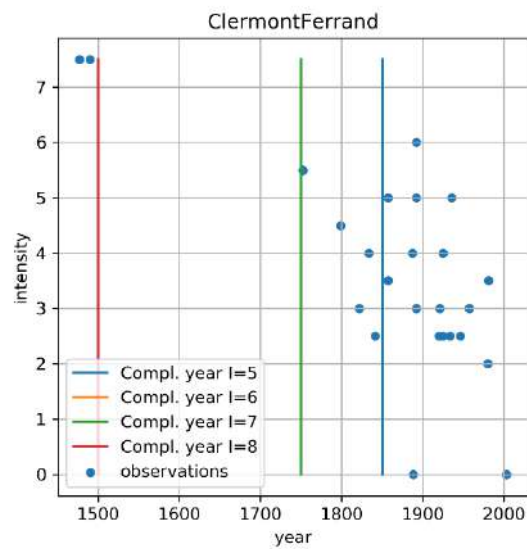
Figure A.6: Observed intensities versus time (blue dots) for Clermont-Ferrand. Completeness years for intensities V, VI, VII and VIII are also plotted (coloured lines).
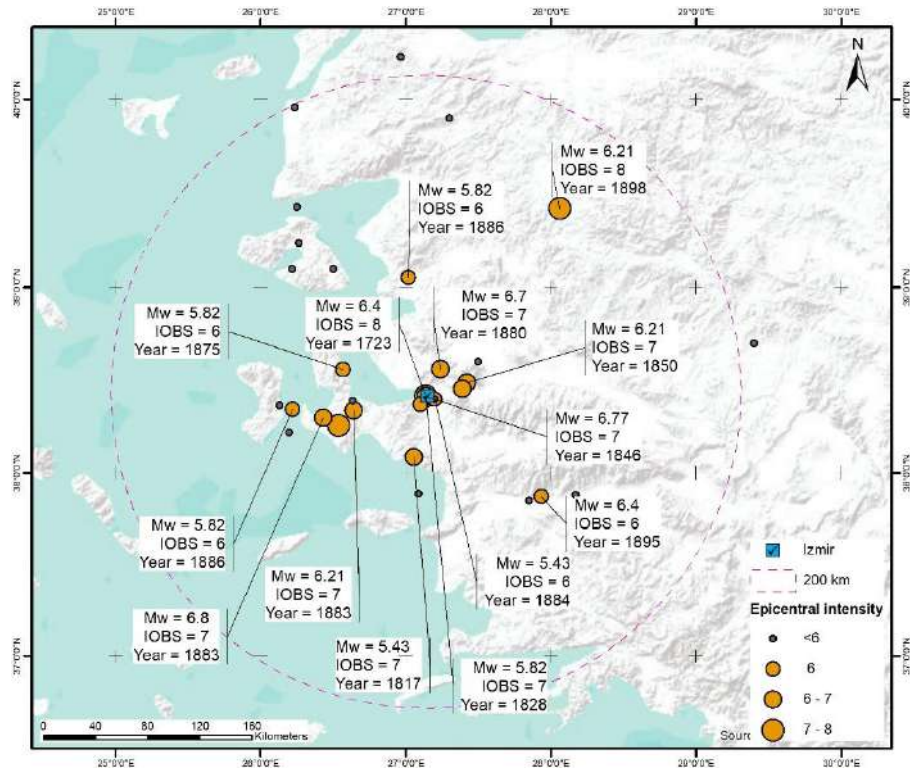
A.1.4   Grenoble
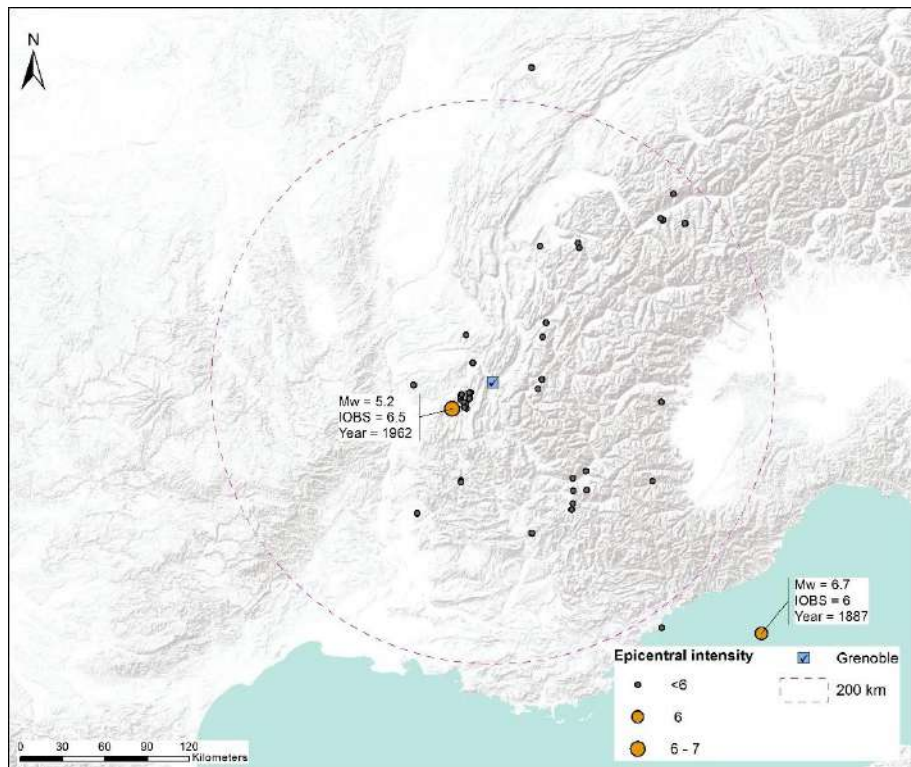
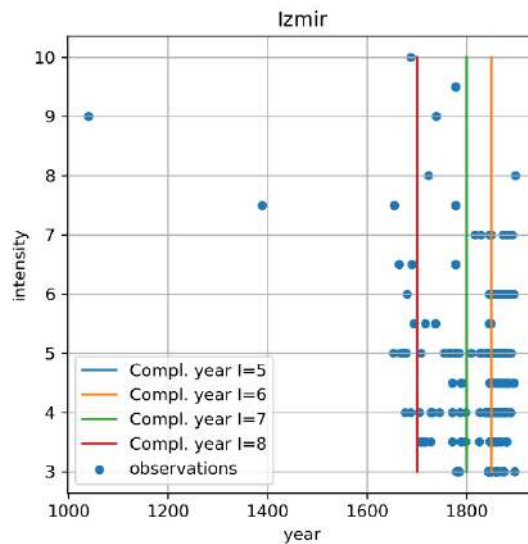Figure A.7: Map of observed intensities for for Grenoble.
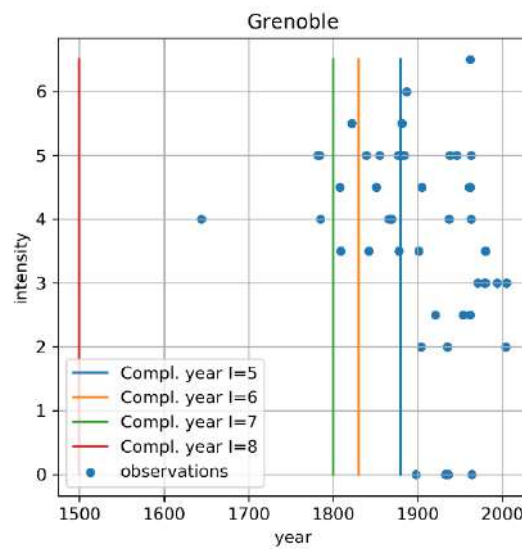
Figure A.8: Observed intensities versus time (blue dots) for Grenoble. Completeness years for intensities V, VI, VII and VIII are also plotted (coloured lines).
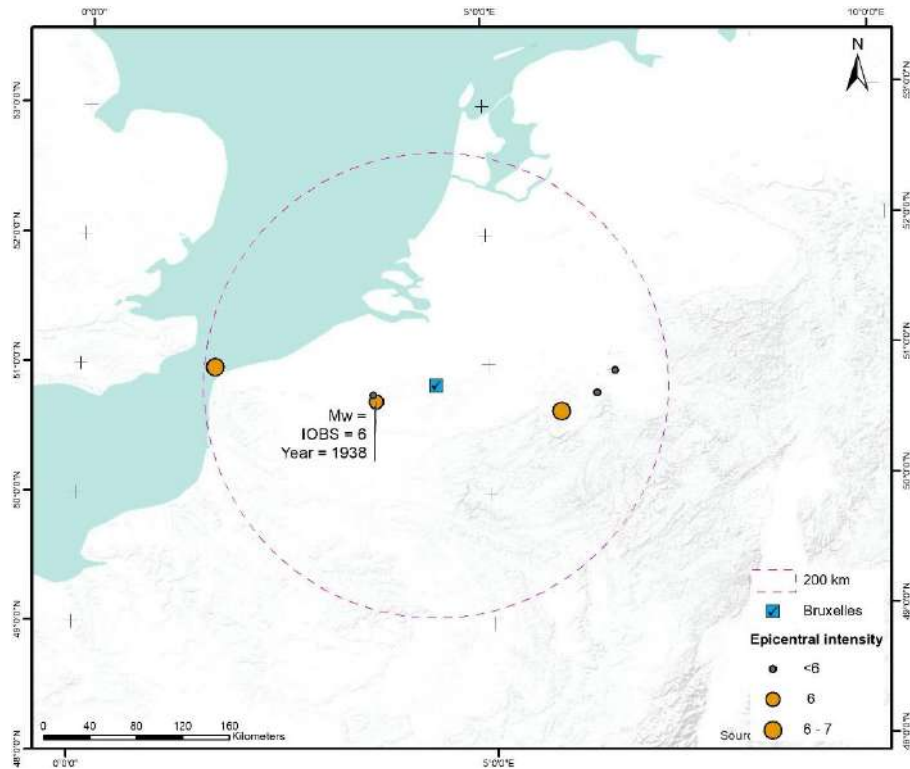
A.1.5 La Rochelle
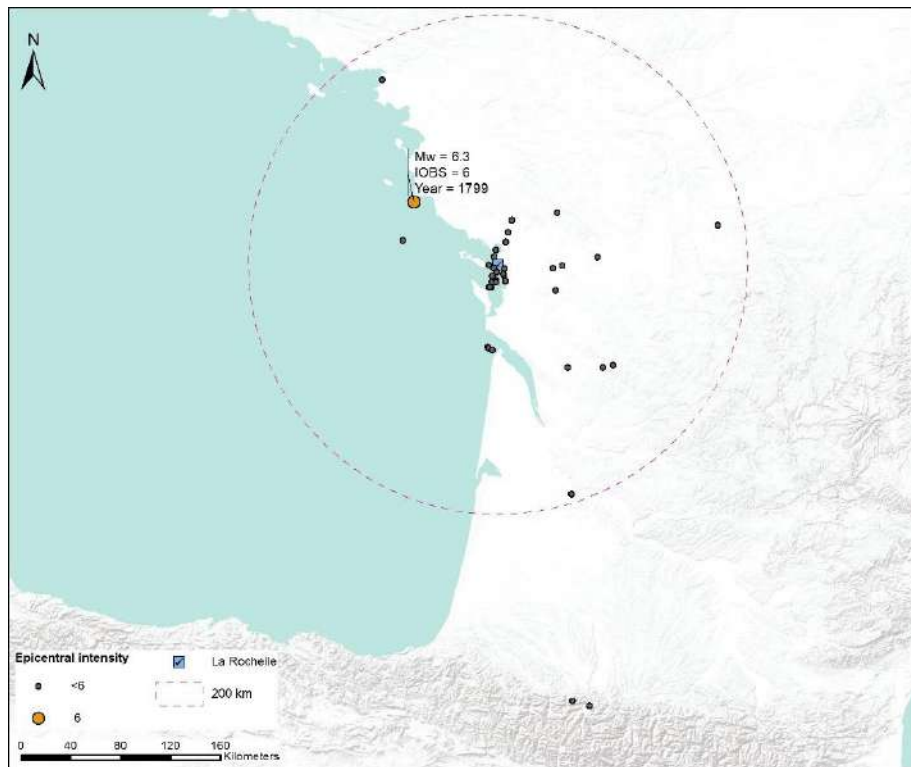
Figure A.9: Map of observed intensities for La Rochelle.
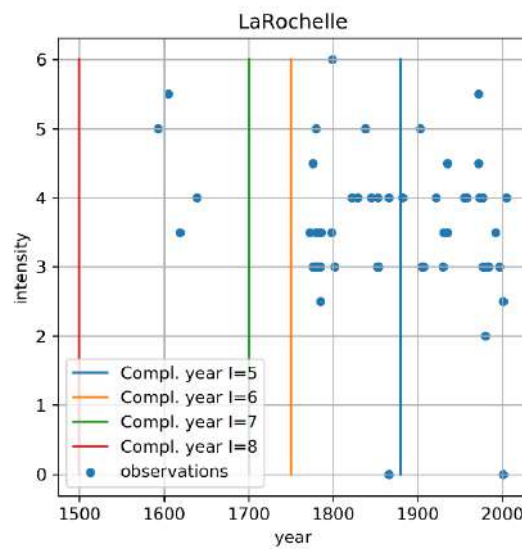
Figure A.10: Observed intensities versus time (blue dots) for La Rochelle. Completeness years for intensities V, VI, VII and VIII are also plotted (coloured lines).

A.1.6 Lille
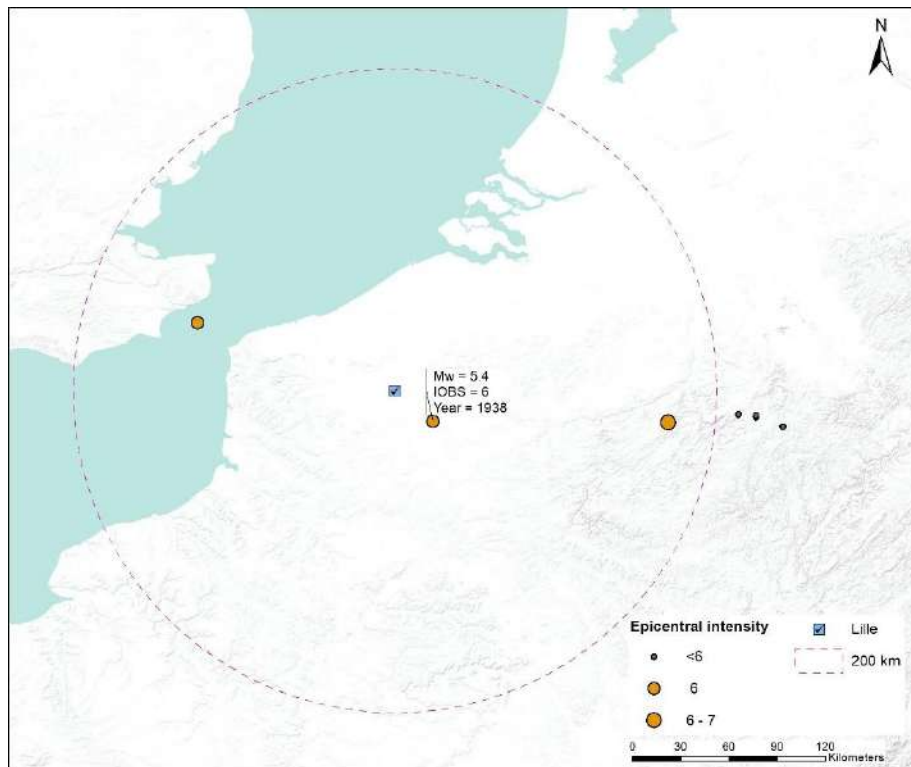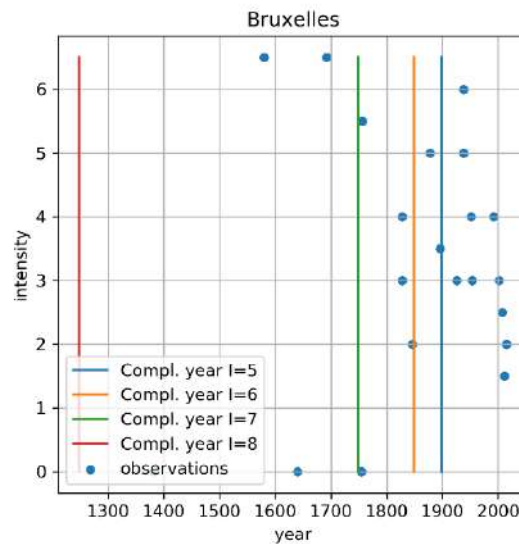

Figure A.11: Map of observed intensities for for Lille.
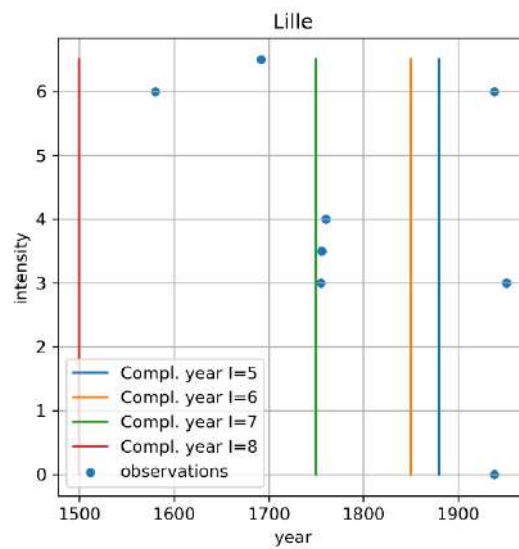
Figure A.12: Observed intensities versus time (blue dots) for Lille. Completeness years for intensities V, VI, VII and VIII are also plotted (coloured lines).
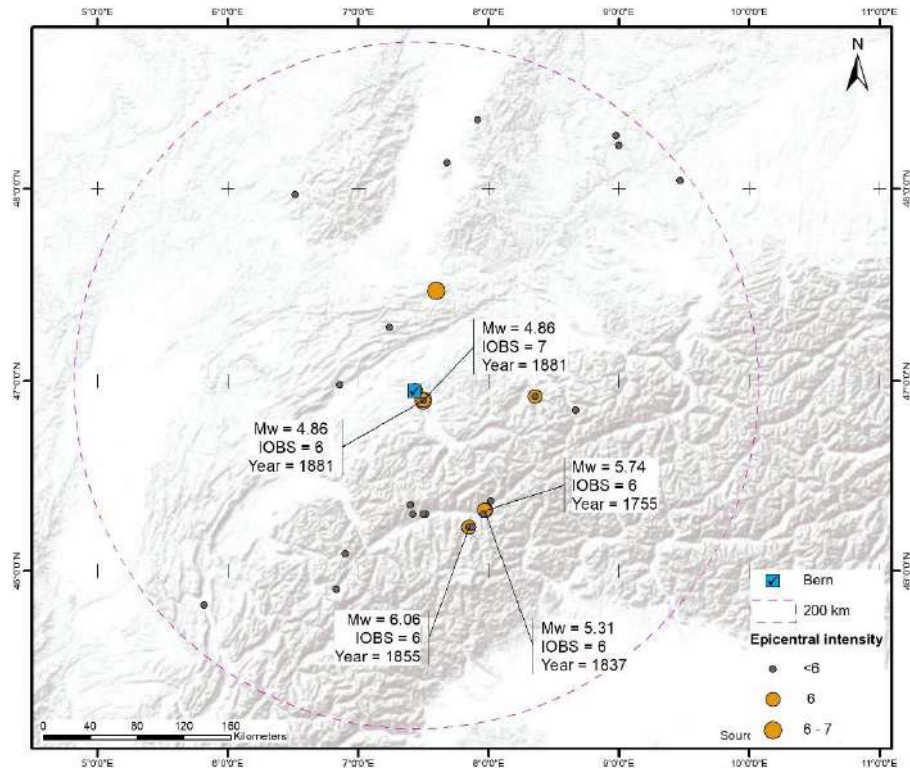
A.1.7 Limoges
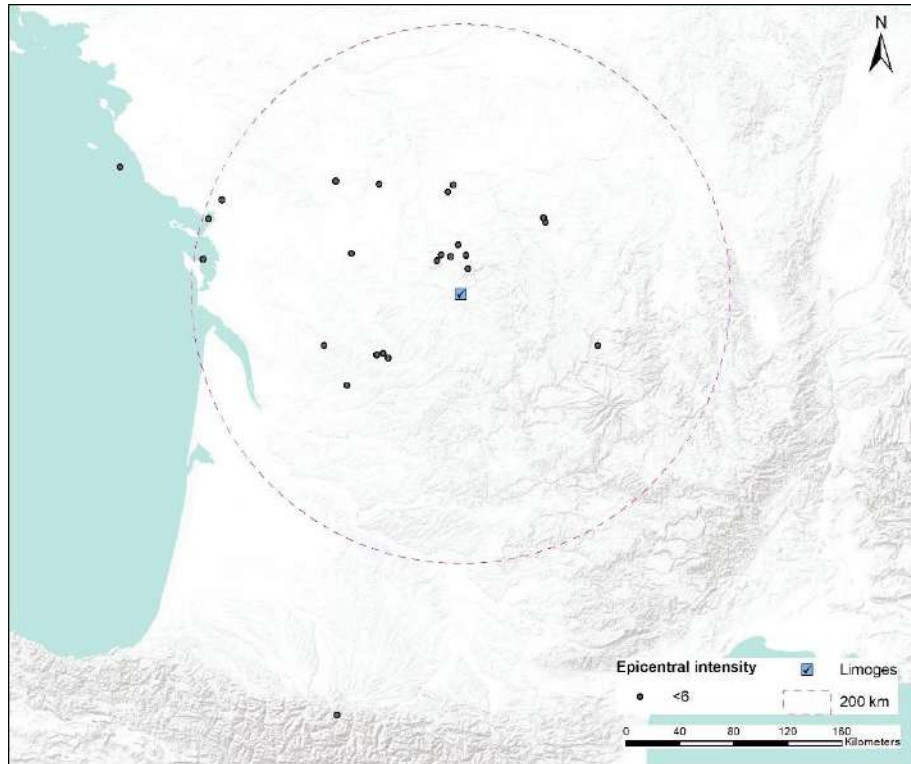
Figure A.13: Map of observed intensities for Limoges.
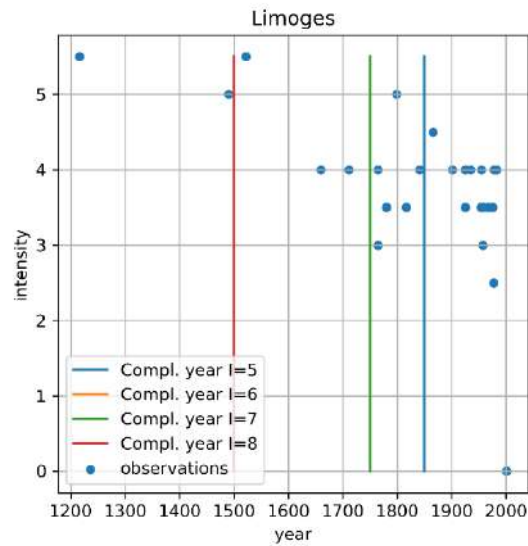
Figure A.14: Observed intensities versus time (blue dots) for Limoges. Completeness years for intensities V, VI, VII and VIII are also plotted (coloured lines).

A.1.8 Lourdes
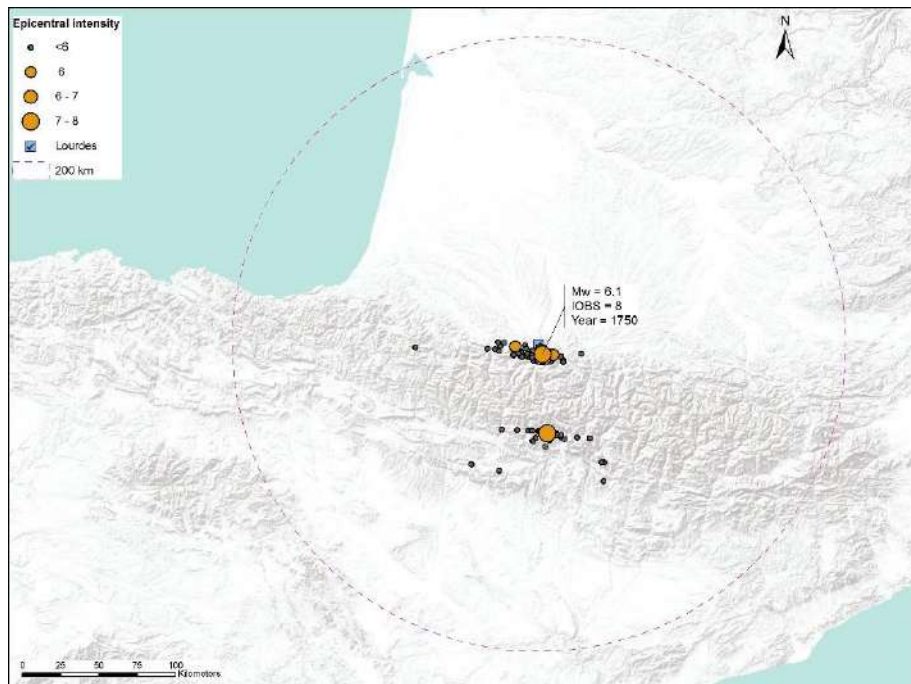
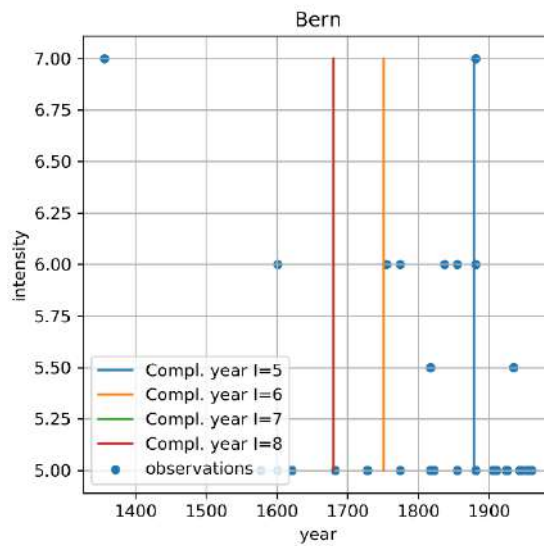Figure A.15: Map of observed intensities for Lourdes.
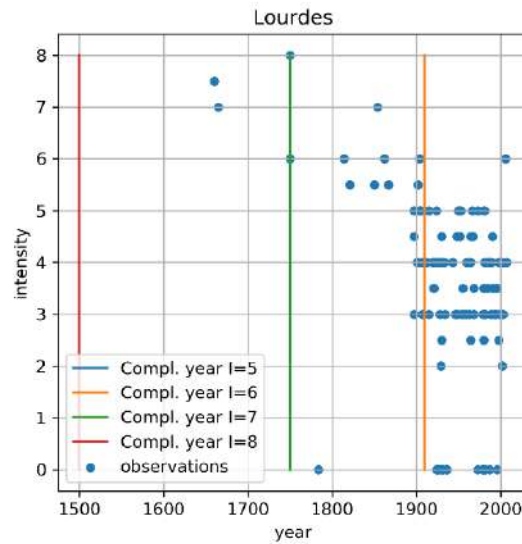
Figure A.16: Observed intensities versus time (blue dots) for Lourdes. Completeness years for intensities V, VI, VII and VIII are also plotted (coloured lines).

A.1.9   Marseille
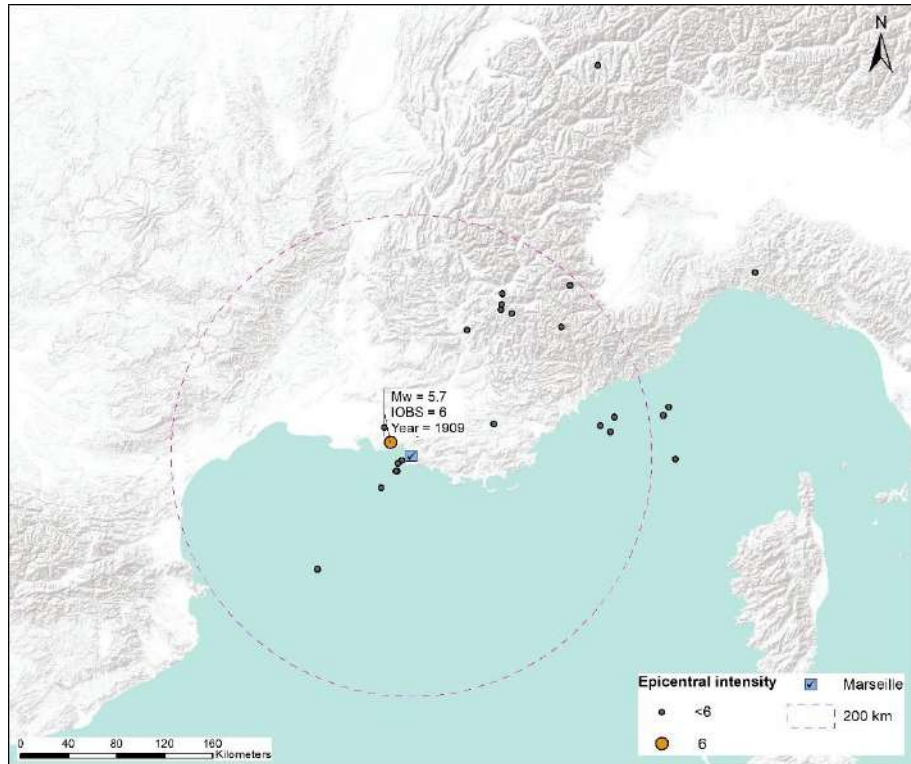
Figure A.17: Map of observed intensities for Marseille.
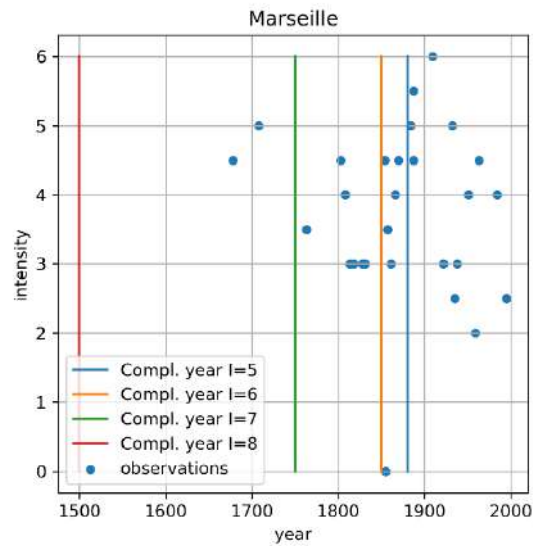
Figure A.18: Observed intensities versus time (blue dots) for Marseille. Completeness years for intensities V, VI, VII and VIII are also plotted (coloured lines).
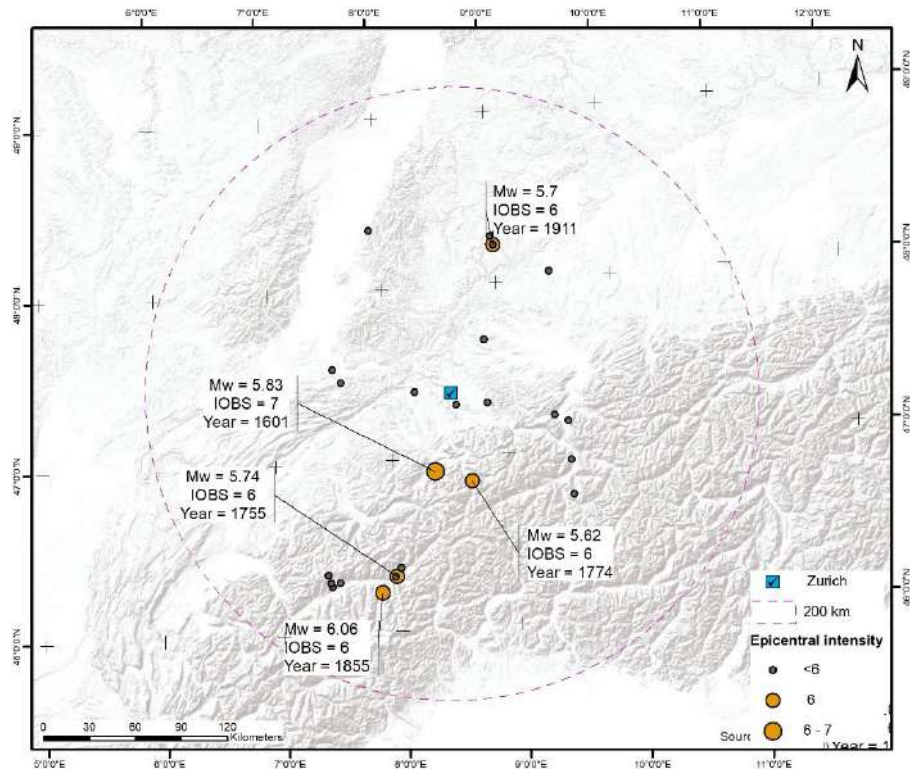
A.1.10   Mulhouse
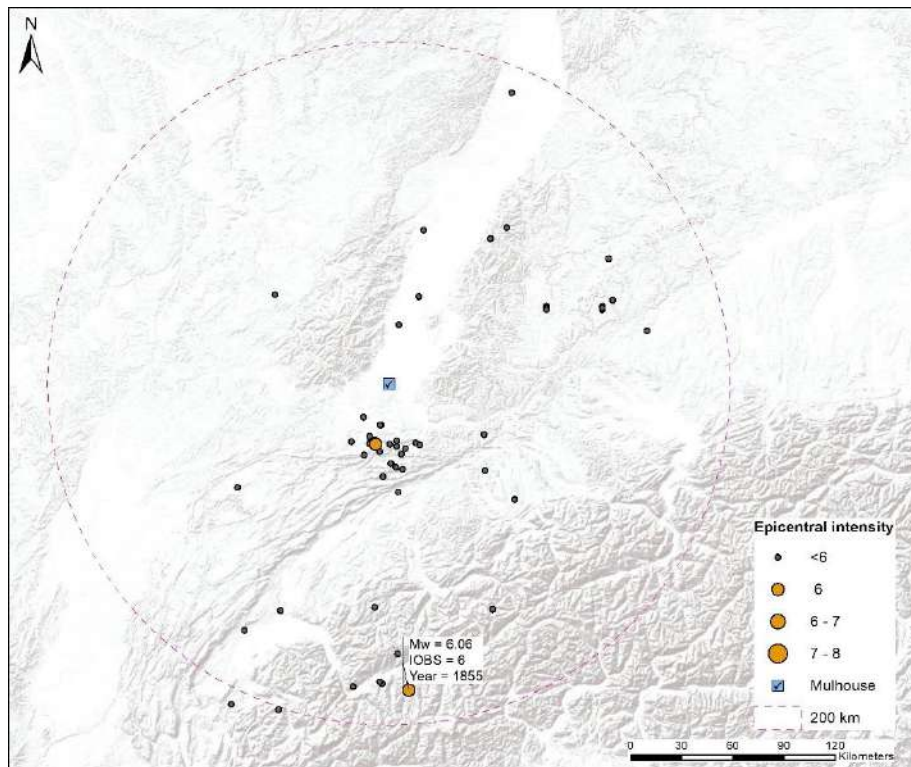
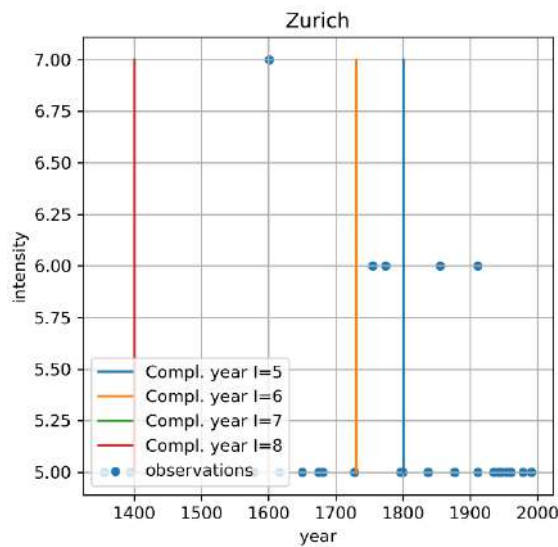Figure A.19: Map of observed intensities for Mulhouse.
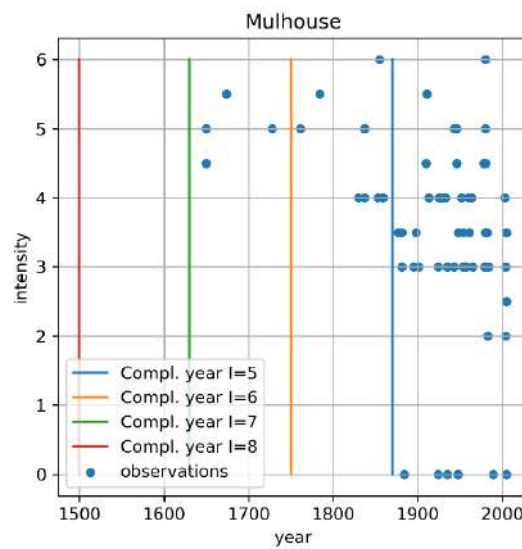
Figure A.20: Observed intensities versus time (blue dots) for Mulhouse. Completeness years for intensities V, VI, VII and VIII are also plotted (coloured lines).

A.1.11   Nice
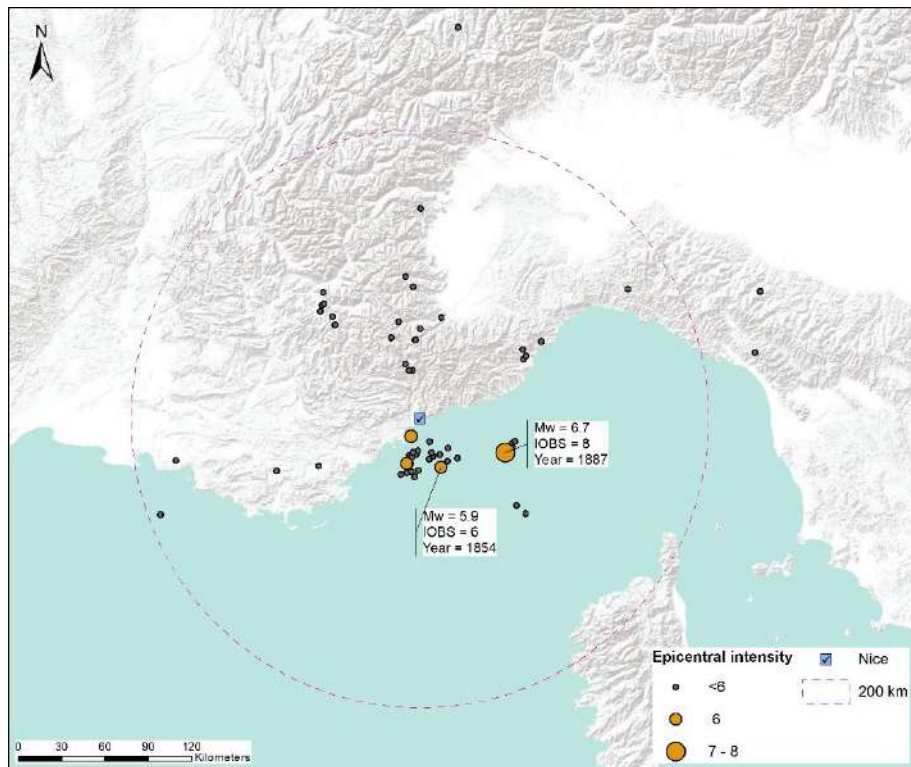
Figure A.21: Map of observed intensities for Nice.
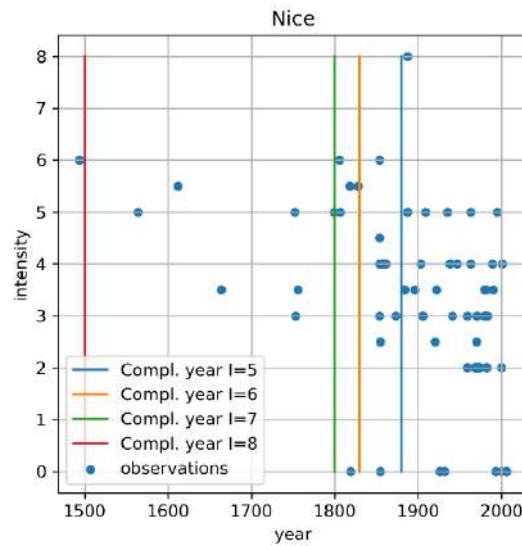
Figure A.22: Observed intensities versus time (blue dots) for Nice. Completeness years for intensities V, VI, VII and VIII are also plotted (coloured lines).

A.1.12 Orleans
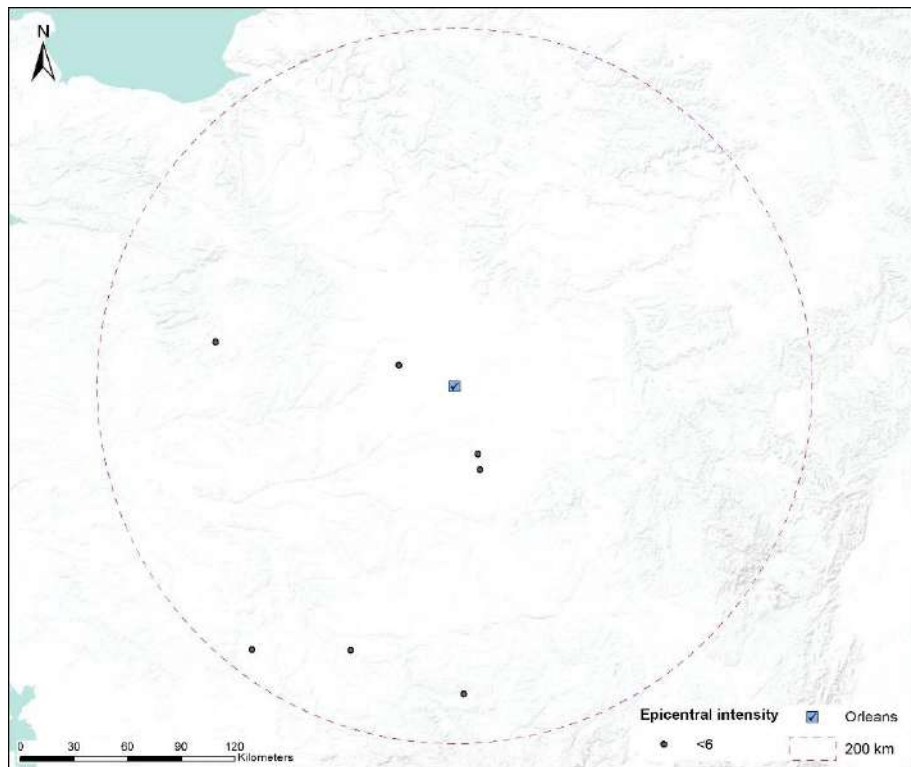
Figure A.23: Map of observed intensities for Orléans.
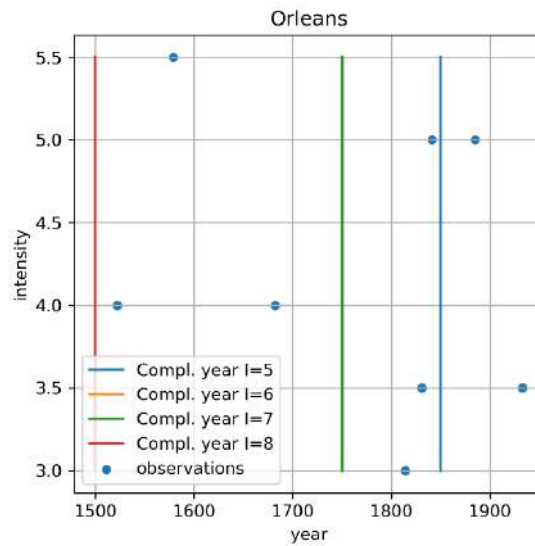
Figure A.24: Observed intensities versus time (blue dots) for Orléans. Completeness years for intensities V, VI, VII and VIII are also plotted (coloured lines).

A.1.13   Paris
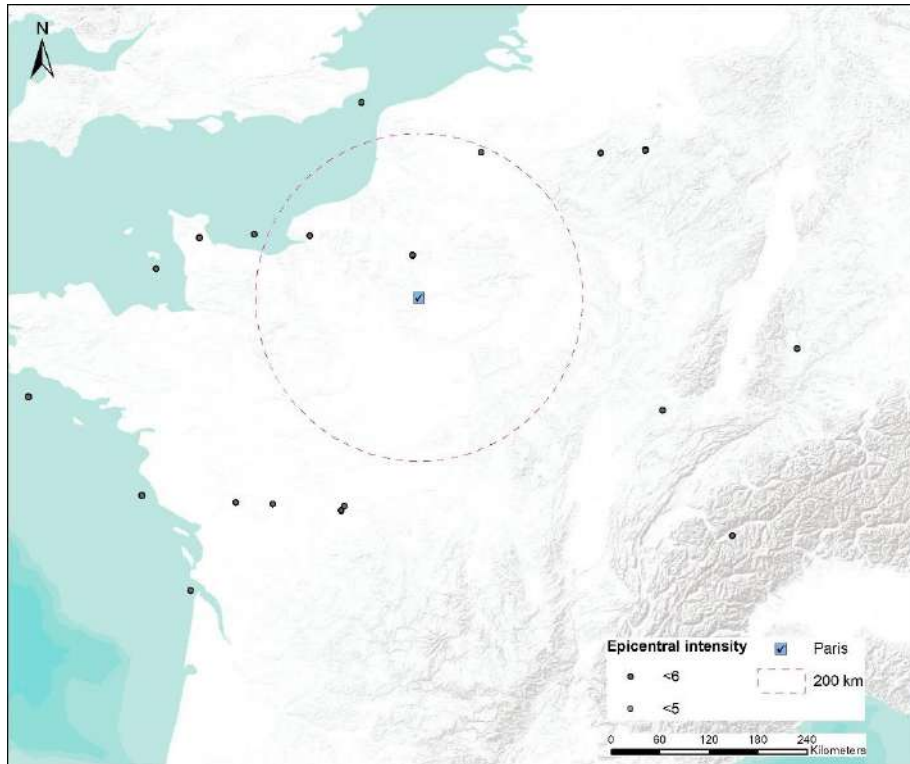
Figure A.25: Map of observed intensities for Paris.
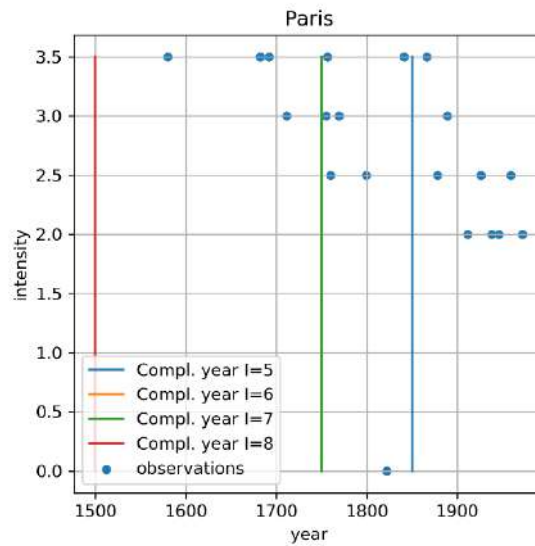
Figure A.26: Observed intensities versus time (blue dots) for Paris. Completeness years for intensities V, VI, VII and VIII are also plotted (coloured lines).

A.1.14   Perpignan

Figure A.27: Map of observed intensities for Perpignan.

Figure A.28: Observed intensities versus time (blue dots) for Perpignan. Completeness years for intensities V, VI, VII and VIII are also plotted (coloured lines).

A.1.15   Toulouse
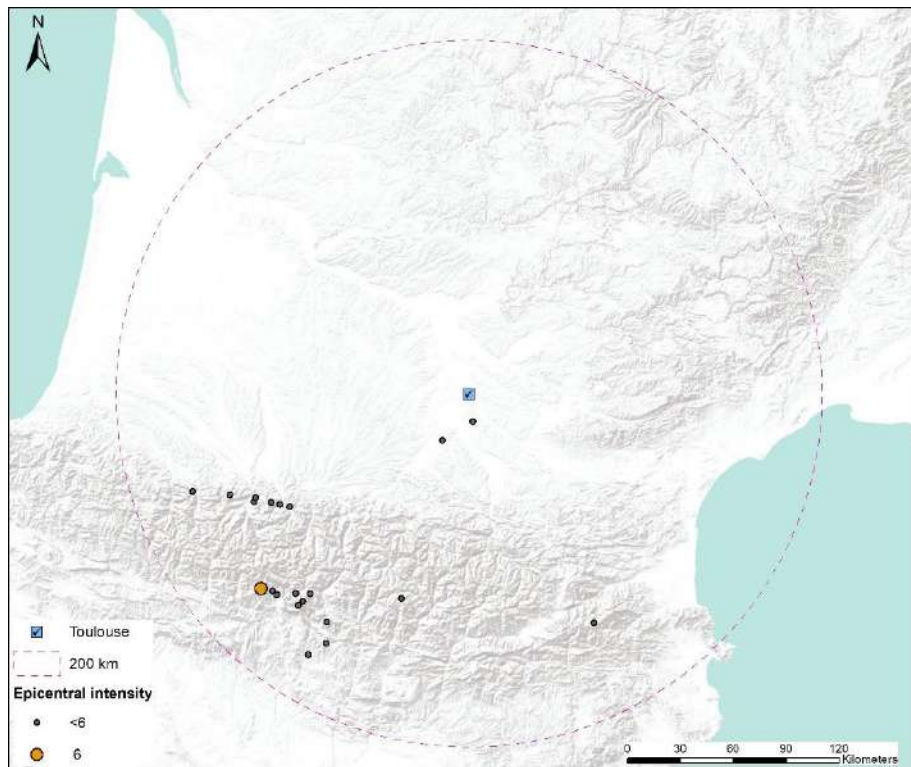
Figure A.29: Map of observed intensities for Toulouse.
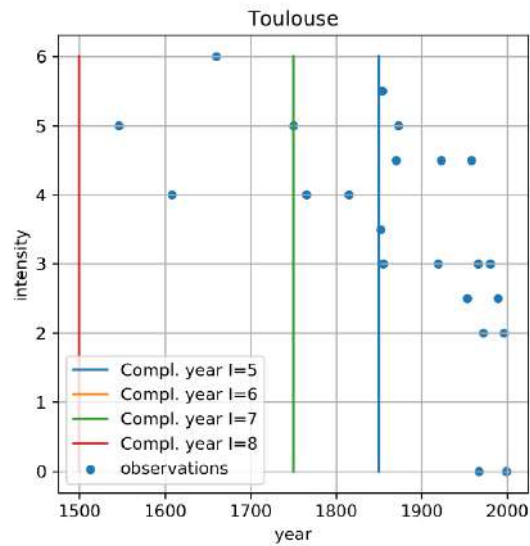
Figure A.30: Observed intensities versus time (blue dots) for Toulouse. Completeness years for intensities V, VI, VII and VIII are also plotted (coloured lines).

A.2 Spain

A.2.1 Barcelona
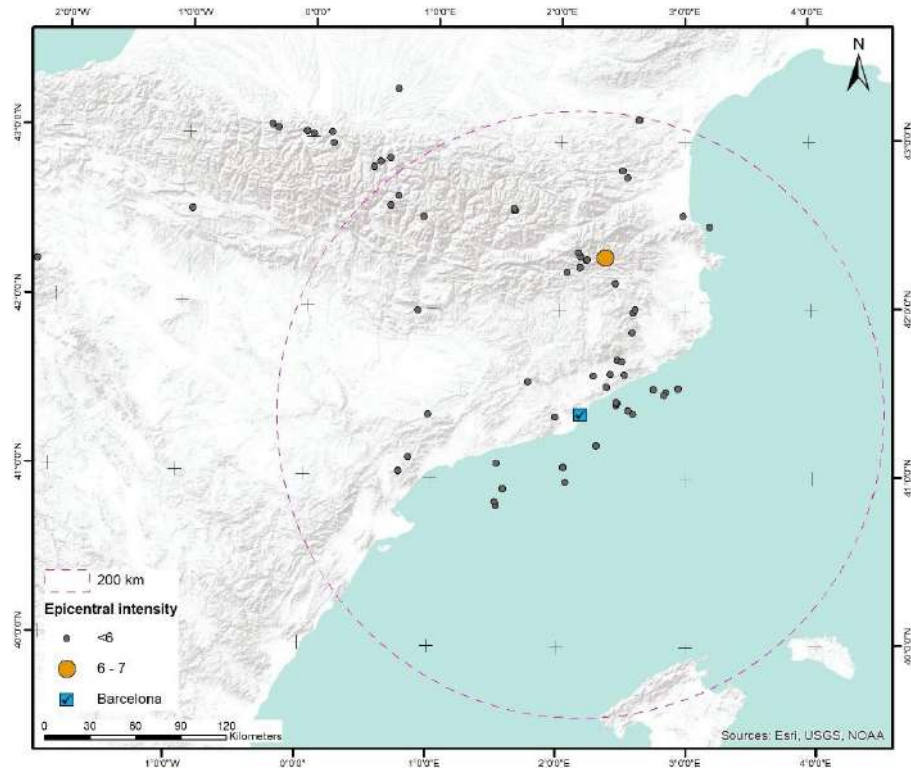
Figure A.31: Map of observed intensities for Barcelona.
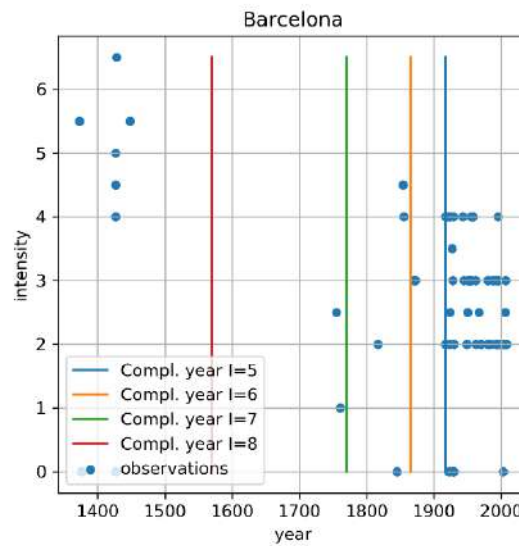
Figure A.32: Observed intensities versus time (blue dots) for Barcelona. Completeness years for intensities V, VI, VII and VIII are also plotted (coloured lines).

A.2.2 Madrid
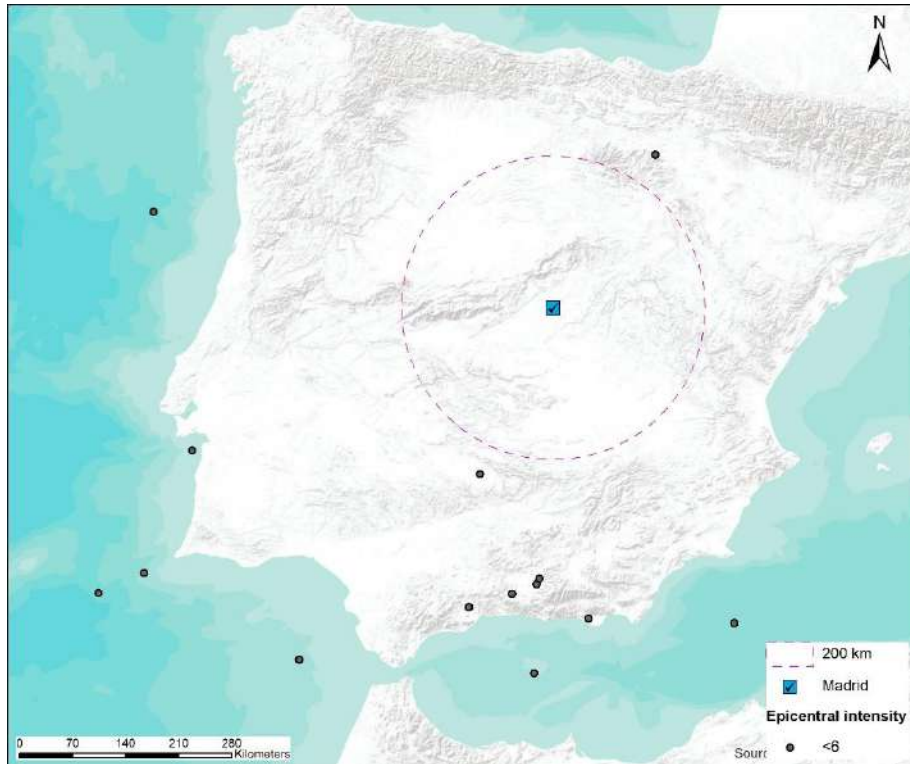
Figure A.33: Map of observed intensities for Madrid.
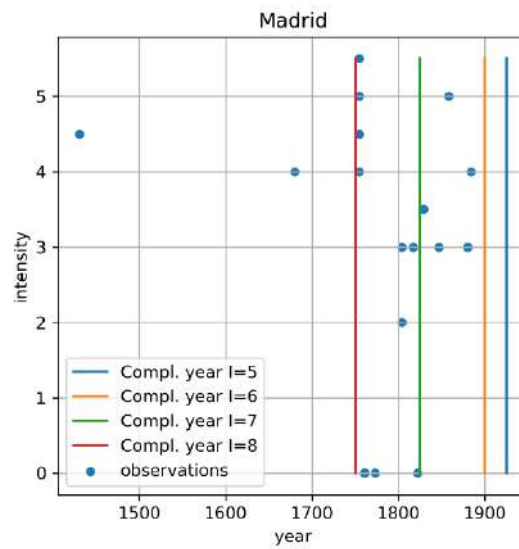
Figure A.34: Observed intensities versus time (blue dots) for Madrid. Completeness years for intensities V, VI, VII and VIII are also plotted (coloured lines).

A.2.3   Malaga

Figure A.35: Map of observed intensities for Malaga.

Figure A.36: Observed intensities versus time (blue dots) for Malaga. Completeness years for intensities V, VI, VII and VIII are also plotted (coloured lines).

A.2.4 Sevilla
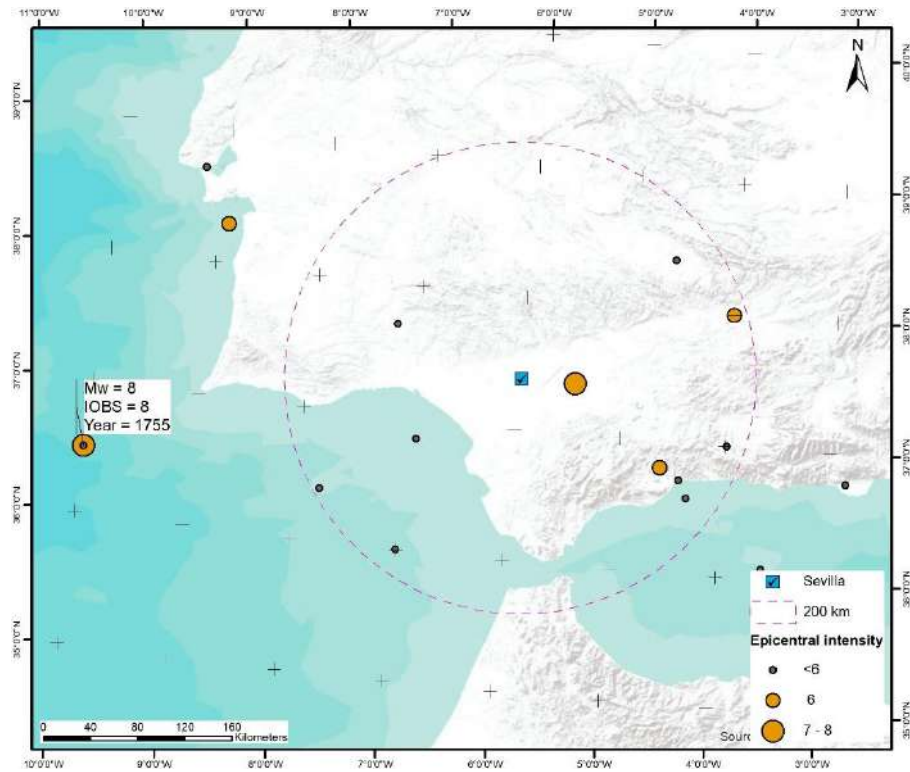
Figure A.37: Map of observed intensities for Sevilla.
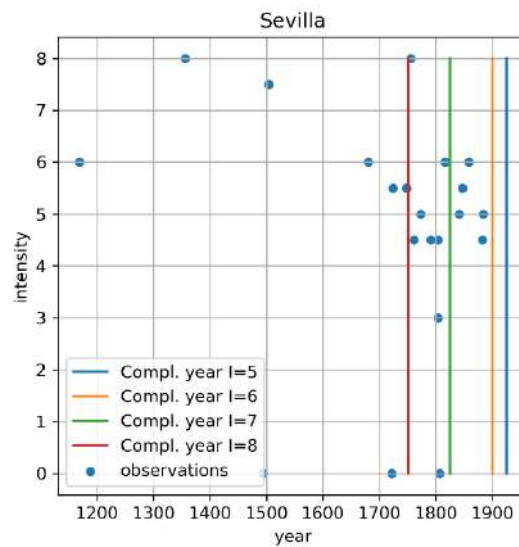
Figure A.38: Observed intensities versus time (blue dots) for Sevilla. Completeness years for intensities V, VI, VII and VIII are also plotted (coloured lines).

A.3 Italy

A.3.1 Bologna
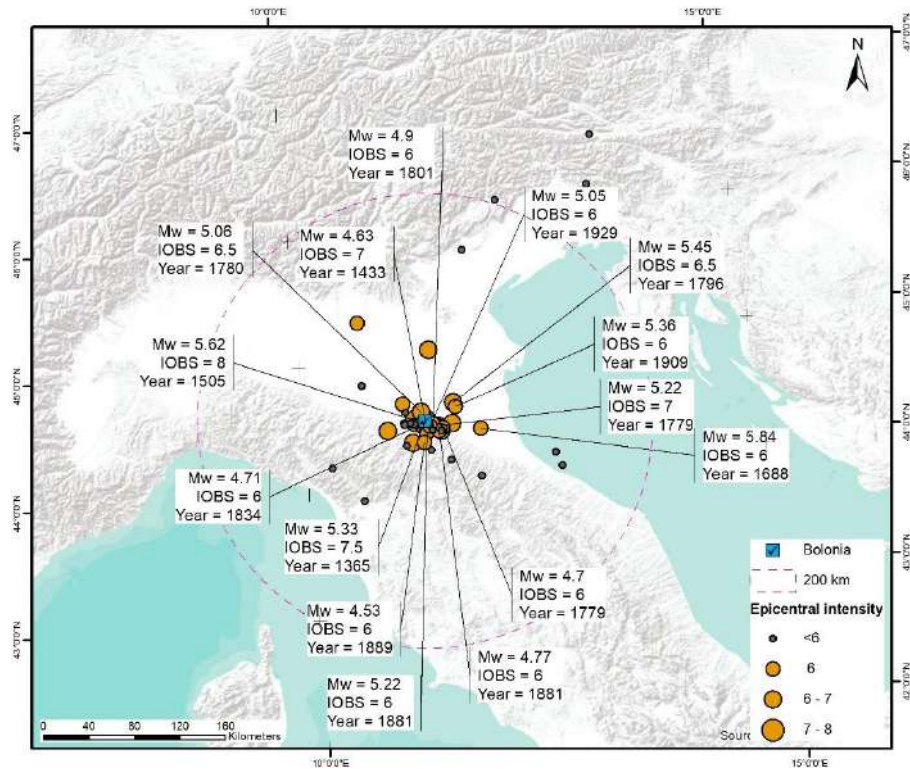
Figure A.39: Map of observed intensities for Bologna.
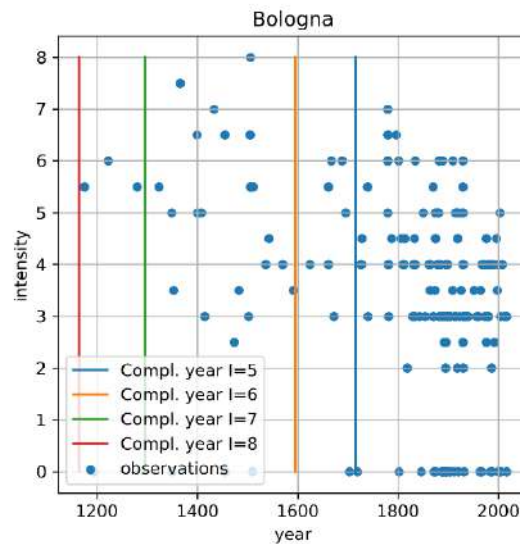
Figure A.40: Observed intensities versus time (blue dots) for Bologna. Completeness years for intensities V, VI, VII and VIII are also plotted (coloured lines).

A.3.2   Catania
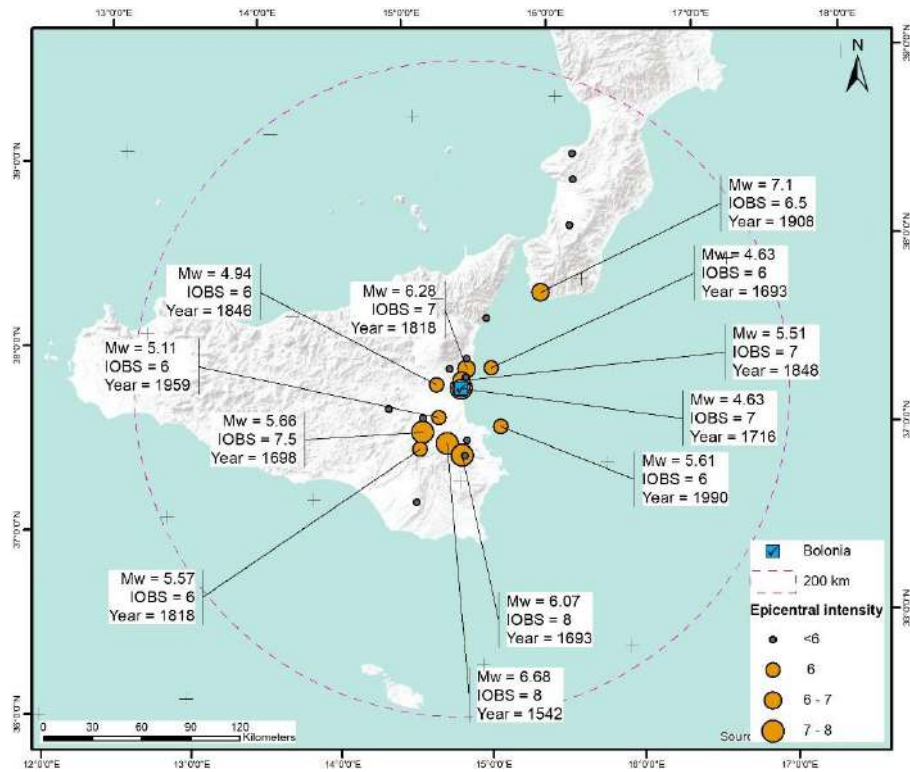
Figure A.41: Map of observed intensities for Catania.
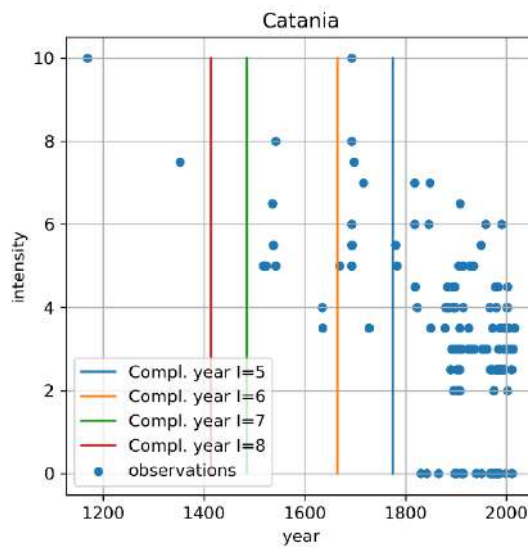
Figure A.42: Observed intensities versus time (blue dots) for Catania. Completeness years for intensities V, VI, VII and VIII are also plotted (coloured lines).

A.3.3   Milan
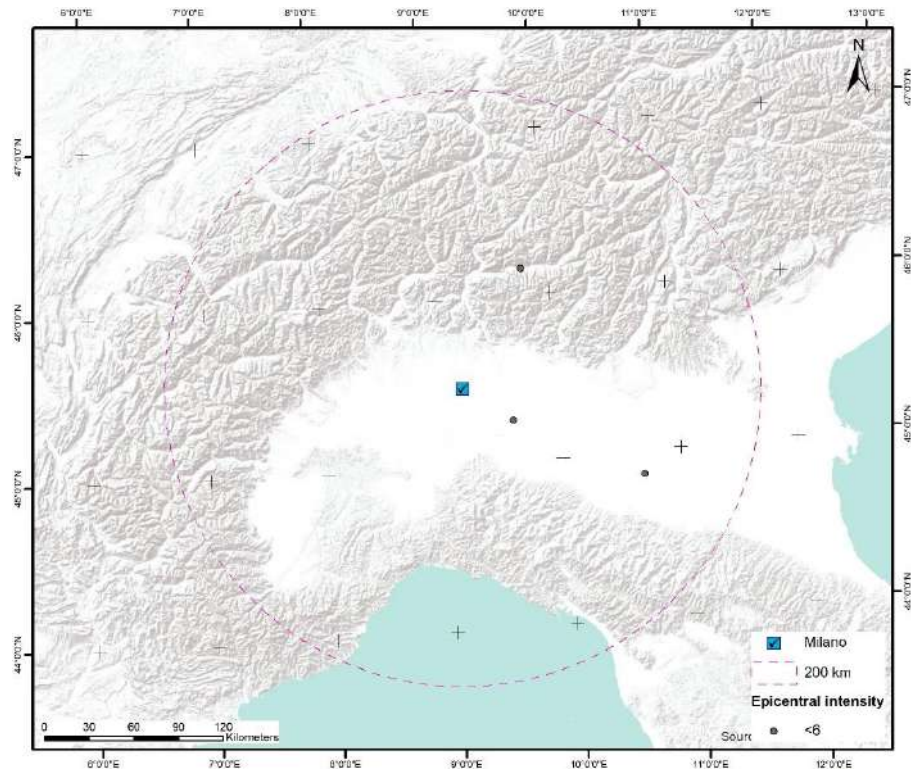
Figure A.43: Map of observed intensities for Milan.
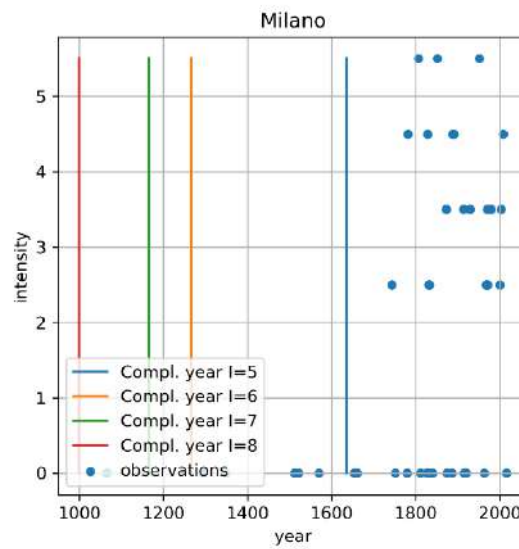
Figure A.44: Observed intensities versus time (blue dots) for Milan. Completeness years for intensities V, VI, VII and VIII are also plotted (coloured lines).

A.3.4   Roma
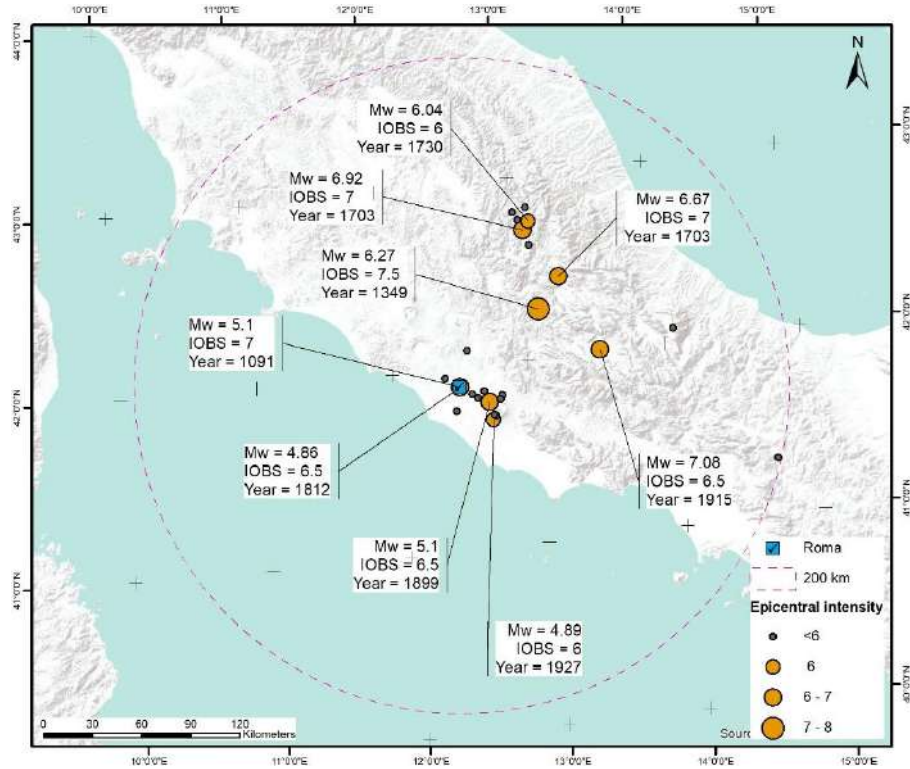
Figure A.45: Map of observed intensities for Roma.

Figure A.46: Observed intensities versus time (blue dots) for Roma. Completeness years for intensities V, VI, VII and VIII are also plotted (coloured lines).

A.4 Greece

A.4.1 Athens

Figure A.47: Map of observed intensities for Athens.

Figure A.48: Observed intensities versus time (blue dots) for Athens. Completeness years for intensities V, VI, VII and VIII are also plotted (coloured lines).

A.4.2   Thessaloniki

Figure A.49: Map of observed intensities for Thessaloniki.

Figure A.50: Observed intensities versus time (blue dots) for Thessaloniki. Completeness years for intensities V, VI, VII and VIII are also plotted (coloured lines).

A.5 Turkey

A.5.1 Izmir

Figure A.51: Map of observed intensities for Izmir.

Figure A.52: Observed intensities versus time (blue dots) for Izmir. Completeness years for intensities V, VI, VII and VIII are also plotted (coloured lines).

A.5.2   Istanbul

Figure A.53: Map of observed intensities for Istanbul.

Figure A.54: Observed intensities versus time (blue dots) for Istanbul. Completeness years for intensities V, VI, VII and VIII are also plotted (coloured lines).

A.6 Belgium

A.6.1 Bruxelles

Figure A.55: Map of observed intensities for Bruxels.

Figure A.56: Observed intensities versus time (blue dots) for Bruxelles. Completeness years for intensities V, VI, VII and VIII are also plotted (coloured lines).

A.7 Switzerland

A.7.1 Bern

Figure A.57: Map of observed intensities for Bern.

Figure A.58: Observed intensities versus time (blue dots) for Bern. Completeness years for intensities V, VI, VII and VIII are also plotted (coloured lines).

A.7.2   Zürich

Figure A.59: Map of observed intensities for Zürich.

Figure A.60: Observed intensities versus time (blue dots) for Zürich. Completeness years for intensities V, VI, VII and VIII are also plotted (coloured lines).

Appendix B

Testing results plots

fUGRO

B.1 Testing ESHM13 – data France

B.1.1 Intensity VII

Caprio et al.
(2015)
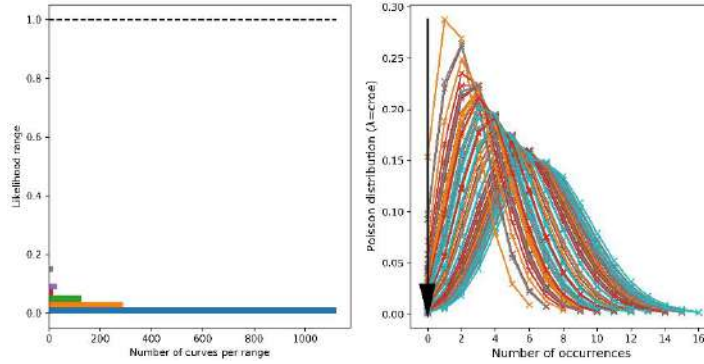
Faenza &
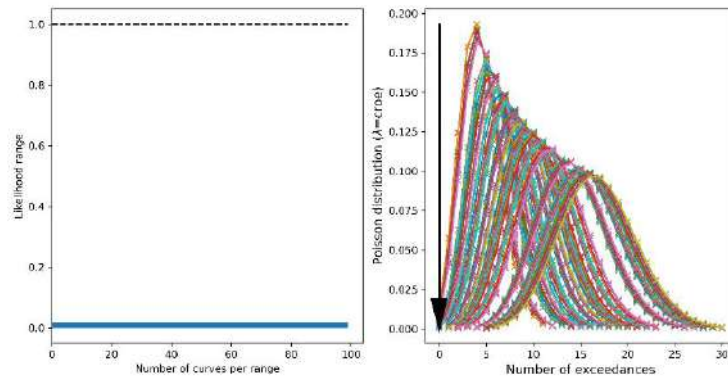Michelini
(2010)
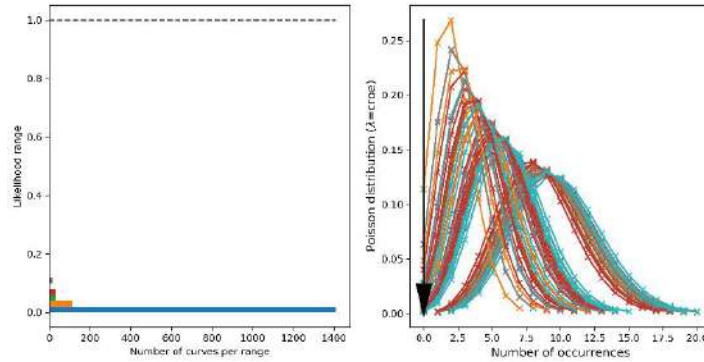
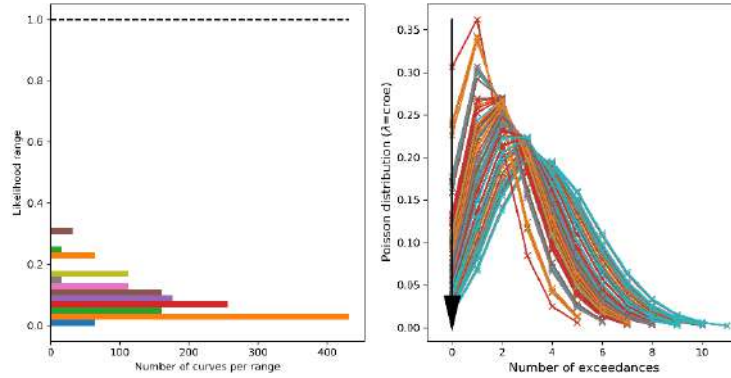Gomez Capera
(2020)
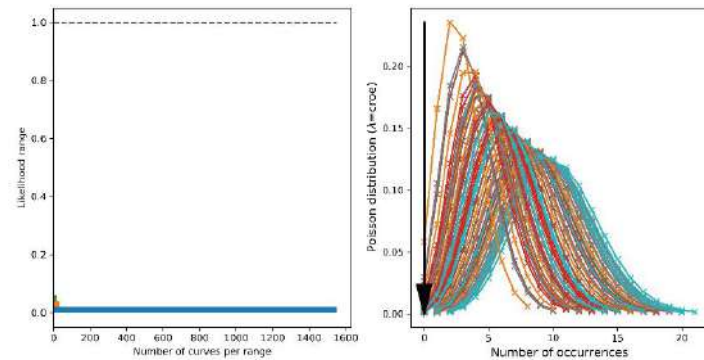
Wald et al.
(1999)
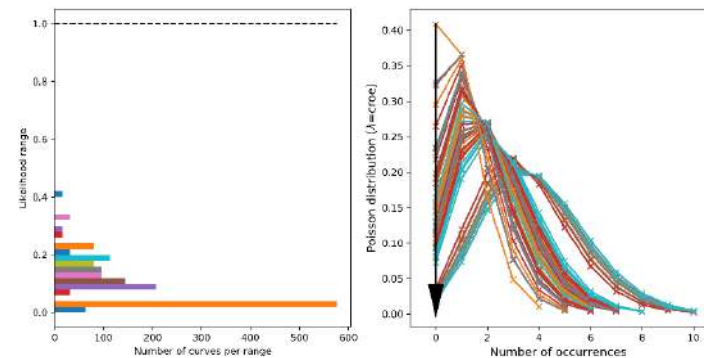
Figure B.1: Left: Likelihood grouped by bins (coloured bars) and maximum theoretical likelihood (dashed line). Right: Poisson distributions generated from the cumulated rates of occurrences for the different branches of the logic-tree considered (coloured bars) and observed number of occurrences (black arrow). Results corresponding to the ESHM13 model (all branches) for intensity VII using data from France and 4 different PGA-to-intensity relationships (from top to bottom).
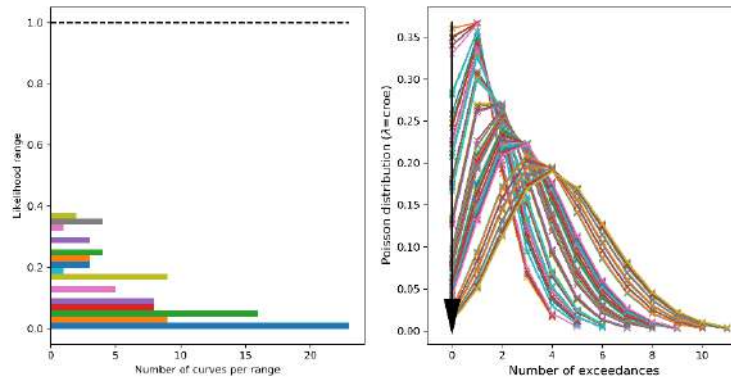
Figure B.2: Left: Likelihood grouped by bins (coloured bars) and maximum theoretical likelihood (dashed line). Right: Poisson distributions generated from the cumulated rates of occurrences for the different branches of the logic-tree considered (coloured bars) and observed number of occurrences (black arrow). Results corresponding to the ESHM13 model (99 fractiles) for intensity VII using data from France and 4 different PGA-to-intensity relationships (from top to bottom).

B.1.2 Intensity VIII

Caprio et al. (2015)
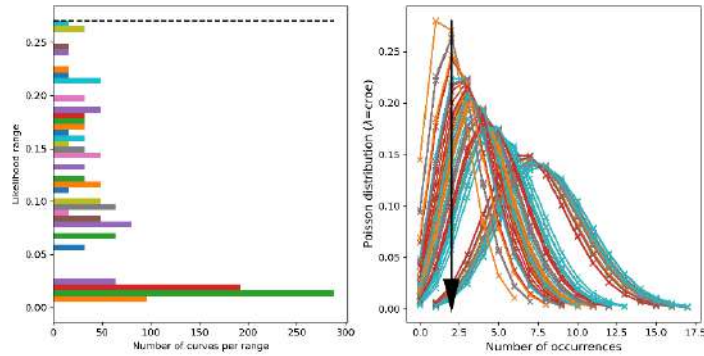
Faenza & Michelini (2010)
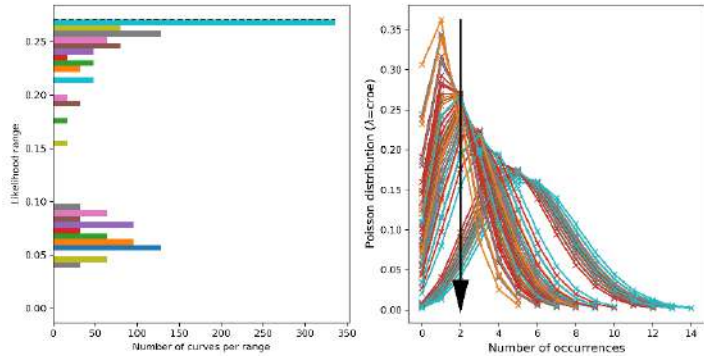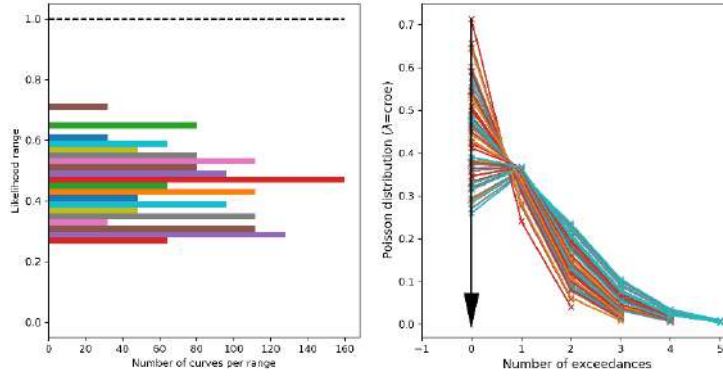
Gomez Capera (2020)
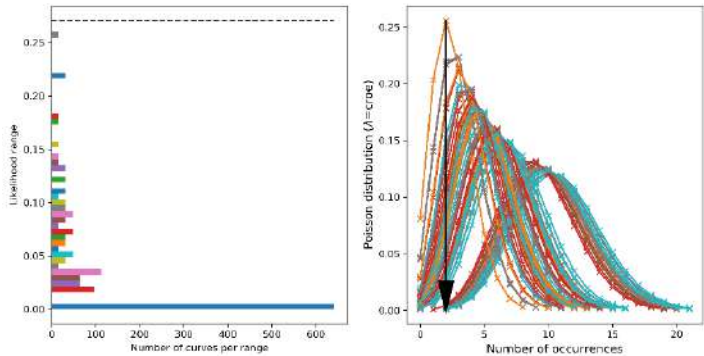
Wald et al. (1999)
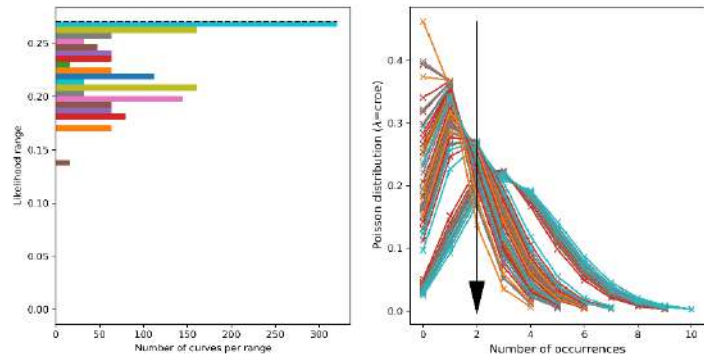
Figure B.3: Left: Likelihood grouped by bins (coloured bars) and maximum theoretical likelihood (dashed line). Right: Poisson distributions generated from the cumulated rates of occurrences for the different branches of the logic-tree considered (coloured bars) and observed number of occurrences (black arrow). Results corresponding to the ESHM13 model (all branches) for intensity VIII using data from France and 4 different PGA-to-intensity relationships (from top to bottom).

Caprio et al.
(2015)
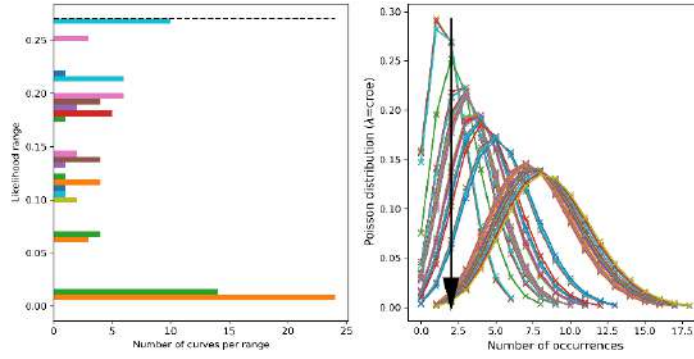
Faenza &
Michelini
(2010)
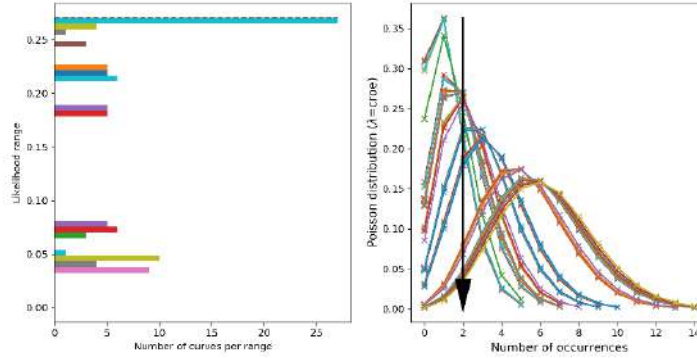
Gomez Capera
(2020)
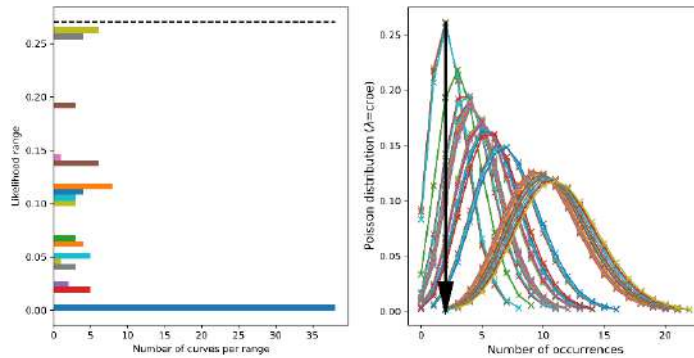
Wald et al.
(1999)
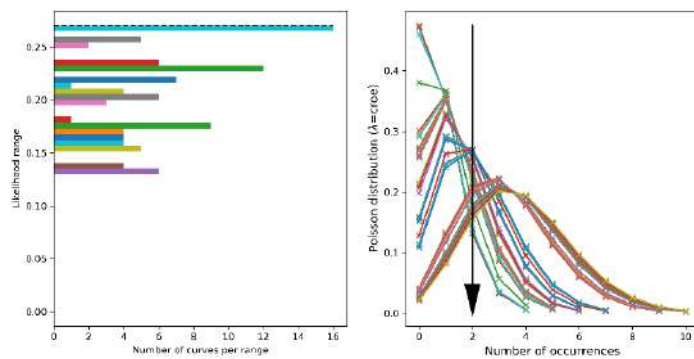
Figure B.4: Left: Likelihood grouped by bins (coloured bars) and maximum theoretical likelihood (dashed line). Right: Poisson distributions generated from the cumulated rates of occurrences for the different branches of the logic-tree considered (coloured bars) and observed number of occurrences (black arrow). Results corresponding to the ESHM13 model (99 fractiles) for intensity VIII using data from France and 4 different PGA-to-intensity relationships (from top to bottom).

B.1.3 Acceleration 0.2 m/s²
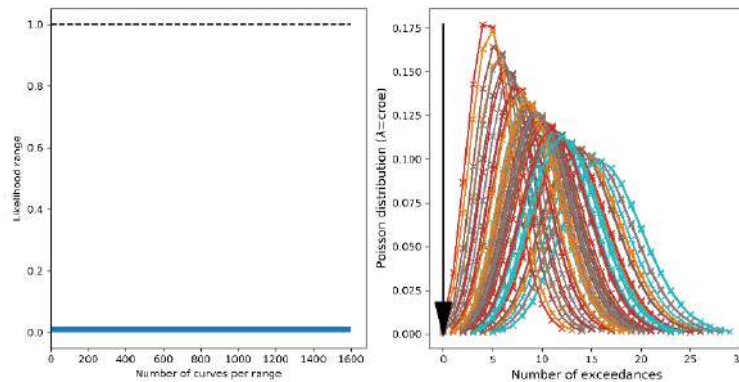
Figure B.5: Left: Likelihood grouped by bins (coloured bars) and maximum theoretical likelihood (dashed line). Right: Poisson distributions generated from the cumulated rates of exceedance for the different branches of the logic-tree considered (coloured bars) and observed number of exceedances (black arrow). Results corresponding to the ESHM13 model (all branches) using data from France for the acceleration threshold 0.1 m/s².
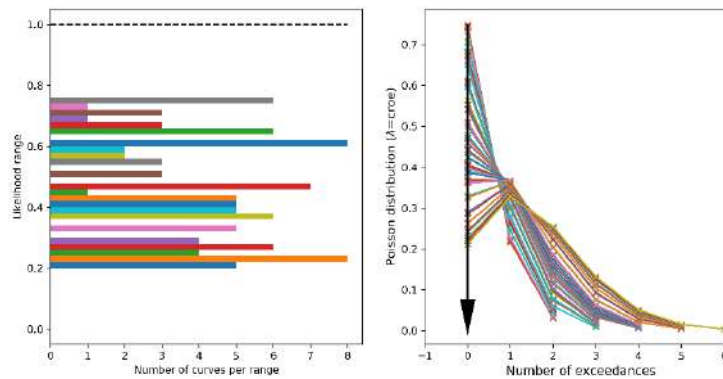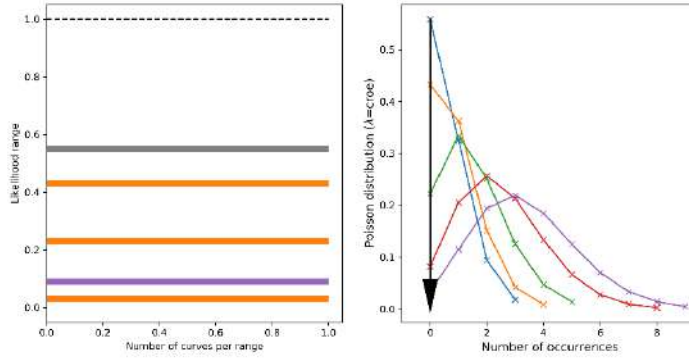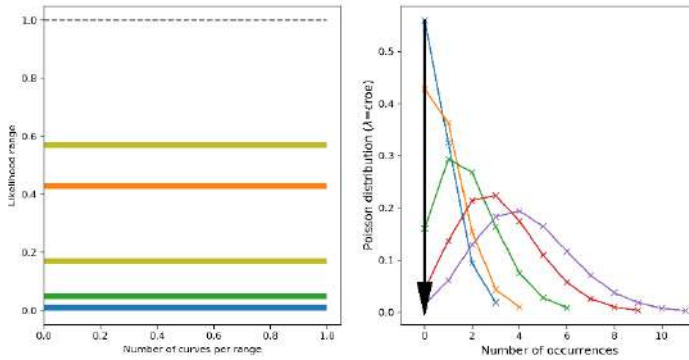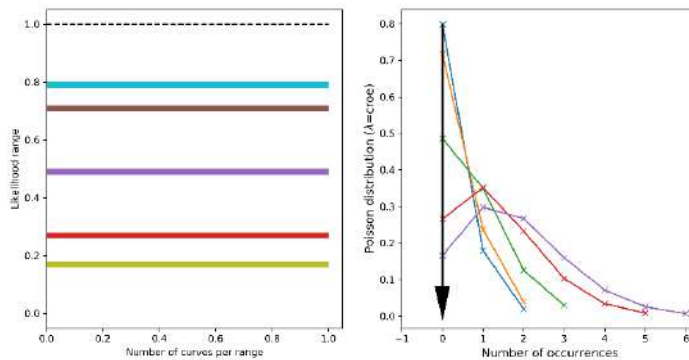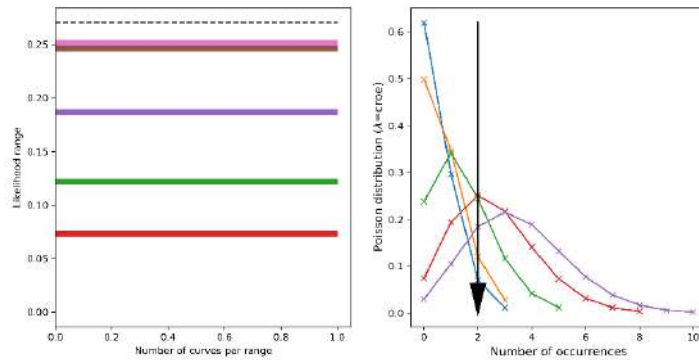

Figure B.6: Left: Likelihood grouped by bins (coloured bars) and maximum theoretical likelihood (dashed line). Right: Poisson distributions generated from the cumulated rates of exceedance for the different branches of the logic-tree considered (coloured bars) and observed number of exceedances (black arrow). Results corresponding to the ESHM13 model (all branches) using data from France for the acceleration threshold 0.1 m/s².
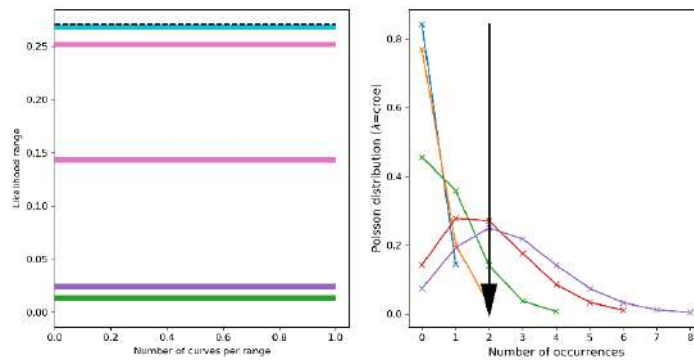
B.1.4 Acceleration 0.5 m/s²

Figure B.7: Left: Likelihood grouped by bins (coloured bars) and maximum theoretical likelihood (dashed line). Right: Poisson distributions generated from the cumulated rates of exceedance for the different branches of the logic-tree considered (coloured bars) and observed number of exceedances (black arrow). Results corresponding to the ESHM13 model (all branches) using data from France for the acceleration threshold 0.1 m/s^2.
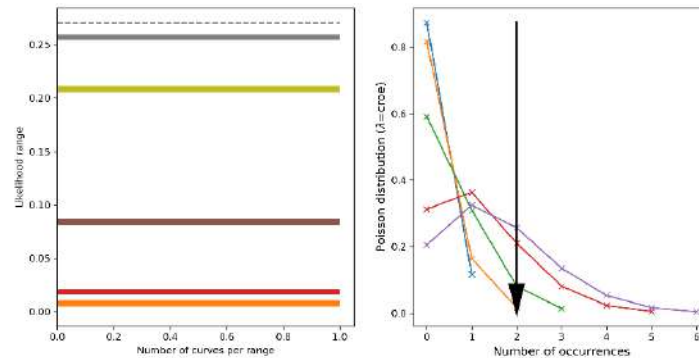

Figure B.8: Left: Likelihood grouped by bins (coloured bars) and maximum theoretical likelihood (dashed line). Right: Poisson distributions generated from the cumulated rates of exceedance for the different branches of the logic-tree considered (coloured bars) and observed number of exceedances (black arrow). Results corresponding to the ESHM13 model (all branches) using data from France for the acceleration threshold 0.1 m/s^2.

B.1.5   Acceleration 1.0 m/s^2

Figure B.9: Left: Likelihood grouped by bins (coloured bars) and maximum theoretical likelihood (dashed line). Right: Poisson distributions generated from the cumulated rates of exceedance for the different branches of the logic-tree considered (coloured bars) and observed number of exceedances (black arrow). Results corresponding to the ESHM13 model (all branches) using data from France for the acceleration threshold 0.1 m/s^2.
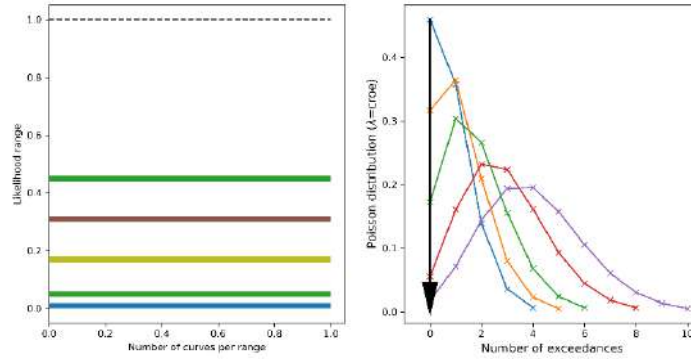

Figure B.10: Left: Likelihood grouped by bins (coloured bars) and maximum theoretical likelihood (dashed line). Right: Poisson distributions generated from the cumulated rates of exceedance for the different branches of the logic-tree considered (coloured bars) and observed number of exceedances (black arrow). Results corresponding to the ESHM13 model (all branches) using data from France for the acceleration threshold 0.1 m/s^2.

B.2   Testing ESHM20 – data France

B.2.1   Intensity VII

Caprio et al. (2015)

Faenza & Michelini (2010)
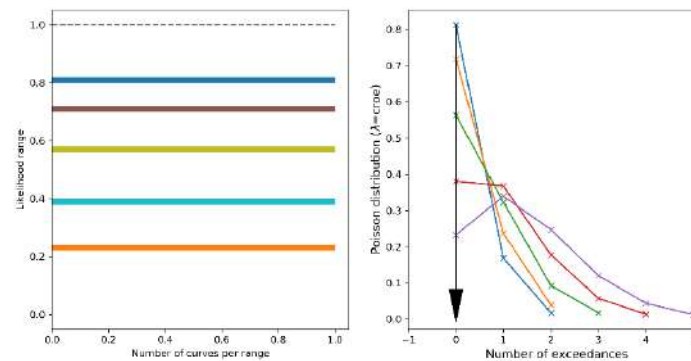
Gomez Capera (2020)
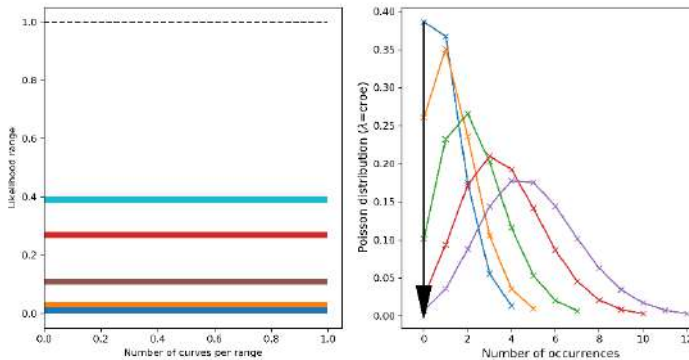
Wald et al. (1999)

Figure B.11: Left: Likelihood grouped by bins (coloured bars) and maximum theoretical likelihood (dashed line). Right: Poisson distributions generated from the cumulated rates of occurrences for the different branches of the logic-tree considered (coloured bars) and observed number of occurrences (black arrow). Results corresponding to the ESHM20 model (5 fractiles) for intensity VII using data from France and 4 different PGA-to-intensity relationships (from top to bottom).
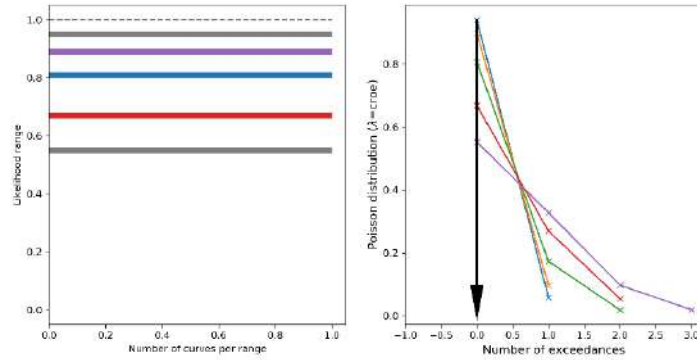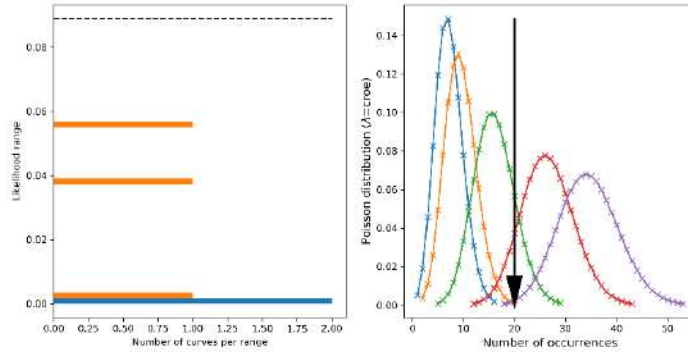
B.2.2 Intensity VIII
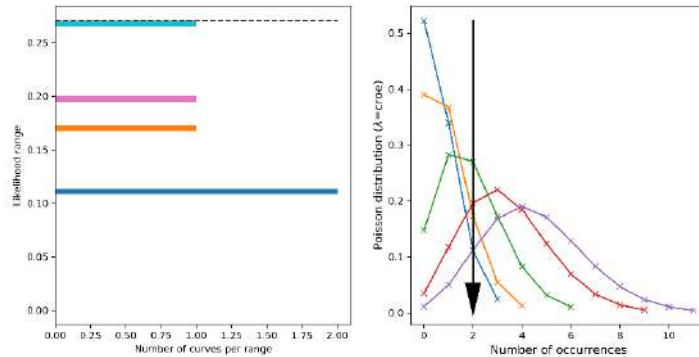
Figure B.12: Left: Likelihood grouped by bins (coloured bars) and maximum theoretical likelihood (dashed line). **Right:** Poisson distributions generated from the cumulated rates of occurrences for the different branches of the logic-tree considered (coloured bars) and observed number of occurrences (black arrow). Results corresponding to the ESHM20 model (5 fractiles) for intensity VIII using data from France and 4 different PGA-to-intensity relationships (from top to bottom).

B.2.3   Acceleration 0.2 m/s²

Figure B.13: Left: Likelihood grouped by bins (coloured bars) and maximum theoretical likelihood (dashed line). Right: Poisson distributions generated from the cumulated rates of exceedance for the different branches of the logic-tree considered (coloured bars) and observed number of exceedances (black arrow). Results corresponding to the ESHM20 model (5 centiles) using data from France for the acceleration threshold 0.1 m/s².
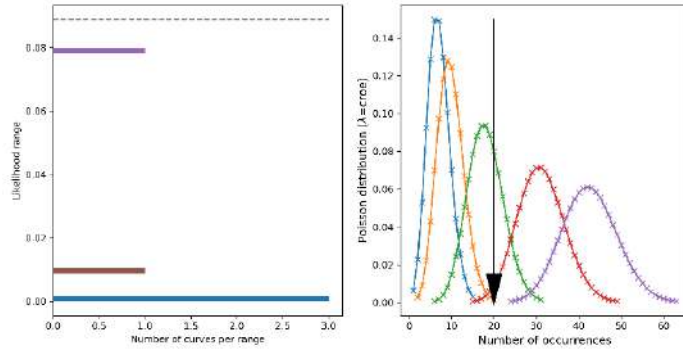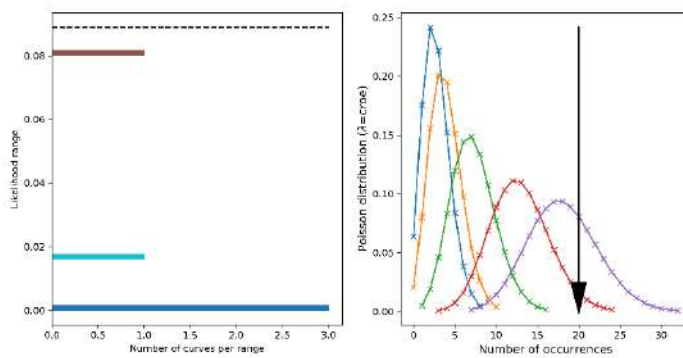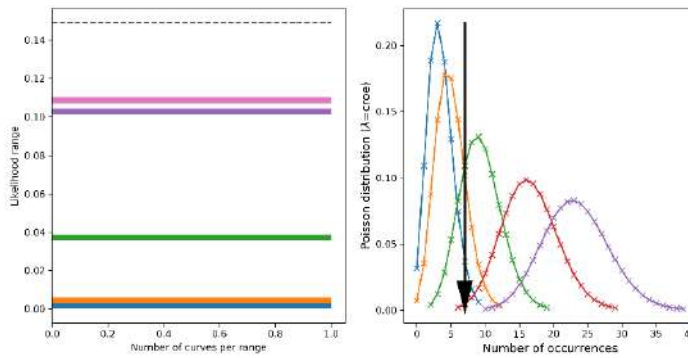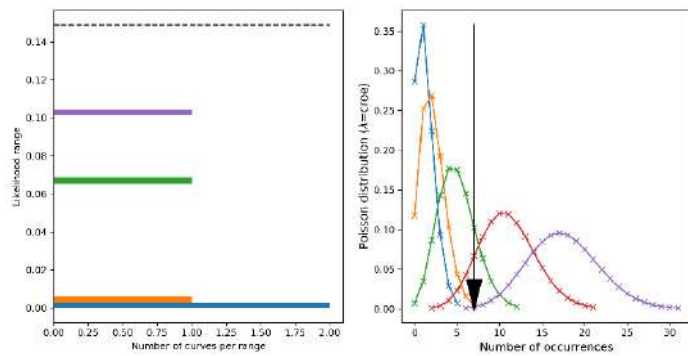
B.2.4   Acceleration 0.5 m/s²

Figure B.14: Left: Likelihood grouped by bins (coloured bars) and maximum theoretical likelihood (dashed line). Right: Poisson distributions generated from the cumulated rates of exceedance for the different branches of the logic-tree considered (coloured bars) and observed number of exceedances (black arrow). Results corresponding to the ESHM20 model (5 centiles) using data from France for the acceleration threshold 0.1 m/s².

B.2.5   Acceleration 1.0 m/s²

Figure B.15: Left: Likelihood grouped by bins (coloured bars) and maximum theoretical likelihood (dashed line). Right: Poisson distributions generated from the cumulated rates of exceedance for the different branches of the logic-tree considered (coloured bars) and observed number of exceedances (black arrow). Results corresponding to the ESHM20 model (5 centiles) using data from France for the acceleration threshold 0.1 m/s^2.

B.3   Testing ESHM20 – data Europe

B.3.1   Intensity VII

B.3.2 Intensity VIII

Figure B.17: Left: Likelihood grouped by bins (coloured bars) and maximum theoretical likelihood (dashed line). Right: Poisson distributions generated from the cumulated rates of occurrences for the different branches of the logic-tree considered (coloured bars) and observed number of occurrences (black arrow). Results corresponding to the ESHM20 model (5 fractiles) for intensity VIII using data from Europe and 4 different PGA-to-intensity relationships (from top to bottom).
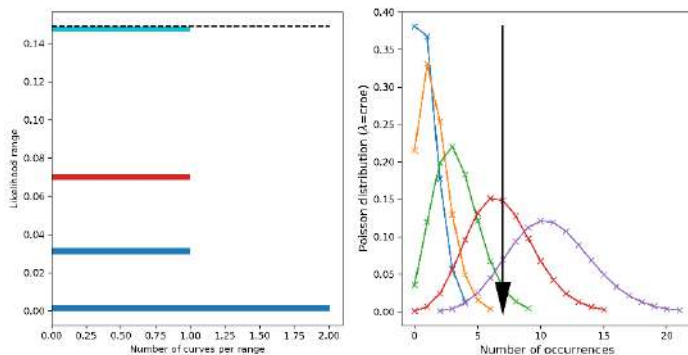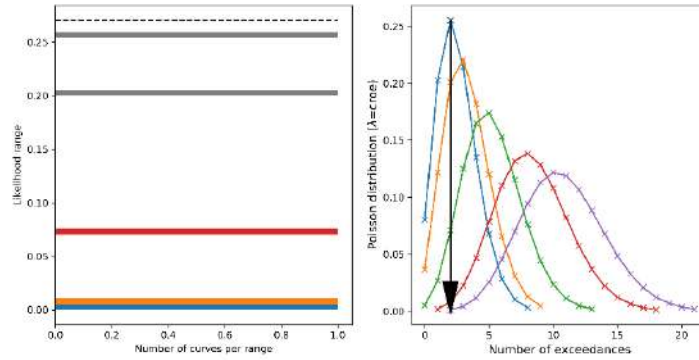
B.3.3   Acceleration 0.2 m/s²

Figure B.18: Left: Likelihood grouped by bins (coloured bars) and maximum theoretical likelihood (dashed line). Right: Poisson distributions generated from the cumulated rates of exceedance for the different branches of the logic-tree considered (coloured bars) and observed number of exceedances (black arrow). Results corresponding to the ESHM20 model (5 centiles) using data from Europe for the acceleration threshold 0.1 m/s².

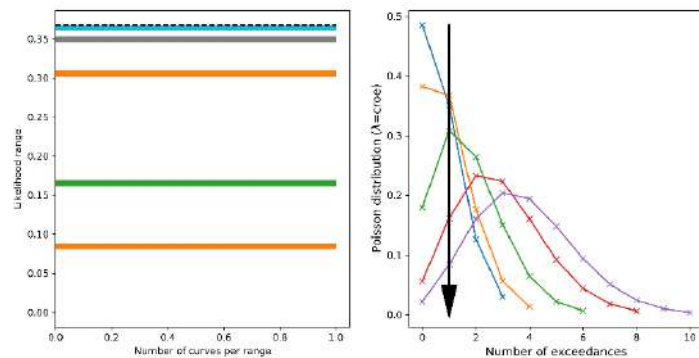## B.3.4   Acceleration 0.5 m/s²

Figure B.19: Left: Likelihood grouped by bins (coloured bars) and maximum theoretical likelihood (dashed line). Right: Poisson distributions generated from the cumulated rates of exceedance for the different branches of the logic-tree considered (coloured bars) and observed number of exceedances (black arrow). Results corresponding to the ESHM20 model (5 centiles) using data from Europe for the acceleration threshold 0.1 m/s².
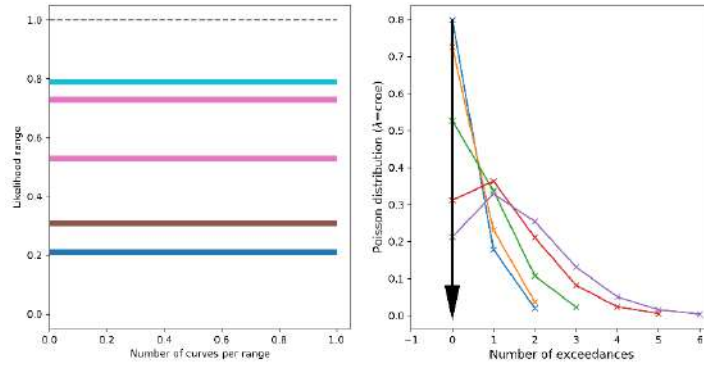
B.3.5   Acceleration 1.0 m/s²

Figure B.20: Left: Likelihood grouped by bins (coloured bars) and maximum theoretical likelihood (dashed line). Right: Poisson distributions generated from the cumulated rates of exceedance for the different branches of the logic-tree considered (coloured bars) and observed number of exceedances (black arrow). Results corresponding to the ESHM20 model (5 centiles) using data from Europe for the acceleration threshold 0.1 m/s^2.